Quarterly Reviews of Biophysics

cambridge.org/qrb

Thermodynamic, kinetic, and structural parameterization of human carbonic anhydrase interactions toward enhanced inhibitor design

Vaida Linkuvienė[1], Asta Zubrienė[1], Elena Manakova[2], Vytautas Petrauskas[1], Lina Baranauskienė[1], Audrius Zakšauskas[1], Alexey Smirnov[1], Saulius Gražulis[2], John E. Ladbury[3] and Daumantas Matulis[1]

[1]Department of Biothermodynamics and Drug Design, Institute of Biotechnology, Life Sciences Center, Vilnius University, Saulėtekio 7, 10257 Vilnius, Lithuania; [2]Department of Protein-DNA Interactions, Institute of Biotechnology, Life Sciences Center, Vilnius University, Saulėtekio 7, 10257 Vilnius, Lithuania and [3]Department of Molecular and Cell Biology and Astbury Centre for Structural Biology, University of Leeds, Leeds, UK

Invited Review

Cite this article: Linkuvienė V *et al* (2018). Thermodynamic, kinetic, and structural parameterization of human carbonic anhydrase interactions toward enhanced inhibitor design. *Quarterly Reviews of Biophysics* **51**, e10, 1–48. https://doi.org/10.1017/S0033583518000082

Received: 30 July 2018
Revised: 14 September 2018
Accepted: 11 October 2018

Key words:
Carbonic anhydrase; drug design; kinetics; protein–ligand binding; thermodynamics; X-ray crystallography

Author for correspondence: Daumantas Matulis, E-mail: matulis@ibt.lt, daumantas.matulis@bti.vu.lt

Abstract

The aim of rational drug design is to develop small molecules using a quantitative approach to optimize affinity. This should enhance the development of chemical compounds that would specifically, selectively, reversibly, and with high affinity interact with a target protein. It is not yet possible to develop such compounds using computational (i.e., *in silico*) approach and instead the lead molecules are discovered in high-throughput screening searches of large compound libraries. The main reason why *in silico* methods are not capable to deliver is our poor understanding of the compound structure–thermodynamics and structure–kinetics correlations. There is a need for databases of intrinsic binding parameters (e.g., the change upon binding in standard Gibbs energy (ΔG_{int}), enthalpy (ΔH_{int}), entropy (ΔS_{int}), volume (ΔV_{intr}), heat capacity ($\Delta C_{p,int}$), association rate ($k_{a,int}$), and dissociation rate ($k_{d,int}$)) between a series of closely related proteins and a chemically diverse, but pharmacophoric group-guided library of compounds together with the co-crystal structures that could help explain the structure–energetics correlations and rationally design novel compounds. Assembly of these data will facilitate attempts to provide correlations and train data for modeling of compound binding. Here, we report large datasets of the intrinsic thermodynamic and kinetic data including over 400 primary sulfonamide compound binding to a family of 12 catalytically active human carbonic anhydrases (CA). Thermodynamic parameters have been determined by the fluorescent thermal shift assay, isothermal titration calorimetry, and by the stopped-flow assay of the inhibition of enzymatic activity. Kinetic measurements were performed using surface plasmon resonance. Intrinsic thermodynamic and kinetic parameters of binding were determined by dissecting the binding-linked protonation reactions of the protein and sulfonamide. The compound structure–thermodynamics and kinetics correlations reported here helped to discover compounds that exhibited picomolar affinities, hour-long residence times, and million-fold selectivities over non-target CA isoforms. Drug-lead compounds are suggested for anticancer target CA IX and CA XII, antiglaucoma CA IV, antiobesity CA VA and CA VB, and other isoforms. Together with 85 X-ray crystallographic structures of 60 compounds bound to six CA isoforms, the database should be of help to continue developing the principles of rational target-based drug design.

Abbreviations

ANS, 1,8-anilinonaphthalene sulfonate; AZM, acetazolamide (also commonly abbreviated as AZA, AAZ, ACTAZ); CA, carbonic anhydrase; DSC, differential scanning calorimetry; DSF, differential scanning fluorimetry; EZA, ethoxzolamide; FPSA, fluorescent (fluorescence-based) pressure shift assay, PressureFluor; FTSA, fluorescent (fluorescence-based) thermal shift assay, alternatively termed ThermoFluor or differential scanning fluorimetry, DSF; *int*, intrinsic; ITC, isothermal titration calorimetry; MZM, methazolamide (also commonly abbreviated as METHZ); NA, not available (attempted but could not be conclusively determined); ND, not determined; *obs*, observed; SFA, stopped-flow assay; SPR, surface plasmon resonance; SULFA, sulfanilamide; TFS, trifluoromethanesulfonamide (also commonly abbreviated as TFMSA).

CAMBRIDGE UNIVERSITY PRESS

Variables

$\Delta\beta$, isothermal compressibility; ΔC_p, constant pressure heat capacity; ΔG, standard Gibbs energy of binding (equivalent to $\Delta G°$); ΔG_{int}, intrinsic standard Gibbs energy change on binding; ΔG_{obs}, observed standard Gibbs energy change on binding; $\Delta G_{pr,CA}$, standard Gibbs energy change on protonation of CA–Zn^{II}-bound hydroxide; $\Delta G_{pr,SA}$, standard Gibbs energy change on protonation of deprotonated sulfonamide amino group; ΔH, standard enthalpy change on binding (equivalent to $\Delta H°$); ΔH_{int}, intrinsic standard enthalpy change on binding; ΔH_{obs}, observed standard enthalpy change on binding; $\Delta H_{pr,buf}$, standard enthalpy change on buffer protonation; $\Delta H_{pr,CA}$, standard enthalpy change on CA–Zn^{II}-bound hydroxide protonation; $\Delta H_{pr,SA}$, standard enthalpy change on protonation of deprotonated sulfonamide amino group; IC_{50}, inhibitor concentration that inhibits 50% of enzymatic activity; k_a, association rate constant; $k_{a,int}$, intrinsic association rate constant; K_b, equilibrium binding constant; $K_{b,int}$, intrinsic equilibrium binding constant; $K_{b,obs}$, observed equilibrium binding constant; K_d, equilibrium dissociation constant; K_D, equilibrium dissociation constant (used in kinetics (SPR), equivalent to K_d); $K_{d,int}$, intrinsic equilibrium dissociation constant; $K_{d,obs}$, observed equilibrium dissociation constant; K_d, dissociation rate constant; $K_{d,int}$, intrinsic dissociation rate constant; K_i, inhibition of enzymatic activity constant; K_M, Michaelis constant of an enzyme; pK_a, negative logarithm of the dissociation constant of acid protons; $pK_{a,CA}$, negative logarithm of the dissociation constant of acid protons from CA–Zn^{II}-bound water molecule; $pK_{a,SA}$, negative logarithm of the dissociation constant of acid protons from the protonated sulfonamide amino group; P_t, total protein concentration; ΔS, standard entropy change on binding (equivalent to $\Delta S°$); $\Delta S_{pr,CA}$, standard entropy change on protonation of CA–Zn^{II}-bound hydroxide; $\Delta S_{pr,SA}$, standard entropy change of protonation of deprotonated sulfonamide amino group; T_m, melting (unfolding, denaturation) temperature of a protein; ΔV, the standard change on binding of the volume of the protein–solvent–ligand system.

Introduction

The quantification of binding of low molecular weight chemical compounds to proteins is a field of great importance in biomedical sciences, especially in drug design. It has been proposed that the optimization of the thermodynamic and kinetic parameters of ligand binding to proteins should lead to compounds with improved interaction characteristics and increased possibilities to become drugs. Despite great efforts, it has become increasingly clear recently that it is difficult to correlate small changes in the thermodynamic parameters of binding with the structure of the chemical compound. As suggested by Krimmer and Klebe (2015), such correlations usually only work for closely related compounds. The limited extent of correlation is exemplified by enthalpy changes upon binding which are strongly influenced by solute effects and/or structural flexibility (Geschwindner *et al.*, 2015). There are at least four types of correlations that are of interest here for drug design, namely, the correlations between compound chemical structure and it's protein-binding thermodynamic and kinetic parameters, and the correlations between the crystallographic structure of the compound-protein complex and it's binding thermodynamic and kinetic parameters.

It is not yet possible to use computational methods to design chemical compounds that interact with a particular binding site on a target protein with a predictable affinity and other binding parameters. There is a need of significantly larger experimental data collections together with improved theoretical models that would explain the correlations between both compound and protein structures and the binding energetics. In the direction towards this goal, we see a need for the following experimental datasets (databases) that need to be assembled or significantly enlarged:

1. Large database of thermodynamic binding data of chemically diverse, but also closely related, e.g., through a pharmacophoric group, chemical compound library to a target protein;
2. Thermodynamic and kinetic databases of chemical compound binding should be assembled for a series of closely related proteins that possess similar structural fold and similar binding sites (e.g., isoforms of the same enzyme, or mutants);
3. All thermodynamic parameters of binding that are possible to measure should be accumulated, not only the affinity (ΔG), but also the changes in the standard enthalpy (ΔH), entropy (ΔS), heat capacity (ΔC_p), and even volume (ΔV) and compressibility ($\Delta\beta$) upon binding;
4. Kinetic parameters of binding, the association rate (k_a) and the dissociation rate (k_d, residence time, residence half period) should be accumulated;
5. All the above-listed thermodynamic and kinetic parameters should be intrinsic, where as many as possible of the undesired contributions are subtracted (e.g., linked protonation, buffer, salt, protein, and ligand conformation changes, etc.) to enable the correlation of binding energies with the structures;
6. Structural characterization (e.g., by X-ray crystallography or NMR) of the unliganded apo-protein and protein-compound complexes, desirably for each binding reaction.

Significant efforts have been devoted to the assembly and curation of protein–ligand binding data and the following databases have been assembled to address each of these goals.

The **BindingDB** (Gilson *et al.*, 2016) (http://www.bindingdb.org/bind/index.jsp) is a public web database of 1 427 022 measured binding affinities between 7026 potential target proteins and 639 152 chemical compounds (as of January, 2018) that were experimentally determined by various techniques including enzyme inhibition and kinetics, isothermal titration calorimetry, NMR, radioligand and competition, and numerous other assays.

The **ChEMBL** (Liu *et al.*, 2015) (https://www.ebi.ac.uk/chembl/) database contains chemical compound bioactivity data against drug targets. The 2018-01-11 version contains 2 101 843 compounds, 14 675 320 activities, 1 302 147 assays, and 11 538 targets. This database of bioactive drug-like small molecules contains compound chemical structures, calculated properties (e.g., log *P*, Molecular Weight, Lipinski parameters, etc.) and bioactivities (e.g., binding constants, pharmacology, and ADMET data). Clinical progress data are currently being integrated into the database.

The **DrugBank** (Wishart *et al.*, 2006) (https://www.drugbank.ca/) is a bioinformatics and cheminformatics resource that combines drug chemical, pharmacological, and pharmaceutical data with drug target sequence, structure, and pathway information. The latest release of DrugBank (version 5.0.11, released 2017-12-20) contained 10 917 drug entries including 2352 FDA-approved small molecule drugs, 926 FDA-approved biotech (protein/peptide) drugs, 108 nutraceuticals, and 5069 experimental drugs.

https://doi.org/10.1017/S0033583518000082

PDBbind database (Liu *et al.*, 2015) (http://www.pdbbind.org.cn/) provides a comprehensive collection of the experimentally measured binding affinity data for complexes deposited in the Protein Data Bank (PDB). The 2017 release provides binding data of a total of 17 900 biomolecular complexes, including protein–ligand (14 761), nucleic acid–ligand (121), protein–nucleic acid (837), and protein–protein complexes (2181), the largest collection of this kind. It connects the energetic and structural information of these complexes, helpful for computational studies on molecular recognition in biological systems.

Binding MOAD (Ahmed *et al.*, 2015) (http://bindingmoad.org/) is focused on well-resolved protein crystal structures with a resolution better than 2.5 Å with clearly identified biologically relevant ligands annotated with experimentally determined binding data. The latest database update in 2014 included 25 769 protein–ligand structural complexes from the PDB, 12 440 non-covalently bound ligands, and 9142 binding data.

The Affinity Database **AffinDB** (Block, 2006) (http://pc1664.pharmazie.uni-marburg.de/affinity/) contains affinity data for protein–ligand complexes of the PDB. Its purpose is to provide direct and free access to the experimental affinity of a given complex structure. As of January 11th, 2018, AffinDB contained 748 affinity values covering 474 different PDB complexes.

The **SCORPIO** database (Olsson *et al.*, 2008) (http://scorpio2.biophysics.ismb.lon.ac.uk/) is a free online repository of protein–ligand interaction enthalpies measured by ITC. It holds 31 different proteins, 173 ligands, approximately 400 ITC datasets, 118 crystal structures, and approximately 90 unique protein–ligand complexes with both thermodynamic and structural data. However, no significant correlations have been observed that would enable a deeper understanding of the recognition phenomenon despite the attempts to select only intrinsic binding data.

All these databases (Inhester and Rarey, 2014) have been of great importance but since most data were presented without a significant selection of intrinsic data, it is difficult to observe systematic correlations that would help to understand the protein–ligand recognition energetics. Figure 1 shows a general illustration of the intrinsic thermodynamic parameters.

In an effort to investigate the correlations between compound structure and the energetics of interaction with the target proteins, we have chosen a system of human carbonic anhydrases (CAs) and their well-known inhibitors, aromatic primary sulfonamides. The system is convenient both from the chemical compound and the protein side thus allowing a large set of data to be accumulated. There are 12 catalytically active isoforms (isozymes) of CAs in the human body. Every isoform contains Zn^{II} in the active site of the enzyme where the amino group of the sulfonamide inhibitor binds via a coordination bond. This pharmacophoric group orients the compounds to bind specifically to the active site and the anchor-like interaction with the Zn^{II} significantly increases the affinity of the inhibitor to the CA. Synthetic variations of the aromatic sulfonamide are quite easy to prepare and thus a large library of aromatic sulfonamide compounds was synthesized by varying the substituents on the aromatic ring. Furthermore, a large set of sulfonamide compounds has already been clinically used as human drugs for several decades. Intrinsic thermodynamic and kinetic parameters of these inhibitors were determined by biochemical enzyme inhibition methods and biophysical direct interaction assays described below. A large collection of X-ray crystal structures have also been determined by a number of laboratories.

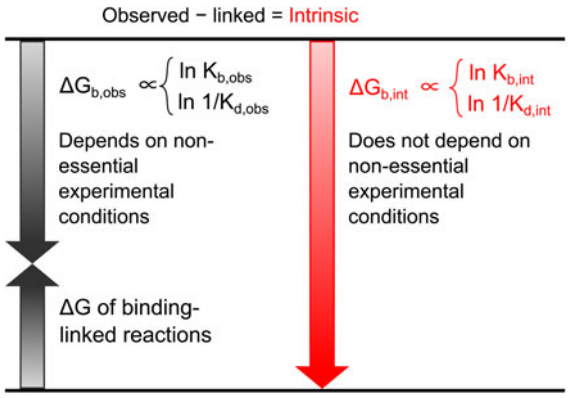

Fig. 1. General illustration of the term *intrinsic*. The standard *observed* Gibbs energy of a protein–ligand binding depends on various non-essential experimental conditions if there are binding-linked reactions that require energy consumption in order for the binding reaction to occur. The standard intrinsic Gibbs energy of binding is obtained by summation of the energies from those linked reactions. The intrinsic energy is thus always greater than the observed and the intrinsic affinity is greater than the observed. The same argument applies to all thermodynamic and kinetic parameters as will be demonstrated below for the case of CA where the binding-linked reactions are protonation reactions of the protein, the ligand, and the compensation by the buffer.

Overview of CA isoforms in the human body

The enzyme that catalyzes liberation of the body's CO_2 from HCO_3^- from blood in the lung was discovered in 1932–33 by Norman U. Meldrum and Francis J. W. Roughton in Cambridge and William C. Stadie and Helen O'Brien at the University of Pennsylvania (Meldrum and Roughton, 1932, 1933*a*, 1933*b*; Stadie and O'Brien, 1933*a*, 1933*b*; Chegwidden *et al.*, 2000; Forster, 2000).

There are several evolutionarily unrelated CA gene families (Dodgson *et al.*, 1991). However, only the enzymes of the alpha family are expressed in humans, of which there are 15 isoforms (isozymes). Twelve of these isoforms are catalytically active, while three are inactive because they lack Zn^{II} in the active site due to mutations of His residues that bind the Zn^{II}. As schematically shown in Fig. 2, human CA isoforms exhibit different cellular localization and multimerization patterns. There are a number of books and reviews that describe CAs from human and other organisms in great detail (Dodgson *et al.*, 1991; Chegwidden *et al.*, 2000; Supuran *et al.*, 2004; Frost and McKenna, 2014).

In this work, we limit the set of proteins to the 12 catalytically active human CA isoforms because a potential drug would have to demonstrate selectivity towards one target isoform and not exhibit a toxic effect by inhibiting other vital non-target isoforms.

The first X-ray crystal structure of a carbonic anhydrase was solved by Liljas *et al.* (1972). It showed that CA is primarily a beta-sheet-structured protein. Later structures of other CA isoforms showed that the proteins have not only highly homologous sequences, but also highly similar 3D structures (as shown in Fig. 3 where five human CA isoforms have been superimposed).

The CAs catalyze the reversible CO_2 hydration reaction:

$$CO_2 + H_2O \rightleftharpoons HCO_3^- + H^+ \quad (1)$$

This reaction is spontaneous but the enzyme may accelerate the achievement of equilibrium by up to approximately a million fold.

https://doi.org/10.1017/S0033583518000082

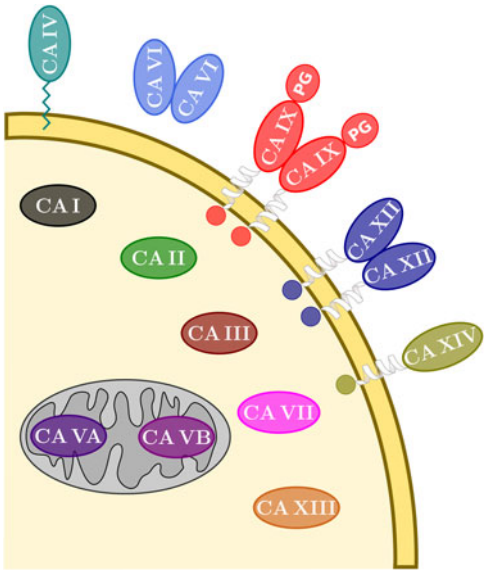

Fig. 2. Localization and multimerization of catalytically active 12 human CA isoforms in the cell. Isoforms CA I, CA II, CA III, CA VII, and CA XIII are cytosolic, CA VA and CA VB are found in mitochondria, CA VI is excreted in human saliva and milk, CA IV is anchored to the membrane via a covalently attached lipid moiety, and CA IX, CA XII, and CA XIV are membrane-bound via a single transmembrane alpha helix with the catalytic domain being outside of the cell. The remaining three isoforms (named CARP – CA-related protein), CA VIII, CA X, and CA XI are catalytically inactive and not shown in the figure. The CA VI, CA IX, and CA XII are dimers while the rest are monomers. The CA IX bears a proteoglycan-like (PG) domain – a unique feature of CA IX.

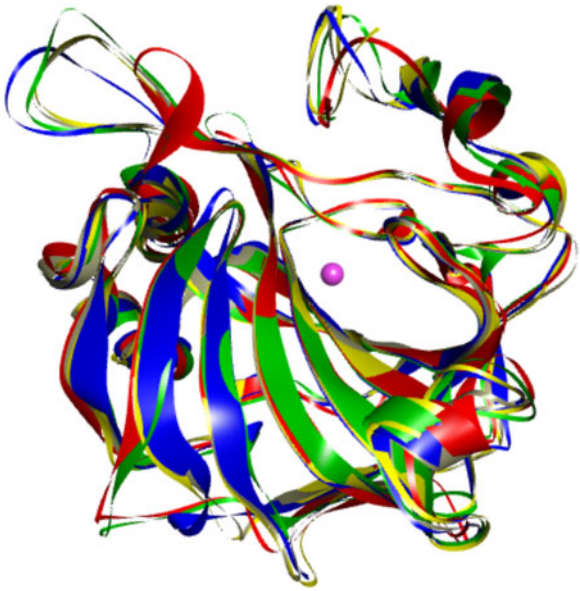

Fig. 3. Overlay of the backbones of five human CA isoforms shown in different colors (CA I – blue, CA II – grey, CA VII – yellow, CA IX – red, and CA XII – green). Their backbones superimpose essentially identically.

Human CA isoforms possess different specific enzymatic activities. Isoforms CA II and CA IX are considered to be the most active (Hilvo *et al.*, 2008) while isoform CA III is the least active isoform. Catalytic activities of recombinant CAs and the catalytic mechanism have previously been described (Krishnamurthy *et al.*, 2008; Supuran, 2008).

The CAs are implicated in numerous diseases. For example, CA IX is scarcely expressed in healthy human tissue (stomach/duodenum, gallbladder, and body cavity linings), but highly overexpressed in numerous solid hypoxic tumors (Pastorekova *et al.*, 2007). This makes CA IX an attractive anticancer target. Indeed, inhibitors that possess high affinity and selectivity towards CA IX over other CA isoforms are currently the focus of anticancer drug development programs.

Overview of CA inhibitors

According to Davenport (1984), the history of CA inhibitors begins with David Keilin who discovered that sulfonamides inhibit CAs. Schwartz tried sulfanilamide as a diuretic in 1940 while Roblin and Clapp at the American Cyanamid Company synthesized acetazolamide in 1949. Later, thiazides and furosemide-type drugs were extensively used for the treatment of hypertension and edema. These and other primary sulfonamides ($R—SO_2NH_2$) are now classical inhibitors of CAs, many of them are still used in the clinic.

The sulfonamide amino group of the inhibitor makes a coordination bond with the catalytic Zn^{II} thus preventing CO_2 or HCO_3^- from binding and competitively inhibiting the CO_2 hydration reaction. The primary sulfonamides may be considered transition state analogs with respect to their mode of active site binding (Fig. 4).

Some clinically used CA inhibitors are not only sulfonamide derivatives, but also sulfamates ($R—O—SO_2NH_2$) (Supuran *et al.*, 2003; Smith and Jones, 2008; Carta *et al.*, 2014). These drugs are used to treat various diseases such as glaucoma (Masini *et al.*, 2013), potentially obesity (Scozzafava *et al.*, 2013), epilepsy (Aggarwal *et al.*, 2013), or act as diuretics (Supuran, 2008). Numerous new sulfonamide derivatives have been reported in published patents and articles describing the development of novel compounds (Carta *et al.*, 2012*a*; Lomelino and McKenna, 2016). Their binding affinity and selectivity depend on the aromatic/heterocyclic scaffold of sulfonamide and the functional groups linked to this scaffold. One of them is in clinical trials for the treatment of hypoxic, metastatic tumors (Lou *et al.*, 2011; Supuran, 2017).

Several new classes of CA inhibitors have been developed, and their inhibitory activity and the binding mechanism extensively reviewed (De Simone *et al.*, 2013; McKenna and Supuran, 2014; Lomelino and McKenna, 2016; Supuran, 2017). Like sulfonamides, various compounds were found to bind directly to the Zn^{II} in the active site i.e. dithio-/monothiocarbamates (Carta *et al.*, 2012*a*), xanthanes (Carta *et al.*, 2013; Abellán-Flos *et al.*, 2015), hydroxamates (Di Fiore *et al.*, 2012), boronic acids and borols (Chazalette *et al.*, 2001; Winum *et al.*, 2009). Among the inhibitors that anchor to the metal ion coordinated water are phenols (Innocenti *et al.*, 2010; Maresca *et al.*, 2015; Karioti *et al.*, 2016), polyamines (Carta *et al.*, 2010; Davis *et al.*, 2014), sulfocoumarins (Tanc *et al.*, 2013; Tars *et al.*, 2013), thioxocoumarin (Ferraroni *et al.*, 2016), and carboxylic acids (Martin and Cohen, 2012). It was found that carboxylic acids can also bind outside of the active site (D'Ambrosio *et al.*, 2015). Another large group of CA inhibitors is coumarins which on hydrolysis bind at the entrance to the active site (Maresca *et al.*, 2009; Touisni *et al.*, 2011). The same binding mechanism is proposed for fullerenes binding to CA (Innocenti *et al.*, 2010*a*). Saccharin and its derivatives were identified as CA inhibitors. However, their binding mechanism has not been determined (Köhler *et al.*, 2007; D'Ascenzio *et al.*, 2014) and there are inconsistencies regarding their affinity measurements derived from different

https://doi.org/10.1017/S0033583518000082

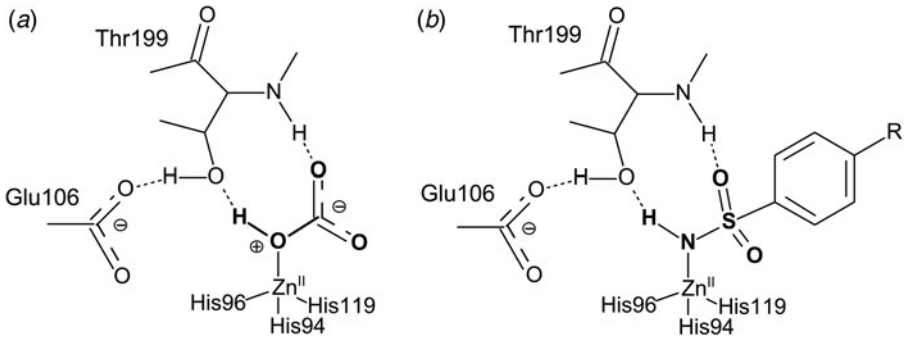

Fig. 4. Comparison between interactions of primary aromatic sulfonamide, and bicarbonate with the CA.

methods (Morkūnaitė *et al.*, 2014). It was shown that secondary and tertiary sulfonamides inhibit CA activity (Alp *et al.*, 2013).

As seen from the above list, there are many chemical compounds that are inhibitors of CA. The newest ones are mostly not sulfonamides. They have been reviewed elsewhere and are not subject of this paper. We limited this work to the primary sulfonamides that have a well-established 1 : 1 molecular binding mechanism and are thus convenient for a detailed structure–thermodynamics analysis. Furthermore, as will be discussed below, it is essential to correlate the *intrinsic* binding parameters with the structures and not the *observed* parameters that are usually listed in the literature on CA inhibitors. We included in this paper only the compounds where the intrinsic binding data has been determined and thermodynamic/kinetic parameters confirmed by several techniques.

Assays to determine small molecule inhibitor interaction with CA

There are many assays of protein–ligand interactions that have been applied to study CA inhibitors. These multiple methods have been extensively reviewed by Krishnamurthy *et al.* (2008). Here we describe and compare five biochemical and biophysical techniques. The methods are not only convenient but also necessary and sufficient for the characterization of CA–sulfonamide interactions:

- SFA – the stopped-flow kinetic assay of inhibition of CA enzymatic activity, hydration of CO_2 to HCO_3^- and H^+,
- ITC – isothermal titration calorimetry, a technique that determines the affinity, enthalpy, entropy, and heat capacity of interaction,
- FTSA – the fluorescent (fluorescence-based) thermal shift assay (commonly termed ThermoFluor or differential scanning fluorimetry (DSF)), an assay that determines the affinity of interaction by following the thermal stabilization of the protein,
- SPR – surface plasmon resonance, an assay that determines the kinetics of interaction including the rates of association and dissociation,
- FPSA – fluorescent pressure shift assay (also known as PressureFluor), a rarely used assay that determines the volume change of the system upon interaction.

We have concluded that at least two assays should be used to confirm novel inhibitors and all of these assays have drawbacks and limitations and contribute a different kind of information as will be discussed below.

Stopped-flow assay of the inhibition of CA enzymatic activity (SFA)

Inhibitors of proteins that possess enzymatic activity and thus are enzymes are often discovered by performing biochemical assays that determine the inhibition of enzymatic activity. Such assays must be developed individually for each enzyme and are often quite tedious and material and time-consuming. The CA activity is often determined by the stopped-flow spectrophotometric method by following the decrease in absorbance of a pH indicator (e.g., phenol red) because of the drop in pH due to the protons appearing from the CO_2 hydration reaction catalyzed by the CA, Eq. (1). The assay is well-described elsewhere (Khalifah *et al.*, 1977; Smirnovienė *et al.*, 2017) and its limitations will be discussed below.

Isothermal titration calorimetry (ITC)

ITC is one of the most commonly used techniques to determine protein–ligand interactions (Chaires, 2008; Krimmer and Klebe, 2015; Callies and Daranas, 2016; Falconer, 2016; Renaud *et al.*, 2016; Vega *et al.*, 2016). However, the technique requires a relatively large amount of pure protein and compound. The technique is isothermal and thus can be fully performed at a physiological temperature, e.g., resembling the conditions in the human body. The reaction is performed by titrating the protein with the compound in the calorimeter cell that measures the heat evolved by the interaction of known quantities of binding partners. The heat is a universal observable in any reaction. Method development is dictated solely by the components of titration and hence straightforward. However, it is not always straightforward to interpret the data obtained. The heat of reaction determined by the calorimeter is equal to the thermodynamic parameter enthalpy, under two conditions that there is no work performed and the pressure is constant. Thus ITC provides a direct route to a determination of the enthalpy of interaction. The experiment is performed in such a way that the ligand is injected in aliquots and thus the evolved heats are proportional to the fraction of ligand bound to the protein. From the direct determination of ligand-bound fraction, one can calculate the equilibrium binding/dissociation constant (and hence affinity) for the interaction. Knowledge of the equilibrium constant permits the calculation of the change in Gibbs energy of binding:

$$\Delta G = -RT\ln(K_b) \tag{2}$$

The standard entropy change upon interaction can also be determined from the same experiment by subtracting the Gibbs

https://doi.org/10.1017/S0033583518000082

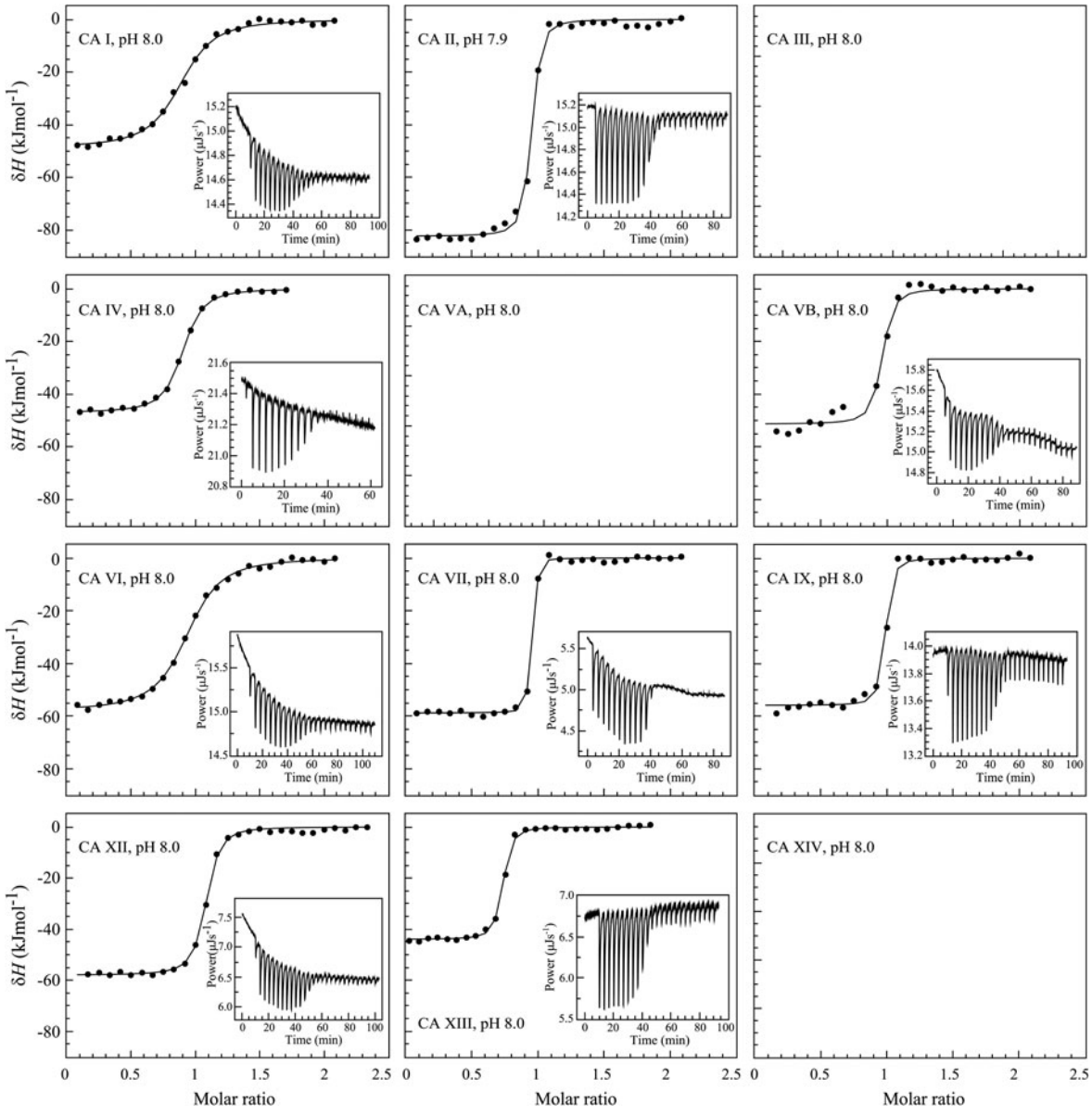

Fig. 5. Examples of ITC data of **1** binding to catalytically active recombinant human CA isoforms at pH 8, 25 °C as determined using the VP-ITC calorimeter. Insets show the raw curves with unflattened baselines, without user-biased interference. Experiments were performed in 50 mM sodium phosphate buffer containing 100 mM NaCl and 2% DMSO as previously described in: CA I and CA II (Morkūnaitė *et al.*, 2015), CA IV (Mickevičiūtė *et al.*, 2017), CA VB (Kasiliauskaitė *et al.*, 2016), CA VI (Kazokaitė *et al.*, 2015), CA VII (Pilipuitytė and Matulis, 2015), CA IX (Linkuvienė *et al.*, 2016*b*), CA XII (Jogaitė *et al.*, 2013), and CA XIII (Baranauskienė and Matulis, 2012). All panels are drawn at the same scale to help visualize the differences both in enthalpies and affinities of binding. No data have been determined at comparable conditions for CA III, CA VA, and CA XIV.

energy from enthalpy:

$$\Delta S = (\Delta H - \Delta G)/T \quad (3)$$

The binding of **1** (EZA, all compound structures are shown in Supplementary Table 1) to the catalytic domains of catalytically active human recombinant CAs as determined by ITC is shown in Fig. 5. It is clear that, for example, **1** bound CA I significantly weaker than CA II under the assay conditions. Furthermore, the observed enthalpy of interaction was significantly more exothermic (more negative) for CA II than for CA I. For every reaction, the molar ratio necessary to reach the midpoint of titration was approximately 1.0. Thus, essentially all 100% of the protein was able to bind the ligand to achieve saturation. This indicates that both the protein and compound preparations were highly pure.

Fluorescent thermal shift assay

FTSA, also commonly termed DSF, or ThermoFluor (when performed in a high-throughput plate format) is the assay that determines the melting (unfolding or denaturation) temperature T_m of the protein in the absence and the presence of increasing concentrations of a ligand. The T_m may be determined by fluorescence or by differential scanning calorimetry (DSC) (Brandts and Lin, 1990). The assay may follow the intrinsic protein fluorescence of tryptophan or tyrosine residues as the protein unfolds and

https://doi.org/10.1017/S0033583518000082

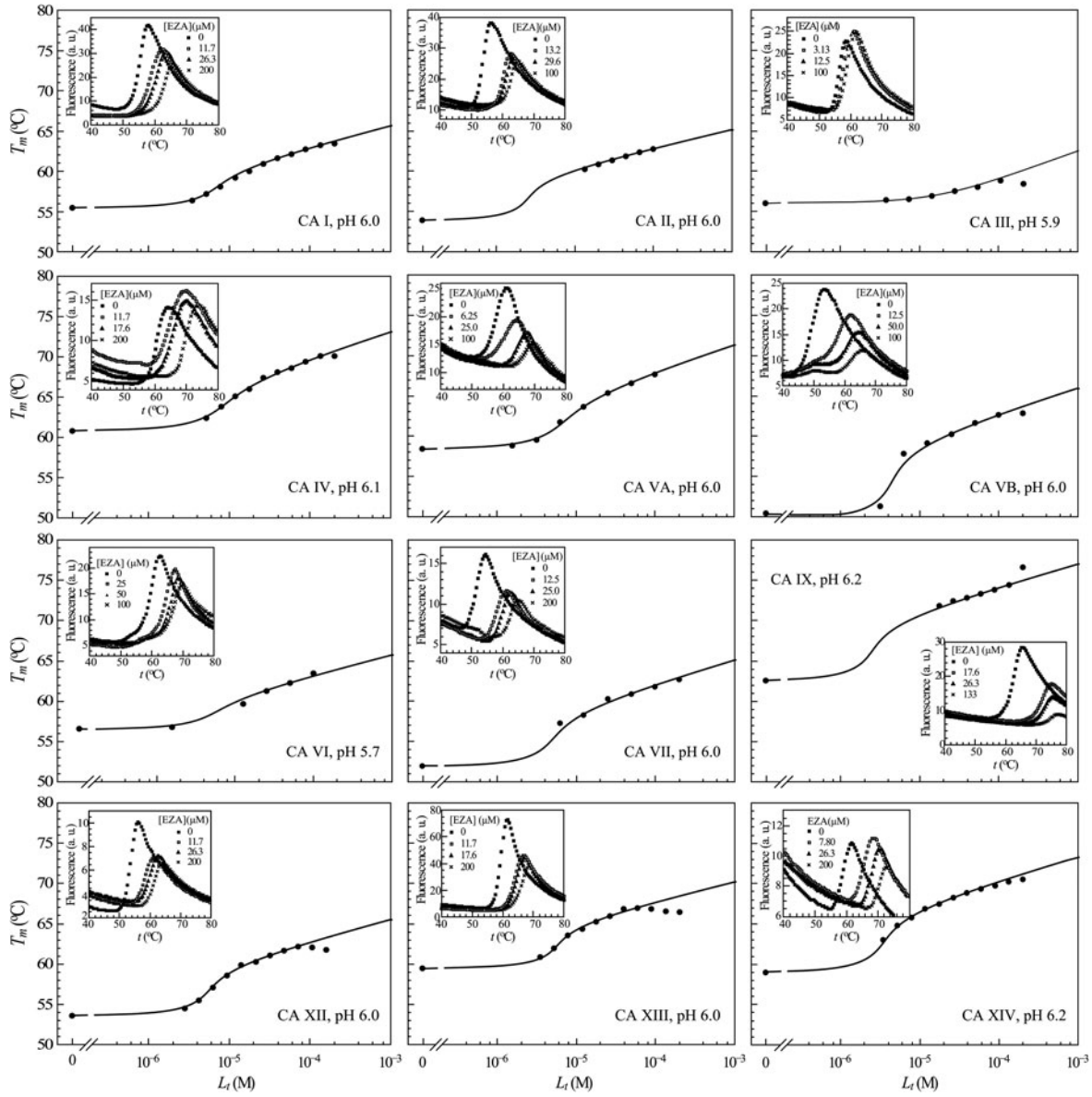

Fig. 6. Example of FTSA data of **1** binding to all 12 catalytically active recombinant human CA isoforms at pH 6. The insets show raw melting curves obtained by following ANS fluorescence. The experiments were performed at pH 6 in universal buffer made of 50 mM sodium phosphate, 50 mM sodium acetate, and 25 mM sodium borate containing 100 mM NaCl and up to 2% DMSO and 50 μM ANS as previously described: CA I and CA II (Morkūnaitė *et al*., 2015), CA IV (Mickevičiūtė *et al*., 2017), CA VB (Kasiliauskaitė *et al*., 2016), CA VI (Kazokaitė *et al*., 2015), CA VII (Pilipuitytė and Matulis, 2015), CA IX (Linkuvienė *et al*., 2016*b*), CA XII (Jogaitė *et al*., 2013), CA XIII (Baranauskienė and Matulis, 2012), and CA XIV (Juozapaitienė *et al*., 2016).

the environment of these residues changes. Alternatively, the fluorescence of a solvatochromic probe such as ANS (1,8-anilinonaphthalene sulfonate) (Anderson and Weber, 1969; Slavik, 1982; Matulis and Lovrien, 1998; Matulis *et al*., 1999; Cimmperman and Matulis, 2011) or Sypro Orange (Lo *et al*., 2004; Niesen *et al*., 2007) can be followed as the probe binds to the exposed hydrophobic residues upon protein unfolding. FTSA is a less-widely used technique than ITC, but its use has significantly increased when compound libraries are screened to determine the best binders to target proteins (Pantoliano *et al*., 2001; Yanchunas *et al*., 2005; McDonnell *et al*., 2009). The assay is relatively easy and robust and does not require assay development for a particular protein–ligand system. However, data interpretation sometimes may not be fully straightforward (Cimmperman *et al*., 2008; Cimmperman and Matulis, 2011).

In the assay, a series of wells with the constant protein concentration are prepared and various compound concentrations are added. The mixture is heated and the melting curves at all compound concentrations are recorded simultaneously in approximately 1 hour. The melting curves are fit to the 2-state (native-unfolded) model (Matulis *et al*., 2005; Cimmperman *et al*., 2008) providing the T_ms at various compound concentrations. These T_m dependencies on compound concentration are fit to the model that includes the thermodynamic parameters of protein unfolding and ligand binding (Cimmperman *et al*., 2008) yielding the affinity of the interaction (the dissociation constant K_d).

The binding affinities of **1** to all 12 catalytically active human CA isoforms determined by FTSA are shown in Fig. 6. The plots show the **1** dosing curves (where the compound concentration is on a logarithmic scale), while the insets show the melting curves

https://doi.org/10.1017/S0033583518000082

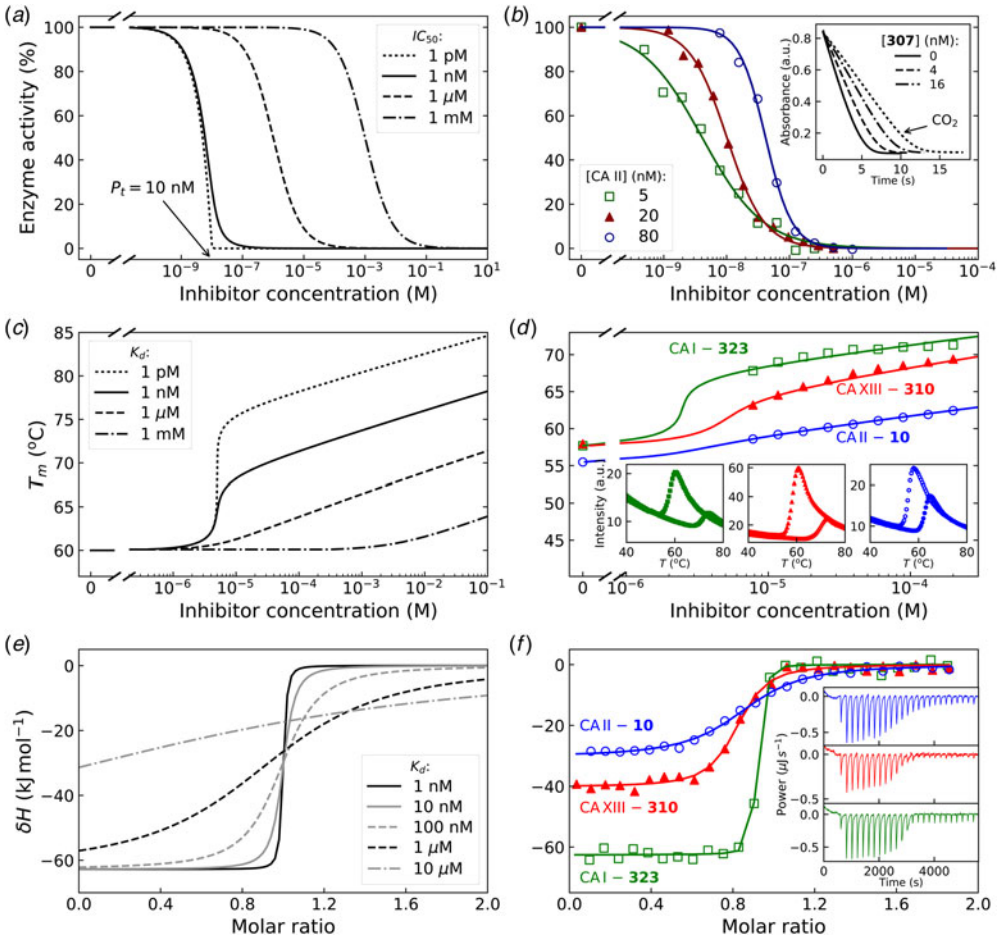

Fig. 7. Comparison of SFA, FTSA, and ITC techniques, their advantages and limitations. Panels on the left show simulated curves, while on the right – the examples of measured data. The figure is adapted from Smirnovienė *et al*. (2017). (*a*) The application of Hill equation at protein concentration P_t = 10nM and various values of apparent IC_{50}. The assay would not distinguish between 1 nM and 1 pM compounds because P_t cannot be reduced to less than 1 nM or 1 pM to obtain distinguishable dosing curves of nanomolar (solid line) or picomolar (dotted line) affinity. (*b*) Experimental data of an interaction between CA II-**307** at several compound concentrations. Data points were fitted according to the Hill equation with varied Hill coefficient. The inset shows the raw absorbance curves at several compound concentrations. (*c*) The simulated FTSA dosing curves for different binding affinities (K_d from 1 pM to 1 mM) are shown. These curves were generated using the following set of parameters: T = 37 °C, P_t = 10 μM, enthalpy of CA II unfolding is 690 kJ mol^{-1}, heat capacity of unfolding is 17 kJ mol^{-1} K^{-1}, enthalpy of binding is −42 kJ mol^{-1}, heat capacity of binding is −0.8 kJ mol^{-1} K^{-1} , and the melting temperature T_m without added ligand is 60 °C. (*d*) Experimental FTSA data of CA I-**323** (squares), CA II-**10** (circles), and CA XIII-**310** (triangles). The insets show raw melting curves at 0 and 200 μM inhibitor concentrations. (*e*) Simulated ITC curves using a single binding site model of different binding affinities at P_t = 10 μM. (*f*) Experimental ITC curves of the same binding interactions as in panel D. Affinity of CA I-**323** is too strong to be determined by ITC but FTSA assay provides accurate K_d.

with various added inhibitor concentrations. Compound **1** stabilized each CA isoform to a different extent. For example, CA III was stabilized by only several degrees, thus showing that this isoform binds the ligand weakly. However, CA IX was stabilized by more than 10° indicating strong interaction. In addition, the assay yielded stabilities of all CA isoforms in the absence of ligand at these assay conditions. It should be kept in mind that direct comparison between the ΔT_ms is usually valid only when the proteins are of similar molecular mass.

Surface plasmon resonance

SPR is also a commonly used technique to determine protein–ligand interactions and has been extensively reviewed (Myszka and Rich, 2000; Patching, 2014; Olaru *et al*., 2015; Renaud *et al*., 2016). The technique determines the protein–ligand association and dissociation rates. Therefore, it is often used to determine the kinetics of interactions. The inverse of the dissociation rate is equal to the residence time, a commonly used characteristic of the drug lead–protein pair. We will go in more detail on the assay in the section on sulfonamide–CA interaction kinetics.

Advantages and limitations of SFA, FTSA, and ITC

Here we emphasize that for the most complete picture of a studied binding reaction a multi-technique-based approach is recommended. We use all of the above-described assays for many CA inhibitors. Each technique has numerous advantages and disadvantages (Renaud *et al*., 2016). However, due to limitations in time and material, and the necessity to test as many chemical compounds as possible, some techniques may be more suited than others.

In Fig. 7, we compare the advantages and limitations of SFA, FTSA, and ITC. Panels on the left show simulated data while examples of observed data are shown on the right. The main limitation of SFA is that the IC_{50} may only be determined down to

https://doi.org/10.1017/S0033583518000082

about $P_t/2$ (half of the protein concentration) (Copeland, 2005). Despite being one of the fastest known enzymes, the concentration of any CA isoform cannot be reduced below 10 nM even for the most active CA II and CA IX and, therefore, the IC_{50} cannot be determined below approximately 5 nM. The dotted and solid curves in Fig. 7*a* show the position of the dosing curves if the protein concentration was 10 nM. The lines almost completely coincide with each other and, therefore, the compounds with picomolar affinities cannot be distinguished from nanomolar ones. In order to distinguish the curves, one would need to significantly reduce the protein concentration. This cannot be done in most cases and thus the K_i of CA inhibitors cannot be determined below approximately 2 nM.

Furthermore, some isoforms possess significantly lower specific enzymatic activity and thus their concentration in the assay must be increased. For example CA I is approximately 10-times less active than CA II. Therefore, the lowest K_i that can be determined for inhibitors of CA I at the same conditions is approximately 20 nM. This may lead to incorrect assignment of inhibitor selectivity towards CA II over CA I based on SFA alone.

Another significant disadvantage of SFA is that, as shown in Fig. 7*b*, if the protein concentration is varied, the dosing curves also shift and thus the K_i could appear to vary dependent on the concentration used in the assay. If the experiment is performed at a single CA concentration, the obtained values may be inaccurate. Therefore, SFA should be used with care keeping in mind the applied protein concentration in the assay that limits the K_i reachable in the assay.

In FTSA (Fig. 7*c*), there are essentially no limitations in affinity determination, thus picomolar and millimolar compounds may be easily distinguished in the same assay. At the simulated conditions, the picomolar compound would shift the temperature by over 20 °C, while the millimolar compound – by only 1° or 2° dependent on the added concentration. In order to detect millimolar compounds, it would be necessary to add a 10 mM compound. Figure 7*d* shows examples of the observed data. The limitation of FTSA is that the assay cannot be used for highly stable proteins that melt at temperatures over 90 °C. However, CAs denature around 55–65 °C. Thus, FTSA has a significant advantage over SFA because strongly-interacting picomolar compound K_ds may be determined correctly by FTSA and not by SFA.

The main disadvantage of FTSA compared with SFA is that it does not determine whether the compound is actually an inhibitor of the enzyme or just a binder. Ligands potentially may bind to various sites on CA surface, stabilize the protein, and be erroneously assigned to be an inhibitor of CA. Therefore, the SFA is a necessary confirmatory technique to demonstrate that the compound is actually an inhibitor of enzymatic activity. However, the affinity of an inhibitor will still be determined more accurately by FTSA than SFA. Since primary sulfonamides bind to the active site in a well-established way, both techniques yield the same K_d or K_i when the assays are properly performed.

The simulated curves of the third assay, ITC, are shown in Fig. 7*e*. The assay has optimal accuracy when the curve is of sigmoidal shape, such as the dashed curves ($K_d = 100 - 1000$ nM). If the compound binds weakly, for example in the micromolar range, the curve becomes too flat and may be indistinguishable from the curve of compound dilution, thus potentially leading to erroneous assignment of the observed data to a binding reaction. In such a situation the protein concentration must be raised, if the solubility of both components permits, expanding the window of affinity determination. On the other hand, if the compound has a K_d of 1 nM or tighter, the curve is too steep and the K_d again cannot be determined. It may be stated that 'the binding is 10 nM or tighter', but the actual affinity cannot be determined. In such a situation, the protein solution may be diluted as long as the signal remains sufficiently above the noise level.

The main advantage of ITC is that it is the only assay that may be used to directly determine the enthalpy of protein–ligand binding. It is also the most accurate technique to obtain the entropy and heat capacity of interaction. The change in enthalpy is most accurately determined when the binding is tight, i.e. nanomolar or tighter. It is nearly impossible to determine the change in enthalpy of weakly binding compounds by direct ITC titration (displacement titration may be sometimes used instead). Raising the protein concentration increases the range, but may not be practical in some cases.

Due to the above-described limitations, it is good to combine FTSA-determined K_d and the enthalpy determined by ITC. It is not possible to accurately determine subnanomolar K_d values from ITC without applying displacement ITC techniques that are not discussed here in detail, but have been introduced and reviewed previously (Krainer *et al.*, 2012; Krainer and Keller, 2015).

Comparison of the observed $K_{d,obs}$ values obtained by the above-described four techniques is shown in Fig. 8. The FTSA is the most robust technique in our opinion, there is essentially no substrate (CO_2) present (concentration of CO_2 from the air is significantly below the K_M of any CA), and the assay is practically without limits of the range (accessing $K_{d,obs}$s from at least pM to mM or greater). Therefore all compound interaction with CA isoforms has been determined by FTSA. Only a fraction of the compound affinities has been determined by the other three techniques.

ITC cannot accurately determine the K_d below 1 nM if we keep the protein concentration around 10 μM because the Wiseman *c* factor, equal to the product of the K_b and protein molar concentration for 1 : 1 binding reactions, which shows the steepness of the titration curve (see Fig. 7 and should be in the range of approximately 5–500), (Wiseman *et al.*, 1989) reaches 1000. Some increase of the accessible range may be achieved by reducing the protein concentration. Here we see (Fig. 8*a*) that there is a decent correlation between the affinities determined by FTSA and ITC in the 100 nM K_d range, but the ITC-determined values tend to show reduced affinities relative to FTSA in the 1–10 nM range. ITC thus tends to underestimate the single-digit nanomolar affinities. It is also important that the spread of data may reach up to 10-fold in affinity when comparing ITC with FTSA.

There was a quite good correlation between the affinities determined by FTSA and SFA (Fig. 8*b*). As discussed above, it is important to use SFA to confirm that the compounds are inhibitors of the enzymatic activity. In the case of CA inhibitors, because all compounds, reviewed in this paper, are primary sulfonamides with a well-described mode of binding by a number of techniques, we do not perform the SFA for all compounds due to several reasons. First, the assay cannot determine the IC_{50}s below the protein concentration, which is approximately 10 nM (Smirnovienė *et al.*, 2017). Second, the assay is significantly more costly both in time and materials to justify its performance for all studied compounds.

The bottom panel (Fig. 8*c*) compares the affinities obtained by FTSA and SPR. The SPR technique is commonly used to determine both the affinity and the kinetics of compound association

https://doi.org/10.1017/S0033583518000082

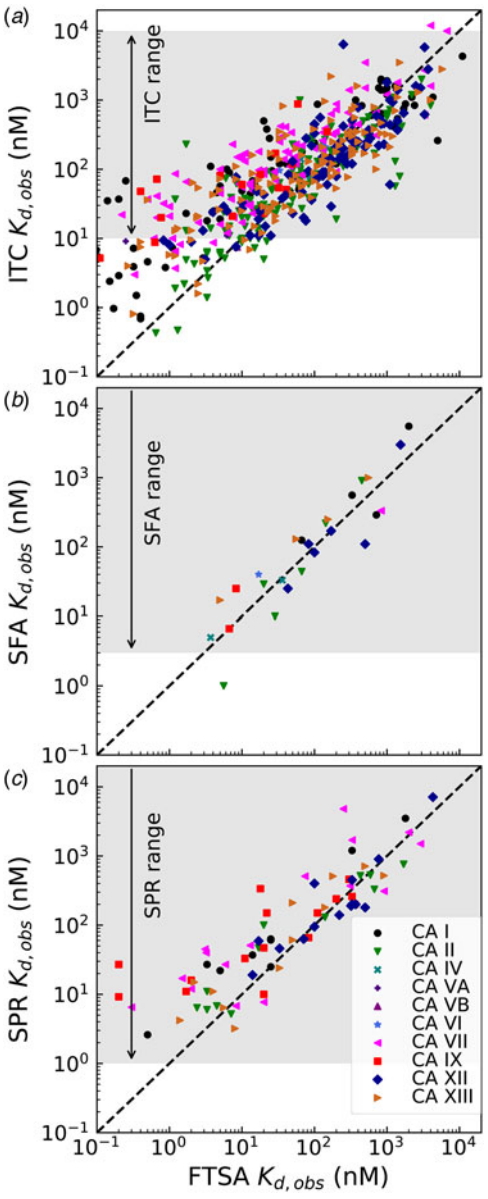

Fig. 8. Comparison of the experimentally determined $K_{d,obs}$ obtained by four techniques: fluorescent thermal shift assay (FTSA), isothermal titration calorimetry (ITC), stopped-flow assay of the inhibition of CA enzymatic activity, CO_2 hydration (SFA), and the surface plasmon resonance (SPR). All K_ds have been determined by FTSA as the most robust and reliable technique and compared with the results obtained for a portion of compounds by ITC, SFA, and SPR. The FTSA practically does not have limits or range of reliable determinations, the compound K_ds may be determined from pM to mM affinity range in a single experiment, while the other three techniques have limitations of the range where reliable determinations may be made, shown with arrows and shaded in grey.

and dissociation from CA (Redhead *et al.*, 2015; Talibov *et al.*, 2016). Similarly to the other three techniques, the spread or uncertainty of the data is quite similar.

Table 1 lists and provides some examples of $K_{d,obs}$ and K_i values obtained by SFA, FTSA, ITC, and SPR (Smirnovienė *et al.*, 2017). In cases, where the four techniques yielded different values, the bold numbers show the correct determination of the affinities. For some ligands of average affinity, all four techniques yielded the same value. For example, the binding and inhibition constants of **187** interactions with CA I, CA II, CA VII, CA XII, and CA XIII were essentially the same by all techniques. However, for example, the binding affinities of **323** to CA I, and of compounds **369** and **341** to CA IX could be correctly determined only by FTSA. The remaining three assays, SFA, ITC, and SPR, confirmed that the interaction is very strong, but could not reach the actual affinity value due to above-described limitations.

Volume change upon protein–ligand binding

The above-described assays provide means to determine inhibition and inhibitor binding thermodynamic and kinetic parameters. However, the picture of protein–ligand interaction can be significantly enhanced by the determination of volumetric properties of the interactions. Unfortunately, the majority of studies are limited to the techniques, which exploit only the temperature as a thermodynamic variable and avoid studying pressure effects because such techniques are much more laborious.

There are several techniques that are capable of determining the volume of protein–ligand binding: the fluorescent pressure shift assay (PressureFluor, FPSA) (Toleikis *et al.*, 2011, 2016; Skvarnavičius *et al.*, 2017), vibrating tube densitometry(Barbosa *et al.*, 2003; Son *et al.*, 2012; Toleikis *et al.*, 2016), and the high-pressure NMR (Wilton *et al.*, 2009; Roche *et al.*, 2012; Toleikis *et al.*, 2016). They can determine the change of system volume and compressibility caused by the bound ligand. The volumetric assays have been described previously by Carey *et al.* (1977); Barbosa *et al.* (2003); Chalikian and Filfil (2003); Wilton *et al.* (2009); Toleikis *et al.* (2011, 2012, 2016); Roche *et al.* (2012); Petrauskas *et al.* (2013); Voloshin *et al.* (2015); Skvarnavičius *et al.* (2017). However, there is relatively little data available in the literature on any protein–ligand system, not mentioning the CA, and it is difficult to judge yet if these approaches will be useful in the design of ligands with desired binding properties.

Observed *versus* intrinsic thermodynamic binding parameters

Intrinsic affinity of binding

Sulfonamides are by far the largest class of compounds that are inhibitors of CAs. However, despite the long history and importance of sulfonamides as CA inhibitors, there still remains uncertainty in their binding mechanism. As first identified by Taylor *et al.* (1970), the binding kinetics of sulfonamide inhibitor to CA II is dependent on pH and the dependence has a U-shape, interaction is fastest near neutral pH and slows down towards acidic and alkaline regions. Application of FTSA, ITC, and SPR techniques also showed that the binding affinity is strongest near neutral pH and decreases both in the acidic and alkaline regions. The affinity decreases exactly tenfold with one pH unit both in the acidic and alkaline regions. This indicates that the CA-sulfonamide binding reaction is coupled to at least two protonation–deprotonation reactions. As pointed by Taylor *et al.* (1970), there are four possible ways for the sulfonamide compound to bind the CA, shown in Eqs. (4)–(7).

$$\mathrm{CA-Zn^{II}-OH^- + RSO_2NH_2} \rightleftharpoons \mathrm{CA-Zn^{II}-NH_2SO_2R + OH^-} \quad (4)$$

https://doi.org/10.1017/S0033583518000082

Table 1. Comparison of binding and inhibition constants of CA I, CA II, CA VI, CA VII, CA IX, CA XII, and CA XIII obtained by SFA (pH 7.0–7.5, 25 °C), FTSA, ITC (pH 7.0, 37 °C), and SPR (pH 7.0–7.4, 25 °C). **SFA**. The used K_M values were, for CA I – 1.4 mM, CA II – 4.7 mM, CA VI – 6.9 mM, CA VII – 11.4 mM, CA IX – 6.9 mM, CA XII – 12 mM, and CA XIII – 13.8 mM, taken from Supuran (2008). The IC_{50} is the 50% inhibition concentration of enzymatic activity obtained by Hill fit of the data. K_i is the inhibition constant obtained after application of the Cheng–Prusoff equation to the IC_{50}. The $K_{d,obs}$ is the dissociation constant obtained via Morrison equation. **FTSA**. The $K_{d,obs}$ is the observed dissociation constant obtained by FTSA at the CA concentration 5 to 10 μM. **ITC**. The $K_{d,obs}$ is the observed dissociation constant obtained by ITC at the CA concentration of 4 to 10 μM. **SPR**. The $K_{d,obs}$ is the observed dissociation constant obtained by SPR at the CA concentration for immobilization of 75 μg ml^{-1} for CA I, 100 μg ml^{-1} for CA II, 25 μg ml^{-1} for CA VII, 100 μg ml^{-1} for CA IX, 25 μg ml^{-1} for CA XII, 75μg ml^{-1} for CA XIII as described by Talibov *et al.* (2016). Values are shown in the regular font when the results match among three methods within an approximate error of ±2 fold. Values are shown in bold to point the most reliable value when results are significantly different among the methods. Values are in italic to emphasize unreliable results when the methods should not be used due to their limitations (for SFA – concentration of the enzyme above the concentration of inhibitor, for ITC – Wiseman *c*-factor outside the required range). SFA, FTSA, and ITC data are taken from the references indicated next to the compound number. The standard error of K_d measurements is ±2 times (Petrauskas *et al.*, 2016; Linkuvienė *et al.*, 2016*a*)

	SFA							FTSA	ITC	SPR
Cpd.	CA	[CA] (nM)	[CO_2] (mM)	*h* coef.	IC_{50} (nM)	K_i (nM)	$K_{d,obs}$ (nM)	$K_{d,obs}$ (nM)	$K_{d,obs}$ (nM)	$K_{d,obs}$ (nM)
2 (Dudutienė *et al.*, 2014) **AZM**	CA I	300	11	1	400	45	290	2400	810	ND
	CA II	13	14	1.3	14	4.6	10	46	46	15
	CA II	50	13	1.1	*⩽35*	*⩽9.2*	**10**	46	46	15
	CA II	100	16	2	*⩽50*	*⩽12*	10	46	46	15
	CA IX	20	12	1.3	18	6.4	6.7	21	22	8.5
	CA XII	40	9.9	1.4	45	25	25	130	130	ND
	CA XIII	100	7.9	2	*⩽60*	*⩽38*	*⩽10*	**120**	60	37
187 (Kišonaitė *et al.*, 2014)	CA I	500	8.6	1	5600	780	5600	4300	2300	3500
	CA II	20	8.9	1	220	76	220	330	430	130
	CA VII	50	7.3	1	830	470	830	710	660	370
	CA XII	100	8.6	1	1100	640	1100	1400	370	180
	CA XIII	500	11	1	450	250	250	330	270	180
323 (Dudutienė *et al.*, 2013)	CA I	33	16	1.1	*⩽12*	*⩽0.9*	*⩽2*	**0.4**	*⩽12*	ND
	CA I	100	11	1.5	*⩽50*	*⩽5.5*	*⩽10*	0.4	*⩽12*	ND
	CA I	300	11	2	*⩽150*	*⩽17*	*⩽20*	0.4	*⩽12*	ND
341 (Dudutienė *et al.*, 2014)	CA I	500	13	1	46 000	4500	46 000	24 000	⩾10 000	ND
	CA II	40	13	1	910	240	910	1000	730	ND
	CA IX	20	10	2	*⩽13*	*⩽5.2*	*⩽5.0*	**0.77**	15	27
	CA XII	40	12	1	170	86	170	240	230	400
	CA XIII	150	14	1.3	180	90	130	98	420	ND
369 (Dudutienė *et al.*, 2014)	CA I	300	14	1	700	65	560	830	1100	ND
	CA II	20	14	1	29	7.4	29	56	59	100
	CA IX	10	14	3	*⩽5*	*⩽1.7*	*⩽10*	**0.032**	*⩽10*	ND
	CA IX	20	17	3	*⩽10*	*⩽2.9*	*⩽10*	0.032	*10*	ND
	CA XII	40	10	2	*⩽20*	*⩽11*	*⩽10*	**2.9**	20	ND
	CA XIII	54	9.7	2	*⩽25*	*⩽15*	*⩽10*	**4.0**	42	15

https://doi.org/10.1017/S0033583518000082

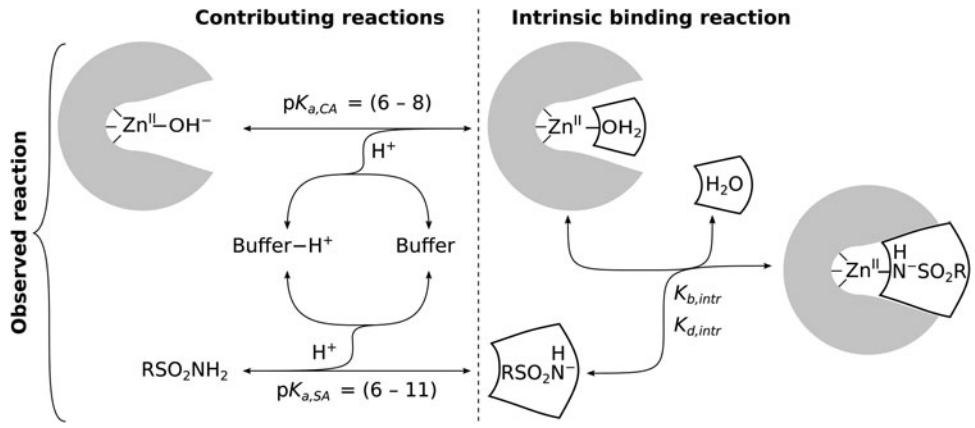

Fig. 9. The model of the linked reactions (also shown as Eq. (8)), occurring upon sulfonamide ligand binding to CA. A sum of several binding-linked reactions occur that we observe by any experimental technique, but the Quantitative Structure–Activity Relationship (QSAR)-type analysis requires that we analyze only the intrinsic reaction and correlate the intrinsic affinity and other intrinsic parameters with the structure of the ligand and the ligand–protein complex. The linked contributing reactions must be subtracted from the observed ones to obtain the intrinsic reaction.

$$\mathrm{CA-Zn^{II}-OH^- + RSO_2NH^-} \rightleftharpoons \mathrm{CA-Zn^{II}-NH-SO_2R + OH^-} \quad (5)$$

$$\mathrm{CA-Zn^{II}-H_2O + RSO_2NH_2} \rightleftharpoons \mathrm{CA-Zn^{II}-NH_2SO_2R + H_2O} \quad (6)$$

$$\mathrm{CA-Zn^{II}-H_2O + RSO_2NH^-} \rightleftharpoons \mathrm{CA-Zn^{II}-NH-SO_2R + H_2O} \quad (7)$$

The first possibility is that the electrostatically neutral (protonated) sulfonamide replaces the OH^- bound to the Zn^{II} in the active site of CA (Eq. (4)). Second, that the negatively charged sulfonamide replaces the OH^- (Eq. (5)), third, that neutral sulfonamide displaces neutral water molecule (Eq. (6)), and the fourth, that the deprotonated sulfonamide (negatively charged SO_2NH^-) replaces the H_2O molecule coordinated by the Zn^{II} in the active site of CA (Eq. (7)). The second and third reactions have been already shown by the authors to be inconsistent with the U-shape dependence on pH. However, both the first and the fourth reactions seemed plausible and were difficult to distinguish.

We are now convinced that the fourth reaction (Eq. (7)) is the only or at least a dominant reaction that takes place when sulfonamides bind to a CA, meaning that the intrinsic binding reaction is between the negatively charged sulfonamide to such form of CA where the fourth ligand bound to the Zn^{II} in the active site is electrostatically neutral water molecule. The first indication that the fourth reaction occurs was the spectral evidence on Co-containing CA enzyme (Engberg and Lindskog, 1984; Tu and Silverman, 1986). However, a more recent neutron-diffraction crystal structure of acetazolamide bound to CA II from McKenna laboratory (Fisher *et al.*, 2012*b*) directly showed that the sulfonamide amino group possesses only one proton and thus the group is deprotonated and negatively charged when bound to the CA II. Our data are consistent with this conclusion. However, it is difficult to distinguish the fourth possibility from the first using thermodynamic methods alone.

At neutral pH 7, most sulfonamides are almost fully protonated since their pK_as are usually around 9 or 10, in the form that is unable to bind. However, a small fraction is deprotonated and binds to CA. When the deprotonated form is depleted, additional sulfonamide deprotonates to keep the fraction unchanged. This additional sulfonamide also binds to CA and so on until the enzyme is fully saturated with the inhibitor.

Similarly, only a part of the Zn^{II}-coordinated molecules are in H_2O form because the pK_as of most human CAs is approximately 7. Thus, approximately half of CA fraction is deprotonated and must undergo protonation in order to bind the sulfonamide anion. When these linked reactions (Eq. (8)) occur, the proton must be uptaken from the buffer or released to the buffer (Fig. 9).

$$\begin{aligned}
&\text{Intrinsic}: \quad \mathrm{CA-Zn^{II}-H_2O + RSO_2NH^-} \rightleftharpoons \mathrm{CA-Zn^{II}-NH-SO_2R + H_2O}\\
&\text{Ligand}: \quad \mathrm{RSO_2NH^- + H^+} \rightleftharpoons \mathrm{RSO_2NH_2}\\
&\text{Protein}: \quad \mathrm{CA-Zn^{II}-OH^- + H^+} \rightleftharpoons \mathrm{CA-Zn^{II}-H_2O} \qquad (8)\\
&\text{Buffer}: \quad \mathrm{Buf + H^+} \rightleftharpoons \mathrm{BufH^+}\\
&\text{Observed}: \quad \text{Intrinsic} + \text{Ligand} + \text{Protein} + \text{Buffer}
\end{aligned}$$

The fraction of deprotonated sulfonamide is dependent on the sulfonamide amino group $pK_{a,SA}$ and can be calculated using Eq. (9):

$$f_{\mathrm{RSO_2NH^-}} = \frac{10^{\mathrm{pH-p}K_{a,SA}}}{1 + 10^{\mathrm{pH-p}K_{a,SA}}} \quad (9)$$

https://doi.org/10.1017/S0033583518000082

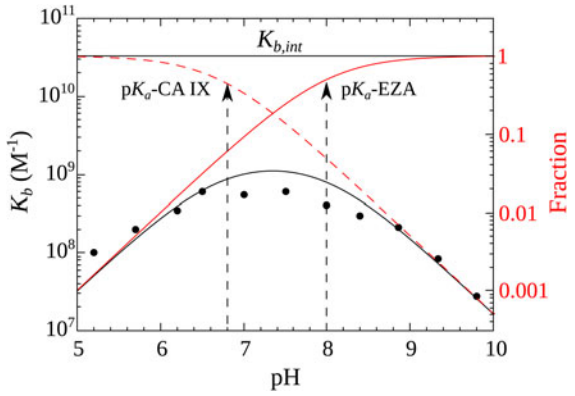

Fig. 10. Relationship between the intrinsic (independent of pH, shown as horizontal line) and observed affinities (filled circles fit by the solid line of overturned U-shape) of **1** binding to CA IX. The observed affinity is reduced both at acidic and alkaline pHs due to reduced fractions of available binding-ready species (negatively charged sulfonamide, shown as solid red line, and CA, bearing the neutral water molecule, shown as a dashed red line).

Similarly, the fraction of binding-ready CA depends on pH and the p$K_{a,\mathrm{CA}}$ of the water molecule in the active site and can be calculated using Eq. (10):

$$f_{\mathrm{CAZnH_2O}} = \frac{10^{pK_{a,\mathrm{CA}}-\mathrm{pH}}}{1+10^{pK_{a,\mathrm{CA}}-\mathrm{pH}}} \tag{10}$$

The affinity of interaction will be reduced by the amount how much the fractions are reduced. In other words, the observed binding constant $K_{b,obs}$ indicates us a diminished $K_{b,int}$ due to reduced fractions. The intrinsic $K_{b,int}$ can be calculated using Eq. (11):

$$K_{b,int} = \frac{K_{b,obs}}{f_{\mathrm{CAZnH_2O}} \times f_{\mathrm{RSO_2NH^-}}} \tag{11}$$

Figure 10 shows the relationship between the intrinsic and observed affinities and the dependence of the latter on pH. The intrinsic affinity is independent of pH, but because there are a reduced fraction of both interacting components at both acidic and alkaline pHs, there is energy needed to overcome this linked reaction and therefore the observed affinity is reduced

In turn, the intrinsic Gibbs energy of binding can be calculated using Eq. (12):

$$\Delta G_{int} = -RT\ln(K_{b,int}) \tag{12}$$

The change in the standard Gibbs energy of ligand binding dependence on pH has a U-shape, similar to the K_d, but upside down as K_b. Figure 11 shows that the U-shapes are obtained for all catalytically active human CAs. All experimental techniques discussed in this paper (FTSA, SFA, ITC, and SPR), yield the U-shape inhibitor binding Gibbs energy dependence on pH. In all cases, the affinity is strongest in near-neutral pH range and decreases in both directions. The observed affinity comes closest to the intrinsic value at near-neutral pH, but usually does not reach it and thus is almost never observed experimentally.

Intrinsic enthalpy of binding

The change in the observed enthalpy on the binding, similarly to ΔG, also has contributions from all linked processes, including inhibitor deprotonation, protonation of the CA-bound hydroxide, and the compensating buffer effects. Therefore, to get the change in the intrinsic enthalpy on binding it is necessary to subtract all linked processes as shown in Eq. (13):

$$\Delta H_{int} = \Delta H_{obs} - n_{\mathrm{SA}}\Delta H_{pr,\mathrm{SA}} - n_{\mathrm{CA}}\Delta H_{pr,\mathrm{CA}} + n_{buf}\Delta H_{pr,buf} \tag{13}$$

where ΔH_{obs} – the observed enthalpy of binding obtained by direct ITC titration, $\Delta H_{pr,\mathrm{SA}}$ – the enthalpy of protonation of deprotonated inhibitor, $\Delta H_{pr,\mathrm{CA}}$ – the enthalpy of protonation of the CA-bound OH^-, and $\Delta H_{pr,buf}$ – the enthalpy of buffer protonation. The ns denote the numbers of protons uptaken or released:

$$n_{\mathrm{SA}} = f_{\mathrm{RSO_2NH^-}} - 1 \tag{14}$$

is the number of protons released from the inhibitor to buffer ($n_{inh} = -1$ to 0),

$$n_{\mathrm{CA}} = 1 - f_{\mathrm{CAZnH_2O}} \tag{15}$$

is the number of protons uptaken by the CA-bound OH^- ($n_{\mathrm{CA}} = 0$ to 1),

$$n_{buf} = n_{\mathrm{SA}} + n_{\mathrm{CA}} \tag{16}$$

is the net sum of protons uptaken by the buffer both from the ligand and protein or released by the buffer to the ligand or protein ($n_{buf} = -1$ to 1).

The enthalpy of protonation of TRIS base is −47.45 kJ mol^{-1} and of HPO_4^{2-} is −5.1 kJ mol^{-1} at 25 °C (Goldberg *et al.*, 2002).

If we perform sulfonamide–CA ITC titrations in various buffers at various pHs as shown in Fig. 12, an X-shape dependence is observed as shown in Fig. 13. At low pH, the observed enthalpies (ΔH_{obs}) in phosphate buffer are low in magnitude, while in TRIS – significantly more exothermic. The difference between the observed enthalpies is equal to the difference between the enthalpies of protonation of the two buffers. In alkaline region, the situation is reversed – the enthalpies in phosphate became much more exothermic, while in TRIS – less exothermic. The red solid line shows the position of the intrinsic enthalpy (ΔH_{int}) of **1** binding to CA I. The intrinsic enthalpy is independent of pH. The dashed line shows a hypothetical situation for the observed enthalpy dependence on pH if the buffer had exactly zero enthalpy of protonation ($\Delta H_{pr,buf} = 0$). The difference between the dashed line and the intrinsic enthalpy in the acidic region is equal to the enthalpy of inhibitor protonation ($\Delta H_{pr,\mathrm{SA}}$), while in the alkaline region – to the enthalpy of protonation of the CA-bound OH^- ($\Delta H_{pr,\mathrm{CA}}$).

The same procedure has been performed with every purified CA isoform and the data is shown in Fig. 14. All of the nine isoforms where the data has been obtained exhibited similar X-shaped curves, but since the protein pK_as were slightly different and the intrinsic enthalpies of binding were also different among isoforms, they yielded slightly different curves. It should be noted that the precision of the enthalpies is really high, but there still

https://doi.org/10.1017/S0033583518000082

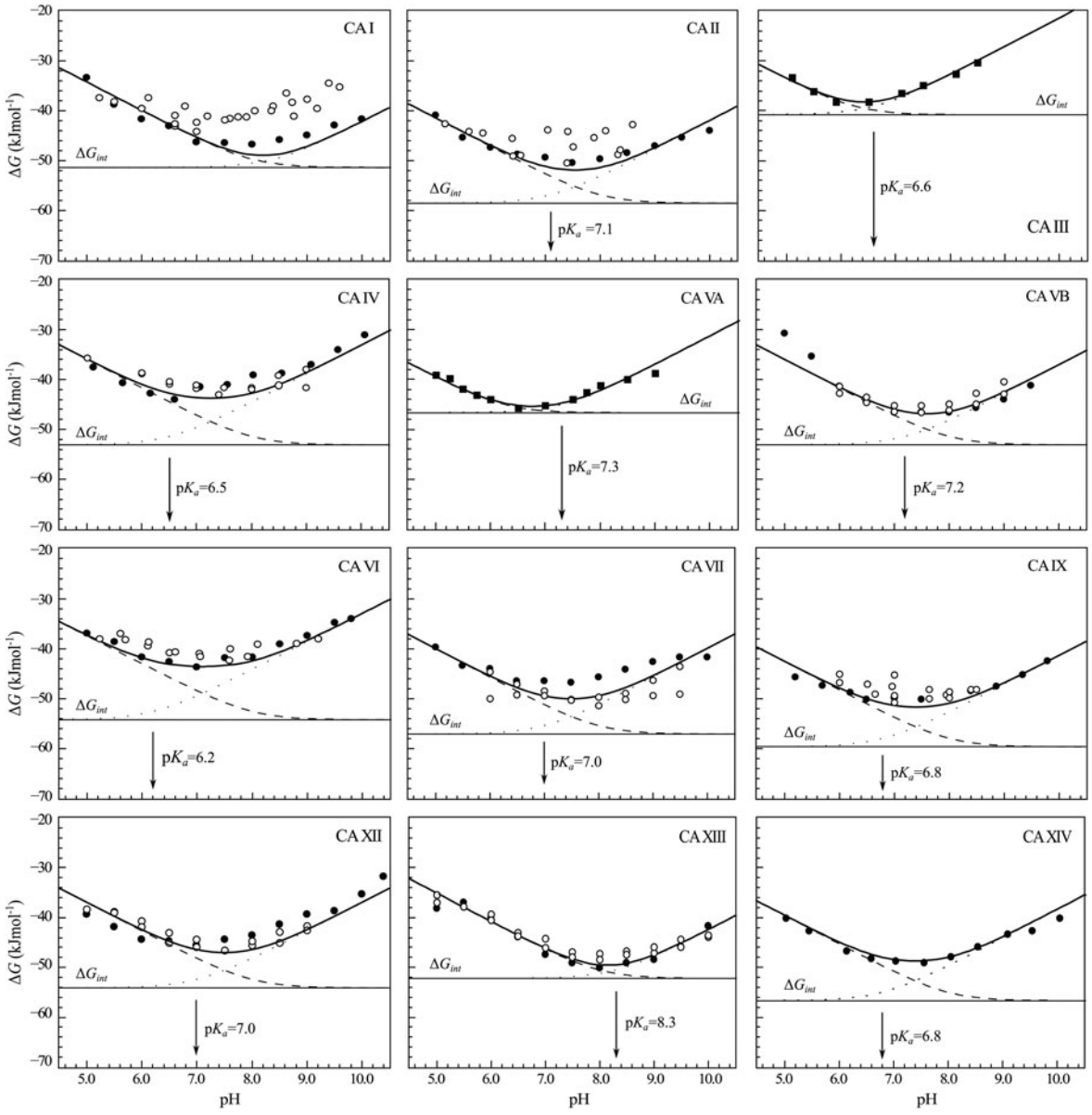

Fig. 11. The dependence of ΔG_{obs} on pH determined by FTSA (filled circles) and ITC (open circles) methods at 25 °C. Circles show the binding of **1** and squares of **303** (to CA III and CA VA). Solid curve is a fit of the model, solid line is intrinsic Gibbs energy of binding, dashed line is a fraction of ligand, dotted line is a fraction of protein. Experiments were performed in universal buffer made of 50 mM sodium phosphate, 50 mM sodium acetate, and 25 mM sodium borate containing 100 mM NaCl and up to 2% DMSO as previously described in: CA I and CA II (Morkūnaitė *et al.*, 2015), CA IV (Mickevičiūtė *et al.*, 2017), CA VB (Kasiliauskaitė *et al.*, 2016), CA VI (Kazokaitė *et al.*, 2015), CA VII (Pilipuitytė and Matulis, 2015), CA IX (Linkuvienė *et al.*, 2016*b*), CA XII (Jogaitė *et al.*, 2013), CA XIII (Baranauskienė and Matulis, 2012), and CA XIV (Juozapaitienė *et al.*, 2016). All panels are drawn at the same scale to help visualize the differences in affinities of binding.

were some discrepancies between the observed data and the model curves, especially at the acidic and alkaline pH. We assume that these discrepancies are due to protein destabilization. However, an attempt was made to determine many more data points for one isoform in one buffer. The data for CA XIII in phosphate buffer are shown in Fig. 15.

Most researchers have based the choosing of the lead compound for development on the observed parameters, observed affinity or observed enthalpy. From the first glance, it may seem that it is sufficient to experimentally determine the physiologically relevant compound affinities. Thus, one may be interested in the affinities observed at the pH 7.4. It seems that it is most relevant to correlate the compound chemical structures with the binding data obtained at such pH. However, this is only partially true and may lead to erroneous conclusions. For example, if the binding affinities of two compounds are compared where the compounds have highly different pK_as (e.g., 8 and 11), then if the compound with the pK_a 8 is 1000-fold stronger binder than the compound with pK_a 11, one may assume that the first compound is better attached to the CA. This conclusion is incorrect because the higher affinity is entirely explained by the difference in the pK_a and both compounds would recognize the protein surface with identical affinity.

As shown in this section, the observed enthalpies are not really informative, instead, it is the intrinsic enthalpy change that describes the interaction. The buffer, ligand, and protein

https://doi.org/10.1017/S0033583518000082

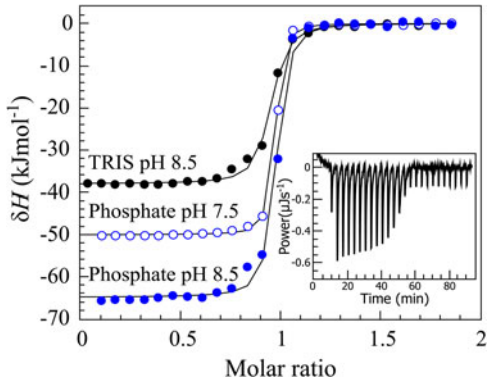

Fig. 12. ITC data of **1** binding to CA IX in two buffers at several pHs at 25 °C. The observed enthalpies depended both on the buffer and on the pH used in the experiment. In such cases, it is necessary to obtain the intrinsic enthalpy to perform any meaningful Structure–Activity Relationship (SAR)-type study. The inset shows a typical ITC raw data curve.

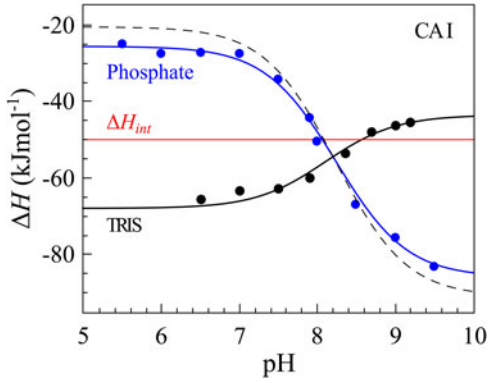

Fig. 13. The observed enthalpies obtained by ITC of **1** binding to CA I in sodium phosphate or TRIS chloride buffer as a function of pH at 25 °C. Blue datapoints show the ΔH_{obs} in phosphate buffer, while black – in TRIS. Solid black and blue lines are global fits to the above-described model (fit in the way where the pK_as are consistent with the FTSA data for each isoform) yielding the intrinsic enthalpy of binding (ΔH_{int}, red line) that is independent of pH. Dashed line shows a hypothetical situation how the observed enthalpy dependence should look like if the enthalpy of buffer protonation was equal to zero.

contributions may be so large that they may overwhelm the enthalpy data and the compounds would thus be ranked in a completely wrong order. Therefore, it is essential to determine the mechanism and calculate intrinsic enthalpies to be able to rank compounds in the order of increasingly exothermic enthalpy.

In this work, we attempted to determine intrinsic thermodynamic parameters of a series of sulfonamide compounds to the 12 catalytically active human CA isoforms. Intrinsic affinities and intrinsic enthalpies were obtained for the structure–thermodynamics correlations.

Protonation pK_a *and enthalpy of CA–*Zn^{II}*-bound water molecule of all 12 human CA isoforms*

It is not straightforward to determine the pK_a and the enthalpy of protonation of the Zn^{II}-bound hydroxide/water molecule. Differently, from the compounds, it is not possible to pH-titrate the protein and record with spectrophotometer or titration calorimeter. Instead, in order to determine the pK_a researchers have determined the pH dependence of inhibition of enzymatic activity or replaced Zn with Co that exhibited visible spectral changes upon the change in pH. However, it is disputable to which extent such non-natural CA represents the native CA.

In addition, we have determined the pK_as of most CA isoforms by fitting the inhibitor affinities at various pHs as explained earlier in the discussion of U-shaped dependencies. The enthalpies of protonation were determined via the global fit of the X-shaped curves obtained by ITC titration of an inhibitor in two buffers. Both the pK_a and the enthalpy of protonation had to be obtained only once with one inhibitor and then can be applied for other inhibitors to obtain the intrinsic energetics of binding to a CA.

These data are summarized in Table 2 which shows the thermodynamic parameters of protonation of the hydroxide anion bound to catalytically active CA isoforms. The pK_as of human CAs have been determined previously by using numerous techniques, see the references in Table 2. Their values span between approximately 6 and 8.5. The values determined by FTSA and ITC were close to the values previously determined by other techniques. However, there were several outliers of up to 1 pK_a unit. It seems that CA I and CA XIII have rather high pK_as, above 8.0. Remaining ones are essentially the same as determined previously. The standard deviation of combined FTSA and ITC determinations in the pH dependencies described above do not exceed 0.2 pH or pK_a units. This accuracy is highly dependent on the correct calibration of the pH-meters and standard buffer preparations. The Gibbs energy changes upon protonation were recalculated according to Eq. (12). The enthalpies were the result of the global fit of ITC titrations of each CA isoform with **1** at a series of pH as explained above. The entropies were obtained by subtracting the Gibbs energy changes from enthalpies (Eq. (3)). The entropy values carry a largest standard deviation, a sum of deviations of the enthalpy and Gibbs energy.

Determination of the pK_a *and the change of enthalpy of protonation of the sulfonamide inhibitor amino group*

Sulfonamide inhibitor amino group deprotonates with a pK_a between approximately 6 and 11. The actual value depends on the chemical structure of the compound, the presence of electron-withdrawing and donating groups, the size of the aromatic conjugated system and other factors. In order to calculate the intrinsic parameters of these sulfonamide inhibitor binding to CAs, it was necessary to determine the pK_as and enthalpies of their protonation.

The sulfonamide amino group pK_a may be roughly estimated from the proton NMR spectrum. The spectrum is determined for every newly synthesized compound thus the information is readily available. The chemical shift of the amino group protons correlates approximately linearly with the spectrophotometrically measured pK_a (Fig. 16).

To determine the pK_a of the sulfonamide, the compound solution may be pH-titrated and the midpoint pH of the titration would correspond to the pK_a, as shown in Fig. 17 (Ladbury and Doyle, 2004; Morkūnaitė *et al.*, 2015). However, as shown by the Whitesides group (Snyder *et al.*, 2011), it is easier to determine the pK_a by preparing the solution of the compound in a series of buffers, made at 0.5 pH unit, and recording the UV spectrum of the solution at each pH. The spectrum changes around the pK_a and it is easy to find the wavelengths of the largest change. The absorbance values at those pH are then used and

https://doi.org/10.1017/S0033583518000082

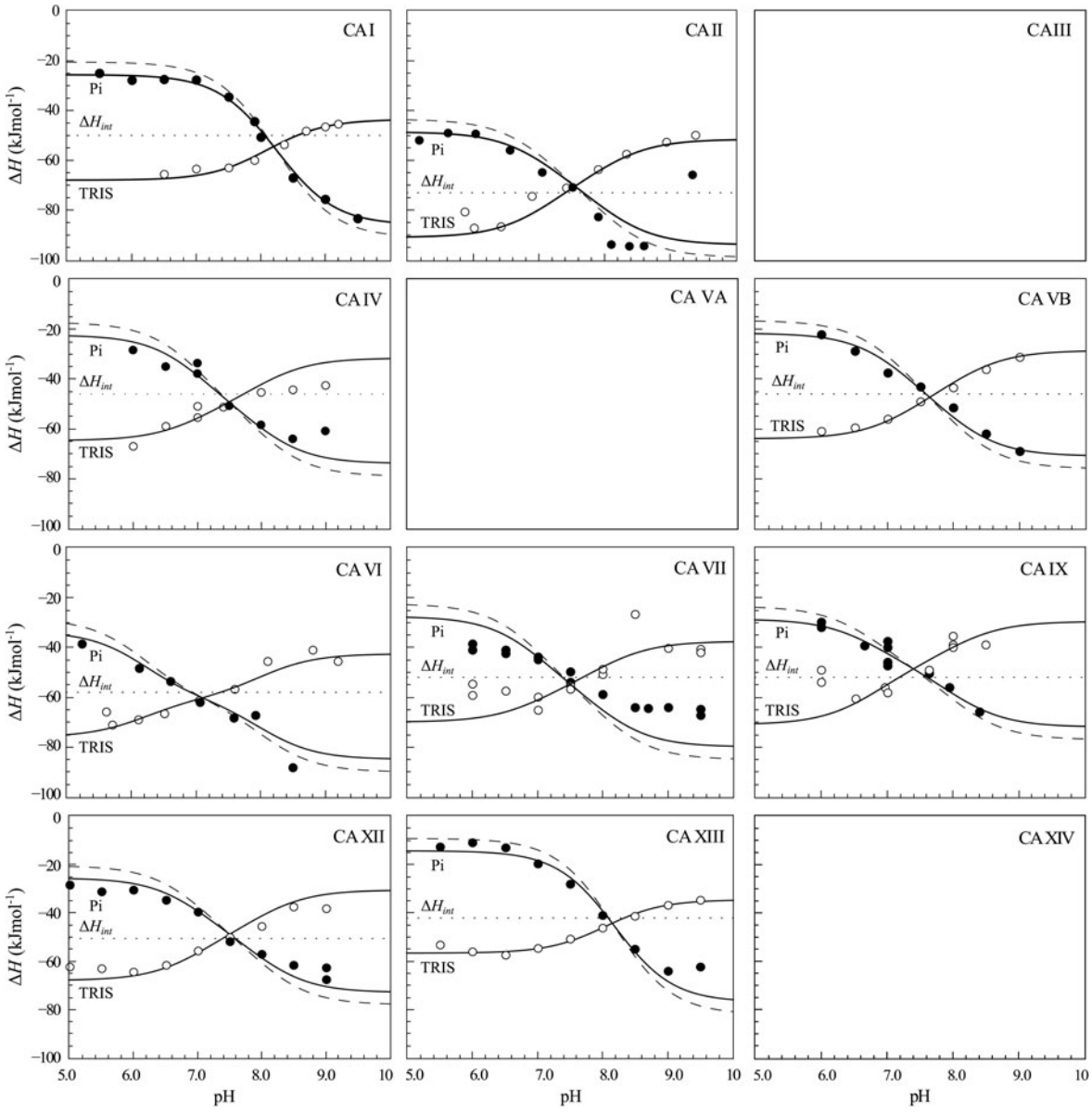

Fig. 14. ITC data of **1** binding to CA isoforms at 25 °C. Filled circles – ΔH_{obs} determined in sodium phosphate buffer, open circles – ΔH_{obs} determined in TRIS buffer, dotted line shows value of ΔH_{int} of **1** binding, solid curves are fits of experimental data, while the dashed curve is a fit of a hypothetical situation if there were no buffer or the enthalpy of buffer protonation ($\Delta H_{pr,buf}$) was equal to zero. The fits were global with the FTSA U-shapes keeping the sulfonamide and CA pK_as the same. Experiments were performed in either 50 mM sodium phosphate or 50 mM TRIS chloride buffer containing 100 mM NaCl and up to 2% DMSO as previously described in: CA I and CA II (Morkūnaitė *et al.*, 2015), CA IV (Mickevičiūtė *et al.*, 2017), CA VB (Kasiliauskaitė *et al.*, 2016), CA VI (Kazokaitė *et al.*, 2015), CA VII (Pilipuitytė and Matulis, 2015), CA IX (Linkuvienė *et al.*, 2016*b*), CA XII (Jogaitė *et al.*, 2013), CA XIII (Baranauskienė and Matulis, 2012). All panels are drawn at the same scale to help visualize the differences in enthalpies of binding. No data has been determined at comparable conditions for CA III, CA VA, and CA XIV. The overall pattern of the X-shapes is similar, but details are different due to different p$K_{a,CA}$ and ΔH_{int} for each isoform.

plotted as a function of pH and normalized to the unit as shown in Fig. 17*a* and *c*.

The enthalpies of sulfonamide amino group protonation may be determined by titrating the compound solution with an acid in an ITC calorimeter at a constant temperature. The compound in a solid pure form exists as a protonated electrostatically neutral sulfonamide. Therefore, it must be deprotonated by applying a sufficient amount of base to achieve the pH sufficiently above the pK_a for accurate determination. We usually apply 50% surplus of the base and therefore the resultant ITC curves appear as two-step ITC reactions. Titration of such solution with a strong acid provides a direct measurement of the enthalpy of protonation as shown in Fig. 17*d*.

Alternatively, the enthalpy of protonation may be determined by applying the van't Hoff relationship and performing the pK_a determination at several temperatures as shown in Fig. 17*e*. However, such determination is not as accurate as ITC because it is assumed here that the enthalpy of protonation is independent of temperature in the studied temperature range. To some extent this assumption is correct, but the enthalpy is temperature-dependent as seen from the ITC determinations at various temperatures (Fig. 17*f*). There is a non-zero heat capacity associated

https://doi.org/10.1017/S0033583518000082

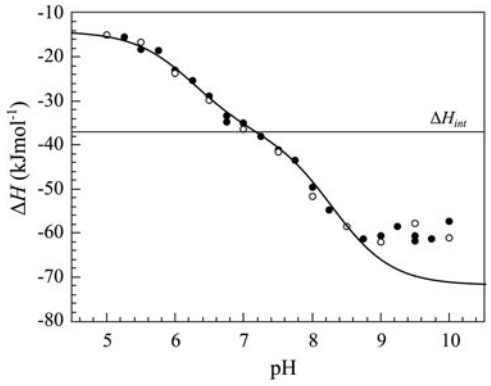

Fig. 15. The enthalpy changes upon compound **303** binding to CA XIII at various pHs. The curve was fit using the following parameters: $pK_{a,SA} = 6.25$, $pK_{a,CA} = 8.3$, $\Delta H_{int} = -37$ kJ mol^{-1}, $\Delta H_{pr,SA} = -28$ kJ mol^{-1}, $\Delta H_{pr,CA} = -40$ kJ mol^{-1}. The open and closed symbols show the data obtained by two independent researchers. The solid curve matched the data resembling all bends in the curve except the discrepancy in the alkaline region. Possibly the protein is slightly destabilized in this region. The horizontal straight line shows the change in the intrinsic enthalpy upon binding if we assume that the reaction occurs according to Eq. (7). However, the same indistinguishable curve would be obtained for Eq. (4) and Eq. (7). The intrinsic enthalpy would then be different. The thermodynamic data alone cannot distinguish the models and we base our decision that Eq. (7) is correct based on crystallographic data.

with the protonation process. The heat capacity change upon protonation is positive (Matulis and Todd, 2004; Morkūnaitė *et al.*, 2015) as usually is the case of ionic binding reactions.

Why intrinsic data is necessary for making compound structure–thermodynamics correlations

It is often thought that it is sufficient to make a SAR-type analysis based on the observed data. This may be true to some extent when the compounds are very similar and there is no need to make explanations why one or another compound binds stronger or weaker to a particular protein. However, if we would like to understand the physico-chemical reasons behind the observed thermodynamic parameters, e.g., determine the contributions of particular atoms to the binding energetics, it is necessary to operate with the intrinsic parameters.

Figure 18 shows the observed and intrinsic K_ds for a series of compound binding to human CA VI. The compounds were arranged in the order of decreasing intrinsic affinity. It is clear that the intrinsic and observed affinities do not correlate for these compounds. The observed K_d for the first and last compound in the figure are almost the same, but the intrinsic affinities differ by more than 300 fold. Not knowing the intrinsic values would yield completely wrong conclusions about the structural determinants of the compounds that cause the affinity to be greater or smaller.

Another example (Fig. 19) shows a different situation when the observed binding constants are quite different, but the intrinsic ones are nearly the same. If only the observed data were available, one could make an erroneous conclusion that fluorines substantially increase the affinity of the compound towards CA I due to the contacts between fluorines and the protein. However, in actuality, fluorines increase the affinity by only 1.5-fold (equal to the ratio of the intrinsic binding constants) due to direct contacts and the remaining 100-fold increase in the observed affinity arises simply due to the reduction of the pK_a of the sulfonamide amino group by electron-withdrawing capabilities of the fluorine atoms.

Intrinsic kinetics of sulfonamide inhibitor interaction with the CAs

It has been shown that sulfonamide inhibitors bind CAs with an unusually slow association kinetics, too slow to be explained by a diffusion-limited association (Linkuvienė *et al.*, 2016*b*). We have performed the kinetic measurements as a function of pH and showed that the apparent discrepancy may be explained by the application of the same model that was applied to determine the intrinsic thermodynamic parameters of binding (Linkuvienė *et al.*, 2018). After the correction of the association rates by the available fractions of the binding-ready deprotonated sulfonamides, the rates appeared to be much more consistent with the diffusion-limited single-step kinetics.

The kinetics of sulfonamide association was determined by SPR. Typical data are shown in Fig. 20. The dependence of the association rates on pH (Fig. 21) shows that the rates exhibit an upside U-shape and may be explained by the fractions of available deprotonated sulfonamide and protonated CA. The intrinsic association rate $k_{a,int}$ is pH-independent but almost never observed experimentally because the fractions are much lower than 1. Contrary, the dissociation rates $k_{d,int}$ appear to be independent of pH as expected for a simple 1 : 1 binding case. Therefore, the intrinsic dissociation rates could be observed experimentally directly by SPR.

The model explaining the pH kinetic data is presented in Fig. 22. The linked protonation-deprotonation reactions explain the apparently slow interaction kinetics. Figure 23 shows two association rates for the same compound, but one dissociation rate. The two association rates are connected by a vertical line. The upper point represents an intrinsic association rate that would be observed under such hypothetical conditions when the fractions of both interacting species are equal to 1. The lower point is the experimentally observed association rate.

The most interesting, strongest-binding compounds were very slow-dissociating ones. Their residence times were approximately equal to several hours and could not be directly determined by SPR. However, they could be estimated from the association rates and the thermodynamic binding constant, available from the equilibrium measurements by FTSA. The position of such compounds is shown in the shaded gray area on the left side of Fig. 23. The residence times of the lead binding compounds for several CA isoforms appear to be in the order of 3–6 h.

The kinetic measurements have further confirmed the mechanism of sulfonamide inhibitor binding to CAs and further validated the necessity to determine the intrinsic binding data, not only observed.

A database of intrinsic affinities of sulfonamide inhibitor binding to all 12 catalytically active human CAs

In Supplementary Table 1, we have assembled a database of 402 primary sulfonamide compounds binding to the 12 catalytically active human CA isoforms. There is limited data in the literature where the intrinsic parameters of interaction have been considered. Major efforts to assemble and analyze sulfonamide–CA interaction intrinsic data have been made by the G. Whitesides laboratory (Krishnamurthy *et al.*, 2008), however, only for one CA isoform, CA II, and thus did not provide information on compound isoform-selectivity. The synthesis, purification, and characterization of chemical compounds **9**–**402**, except **303**, presented in Supplementary Table 1 have been previously described by

https://doi.org/10.1017/S0033583518000082

Table 2. Thermodynamic parameters of protonation of CA-Zn^{II}-bound hydroxide anion (Eq. (8), third reaction) for all 12 catalytically active CA isoforms. The pK_a values determined by various methods and taken from the earlier literature are listed in the second column together with the references. Other values were determined by FTSA and ITC with the references listed in the first column next to the CA isoforms. The uncertainty of the pK_a values determined by FTSA and ITC is approximately 0.2 pH units, while for the change in Gibbs energies and enthalpies it is approximately 2 kJ mol^{-1}

		$pK_{a,CA}$		$\Delta G_{pr,CA}$ (kJ mol^{-1})		$\Delta H_{pr,CA}$ (kJ mol^{-1})		$T\Delta S_{pr,CA}$ (kJ mol^{-1})	
CA isoform	$pK_{a,CA}$	25 °C	37 °C	25 °C	37 °C	25 °C	37 °C	25 °C	37 °C
Technique -	Inhibition				FTSA, ITC				
CA I (Morkūnaitė *et al.*, 2015)	8.1 (Coleman, 1967)	8.4 ± 0.2	8.1	−47.9	−48.2	−41.0	−38.5	6.9	9.7
	6.9 (Innocenti *et al.*, 2009)								
	7.1 (Engstrand *et al.*, 1995)								
	7.3 (Whitney and Brandt, 1976; Khalifah, 1977; Khalifah *et al.*, 1977)								
CA II (Morkūnaitė *et al.*, 2015)	6.9 (Duda *et al.*, 2001; Mikulski *et al.*, 2011*a*)	7.1	6.9	−40.5	−41.1	−26.0	−23.5	14.5	17.6
	7.1 (Innocenti *et al.*, 2009)								
	6.8 (Tu *et al.*, 2002)								
CA III	~5 (Tu *et al.*, 2002)	6.6	6.5	−37.7	−38.6	ND	ND	ND	ND
	~5 (Jewell *et al.*, 1991; Qian *et al.*, 1997)								
	<6 (Elder *et al.*, 2007)								
Escherichia coli CA IV (Mickevičiūtė *et al.*, 2017)	6.2 (Baird *et al.*, 1997)	6.8	6.6	−38.8	−39.0	−33.0	−30.5	5.8	8.5
Murine CA IV	6.6 (Hurt *et al.*, 1997)								
CA VA	ND	7.3	7.3	−41.7	−43.3	ND	ND	ND	ND
CA VB (Kasiliauskaitė *et al.*, 2016)	ND	7.2	7.0	−41.1	−41.5	−30.0	−27.5	11.1	14.0
E. coli CA VI (Kazokaitė *et al.*, 2015)	ND	6.2	6.0	−35.4	−35.6	−32.0	−29.0	3.4	6.6
Saliva CA VI (Kazokaitė *et al.*, 2015)		5.5		−31.4					
Mammalian CAVI (Kazokaitė *et al.*, 2015)		5.5		−31.4					
CA VII (Pilipuitytė and Matulis, 2015)		7.0	6.8	−40.0	−40.2	−33.0	−30.5	7.0	9.7
Murine CA VII	6.2 (Earnhardt *et al.*, 1998)								
CA IX (Linkuvienė *et al.*, 2016*b*)	6.3 (Wingo *et al.*, 2001)	6.8	6.6	−38.8	−39.4	−24.0	−21.5	14.8	17.9
cdCA IX (catalytic domain)	7.01 (Innocenti *et al.*, 2009)								
CA IX (full length)	6.49 (Innocenti *et al.*, 2009)								
CA XII (Jogaitė *et al.*, 2013)	7.1 (Ulmasov *et al.*, 2000)	7.0	6.8	−40.0	−40.4	−28.0	−25.5	12.0	14.9
	6.9 (Innocenti *et al.*, 2009)								
CA XIII (Baranauskienė and Matulis, 2012)	ND	8.3	8.0	−47.4	−47.5	−44.0	−41.5	3.4	6.0
CA XIV (Juozapaitienė *et al.*, 2016)	6.92 (Innocenti *et al.*, 2009)	6.8	6.8	−38.8	−40.4	ND	ND	ND	ND

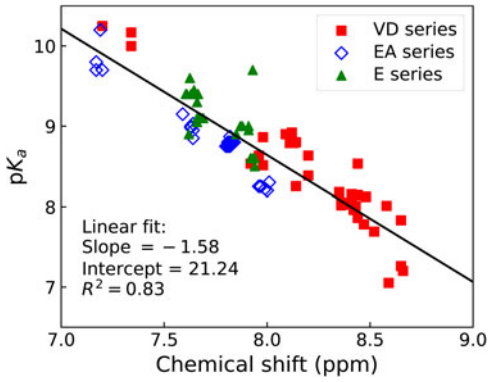

Fig. 16. Correlation between the pK_as of sulfonamide amino group (determined spectrophotometrically) and the chemical shift of the sulfonamide amino group protons as determined by NMR in deuterated DMSO solvent. Three series of compounds are distinguished in three colors and symbol shapes, VD series are mostly fluorinated benzenesulfonamides, EA and E series are mostly chlorinated compounds. The correlation is approximately linear. The plot may be used to obtain an estimate of the amino group pK_a from proton NMR data when characterizing newly synthesized primary sulfonamides.

Dudutiene *et al.* (2007); Baranauskienė *et al.* (2010); Čapkauskaitė *et al.* (2010, 2012, 2013, 2017); Sūdžius *et al.* (2010); Dudutienė *et al.* (2013, 2014, 2015); Kišonaitė *et al.* (2014); Morkūnaitė *et al.* (2014, 2015); Rutkauskas *et al.* (2014, 2017); Zubrienė *et al.* (2014, 2015, 2017); Kazokaitė *et al.* (2015); Pilipuitytė and Matulis (2015); Juozapaitienė *et al.* (2016); Kasiliauskaitė *et al.* (2016); Linkuvienė *et al.* (2016*b*); Mickevičiūtė *et al.* (2017); Vaškevičienė *et al.* (2017). The other compounds were purchased from Sigma-Aldrich Chemical Co. and used without further purification.

Instant JChem was used for structure database management, search and prediction, Instant JChem 6.1.3, 2013, ChemAxon (http://www.chemaxon.com).

A database of intrinsic enthalpies and entropies of sulfonamide inhibitor binding to all 12 catalytically active human CAs

In Supplementary Table 2, we put together available data on the intrinsic enthalpies and entropies of primary sulfonamide binding to human CAs. The table lists the intrinsic Gibbs energies, enthalpies, and entropies of binding together with the experimentally determined (or estimated) pK_as of the sulfonamide amino group of the compounds. These listed pK_as were used to calculate the intrinsic parameters of binding as explained in the previous sections.

The observed and intrinsic binding affinity data in Supplementary Table 1 and the intrinsic enthalpy–entropy data in Supplementary Table 2 needs detailed analysis and we hope that it will be useful for computational chemists who are designing *in silico* binding models that would enable prediction of binding thermodynamic parameters.

Some analysis of the compound affinity and selectivity towards each CA isoform has been provided in the references. However, the much deeper analysis may be performed. Here, we concentrate on the most general observations and structure–thermodynamics correlations.

The intrinsic enthalpies and entropies were plotted on a so-called enthalpy–entropy compensation plot (Chodera and Mobley, 2013; Ahmad *et al.*, 2015; Dragan *et al.*, 2017) and shown in Fig. 24. The plot is drawn as a square with the same enthalpy and entropy scale spreading from compounds that exhibit high exothermic enthalpy to compounds that are fully entropy-driven. Diagonal lines represent isoaffinity areas. Most compounds in this study are bound with an intrinsic affinity ($k_{d,int}$) between 10 μM and 1 pM. The intrinsic Gibbs energies of binding spread from approximately −40 kJ mol^{-1} to −70 kJ mol^{-1}. However, the ranges of enthalpies and entropies were significantly larger. The enthalpies spread from −90 kJ mol^{-1} to 10 kJ mol^{-1} while entropies – from −50 kJ mol^{-1} to 20 kJ mol^{-1}.

The thermodynamic parameters to various CA isoforms tended to assemble in groups. For example, CA I bound ligands with highly exothermic enthalpy and near-zero entropy, while CA IX bound compounds with only slightly exothermic enthalpy and a significant positive entropy contribution. Thus CA I bound ligands due to primarily enthalpic reasons, while CA IX binding was dominated by the positive entropy contribution. This effect is puzzling and the exact values most likely depend on exact positions of water molecules at the protein–ligand surface prior and post-binding.

We took great care to ensure as high precision of the data as possible. The standard deviation, uncertainty, repeatability, and precision of FTSA measurements have been discussed in Cimmperman and Matulis (2011) and ITC (Linkuvienė *et al.*, 2016*a*). Several orthogonal methods have been used where possible to ensure as precise data as possible. However, the standard deviation of all methods for all thermodynamic parameters, including Gibbs energies, enthalpies, and entropies, essentially cannot be reduced below approximately ±1 kJ mol^{-1}. Therefore, the precision of the data should not be overstated. For example, if the affinities (K_d) of two compounds differ by 2-fold it means that the values are within the error margin and it is insufficient data to reliably conclude which compound is a stronger binder. Similar precision could be applied for enthalpies and entropies.

Recombinant preparation and characterization of the human CAs

The quality of prepared CA proteins

All 12 catalytically active human CA isoforms have been prepared in our laboratory. There was always of a concern how pure those preparations are and whether the preparations exhibit a specific activity that is comparable with the proteins described in the literature.

The proteins have been confirmed by such standard techniques and SDS-PAGE and high-resolution mass spectrometry. They were of correct molecular weight on resolving gels and exhibited a mass that was within a single Da from the mass predicted from the amino acid sequence. However, we think that in addition, it is of most importance to demonstrate that the entire protein preparation is catalytically active by titrating it with an inhibitor and thus demonstrate that the entire preparation of the protein is catalytically active and it is not contaminated by non-active fraction of the same protein that may be indistinguishable by other techniques.

Figure 25 shows the activity titration of CA XIV. First, it is necessary to titrate the active fraction of the protein. The known large concentration of CA XIV, 500 nM, was added to the solution and various concentrations of a strongly-binding inhibitor **1** were

https://doi.org/10.1017/S0033583518000082

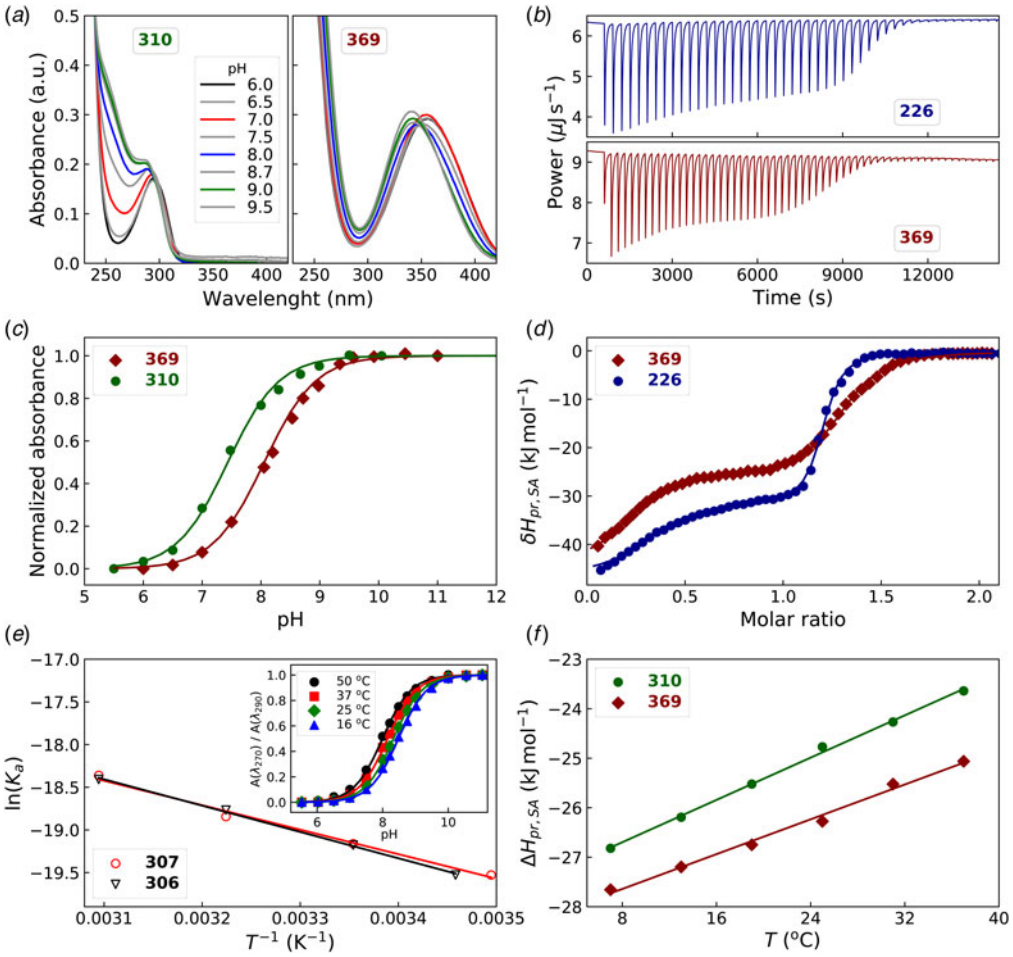

Fig. 17. Determination of the pK_a and enthalpy of protonation ($\Delta H_{pr,SA}$) of the sulfonamide amino group. Left panels (*a*), (*c*), and (*e*) show the spectrophotometric, while right panels (*b*), (*d*), and (*f*) show the ITC data. (*a*) UV-Vis spectra of the compound solution in buffers of various pH. (*c*) The normalized absorbance change at a chosen wavelength or ratio of two wavelengths. (*e*) Determination of the $\Delta H_{pr,SA}$ via van't Hoff relationship, the dependence of the pK_a on temperature. (*b*) ITC raw data of titrating a base-neutralized (with 1.5 equiv.) sulfonamide with HNO_3. (*d*) Integrated ITC curves of the sulfonamide titration with acid. (*f*) Determination of the heat capacity of protonation by performing the ITC titrations at various temperatures. The ΔC_p values for **310** and **369** were equal to 107 J mol^{-1} K^{-1} and 88 J mol^{-1} K^{-1}, respectively.

added. Two straight lines should intersect at exactly 500 nM as was experimentally observed (Fig. 25) if the inhibitor is of sufficient binding affinity.

Protein purity can be further confirmed by demonstrating inhibition by several known inhibitors. Then, it is useful to demonstrate using a strong inhibitor that the compound binding stoichiometry by ITC is near 1. Determination of the protein stability in various buffers and various compounds that are known binders is also useful. Finally, X-ray crystallographic structural characterization of the protein is one of the most widely accepted techniques to show that the protein is of high purity. All these techniques are orthogonal and complementary and add to the overall picture that we need in order to understand the structure–thermodynamics of protein–ligand binding.

The recombinant CAs may not be fully representative of their behavior in live human cells. First, here we produced only the catalytic domains of isoforms that contain transmembrane domains (CA IX, CA XII, and CA XIV). The dimerization of these and other isoforms may also be affected thus changing the compound affinities. Furthermore, different isoforms may be posttranslationally modified in human and not represented in bacterial preparations. Therefore, despite the recombinant proteins being the best models representing proteins in the human body, it should be used with some caution.

However, for several monomeric isoforms that were produced in bacteria in full length and where no glycosylation or other posttranslational modifications are known, the bacterial recombinant isoforms are an excellent model to represent their binding of a potential drug in the human body.

The most interesting and compelling case is of CA VI which can be affinity-purified from human volunteer saliva. We have demonstrated that the CA VI preparations from human saliva and the protein recombinantly prepared from mammalian cells, as previously described by Kazokaitė *et al.* (2015), exhibited essentially the same affinity towards a large series of sulfonamide compounds (Fig. 26).

Thermal stability of CA isoforms

Figure 27 shows the thermal stabilities of all 12 catalytically active CA isoforms in various buffers as a function of pH. The stability profiles are quite similar among the isoforms, with stability maximal and minimal pH dependence between pH 6 and 9. Isoform CA VI is somewhat exceptional with the pH stability maximum

https://doi.org/10.1017/S0033583518000082

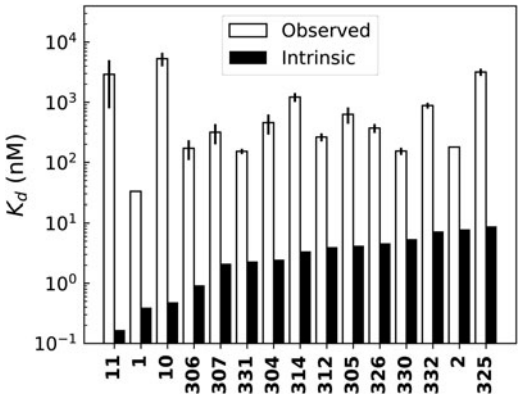

Fig. 18. The observed and intrinsic K_d of a series of sulfonamide compound interaction with CA VI (Kazokaitė *et al*., 2015). There is clearly no correlation between the observed and intrinsic binding affinities.

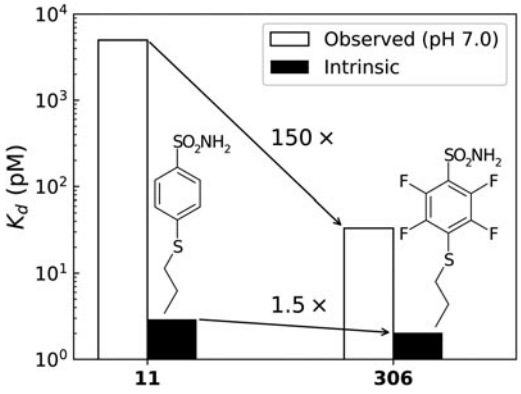

Fig. 19. The observed and intrinsic K_d of two sulfonamide compound interaction with CA I. The compounds are *para*-substituted benzenesulfonamides, one of them with four fluorines on the benzene ring. The observed affinity showed that the F-bearing compound bound CA I significantly stronger than the non-fluorinated compound. The intrinsic K_ds were practically equal for both compounds, but the observed ones differed by 150-fold mostly due to the reduction of the pK_a of the fluorinated compound and not direct recognition between the F atoms and the protein surface.

between pH 5 and 6. The most stable isoform is CA IX, the next is CA IV, while CA VII and CA XII are the least stable isoforms. It should be kept in mind that these are stabilities of catalytic domains and may not fully represent native CAs that contain transmembrane parts.

Interestingly, the citrate buffer exhibits a strong destabilizing effect on most CA isoforms, most likely because citrate binds Zn^{II} and thus destabilizes CAs by pulling the metal cation from the active site.

X-Ray crystallographic studies of human CA isoforms

In this section, the X-ray and neutron crystallographic structures of human recombinant unliganded CA isoforms and with bound ligands in the active site are reviewed that were deposited to the PDB up to the Fall of 2017. First, we concentrate on the apoprotein and later review the ligand binding studies.

CA I

The very first crystal structure of CA reported as the human erythrocyte CA form B, was the structure of CA I (Kannan *et al*., 1975). The crystallization report appeared earlier (Kannan *et al*., 1972*a*) and the structure was revisited and refined to the resolution of 2 Å (Kannan *et al*., 1984). The bicarbonate in CA I was found as a monodentate ligand in the tetrahedral coordination sphere of Zn ligands (Kumar and Kannan, 1994). This position differs from that in the crystal structure of CA II-Co-HCO_3^- complex, where cobalt substitutes for the zinc (Haakansson and Wehnert, 1992). In this structure, the bidentate binding of HCO_3^- was found. Further crystal structures of CA I with anionic inhibitors (Kumar *et al*., 1994) revealed differences in the binding of two anions: iodide replaced the Zn-bound water, whereas gold cyanide did not bind to the zinc directly. One of CN^- atoms made H-bond with the Zn-bound water. Thus, $Au(CN)^{2-}$ can inhibit CA I because it occupies a substrate binding site, whereas I^- directly binds to Zn.

An interesting naturally occurring genetic variant of CA I, Michigan 1(Ferraroni *et al*., 2002), where His67 residue is replaced with Arg, could bind an additional zinc ion. An additional Zn-binding site was formed by His64, His200 and Arg67 side chains. Coordination of Zn^{II} by arginine side chain is rare.

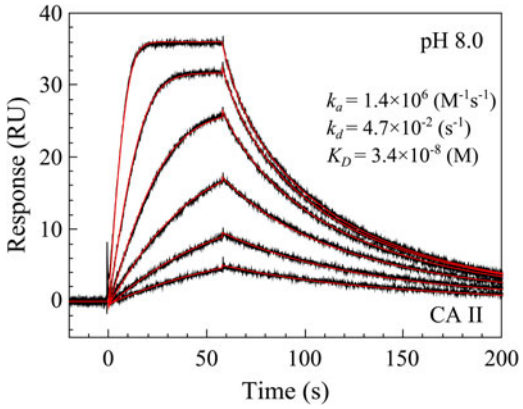

Fig. 20. An example of raw SPR data. Interaction of **368** with CA II at pH 8.0 as described by Linkuvienė *et al*. (2018). The data are shown in black while the globally fitted curves – in red. Each consecutive curve was obtained at a half concentration of the compound as compared with the previous one.

CA II

Crystallographic studies of CA II play a very important role in the field of human CAs. First CA II structure was described in 1972 (Kannan *et al*., 1972*b*; Liljas *et al*., 1972) as the human erythrocyte CA form C. First CA II crystal structures of limited resolution 2 Å were obtained by Liljas *et al*. (1972) as early as in 1972 (Liljas *et al*., 1972), then revisited and refined in 1988 (Eriksson *et al*., 1988*a*). Additional restrained refinement allowed to identify water molecules in the active site, one of them bound to the Zn^{II}. The structure helped to elucidate the reaction mechanism. High-resolution crystal structures of CA II appeared later and helped to understand the water network in the active site (Fisher *et al*., 2007*a*; Avvaru *et al*., 2010*b*). There was also some variability in crystal forms of CA II, first mentioned by Robbins *et al*. (2010).

Coordination of Zn

Numerous mutational studies were attempted in order to modify the tetrahedral coordination sphere of Zn^{II} that in α-class CAs is formed by three histidine side chains and a water molecule as a

https://doi.org/10.1017/S0033583518000082

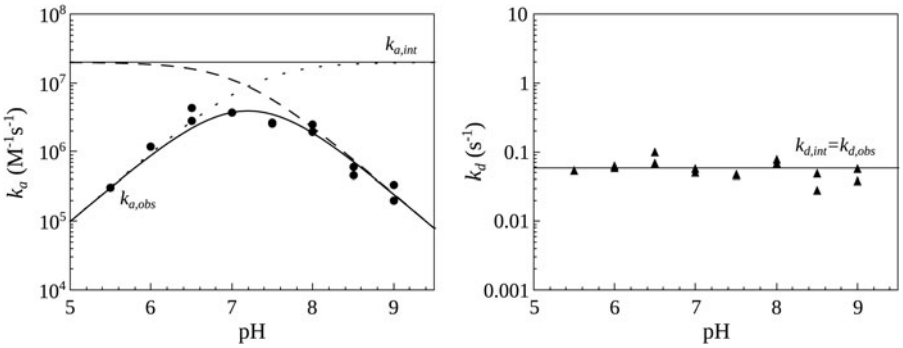

Fig. 21. The dependence of observed k_a (left graph) and observed k_d (right graph) on pH at 25 °C. It is obvious, as previously observed by Taylor *et al.* (1970), that the on-rate k_a depends on pH in a similar fashion as the thermodynamic K_D. However, the dissociation rate k_d is independent of pH as shown on the right graph drawn at the same scale as the left one.

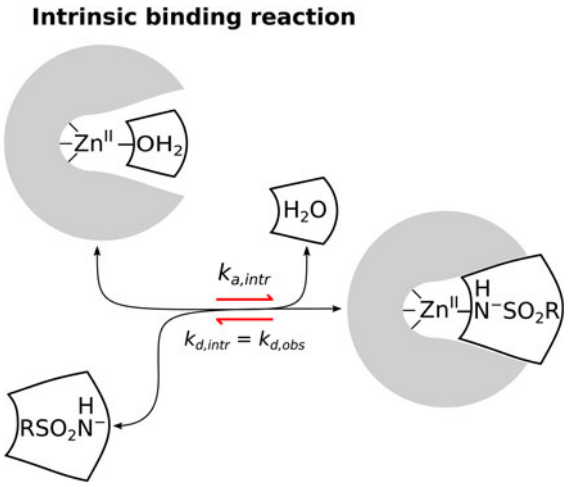

Fig. 22. The model of linked reactions, similar to the model explaining the intrinsic thermodynamics described above, that explains the pH dependence of the association rate. The observed association rate depends on pH while the observed dissociation rate is independent of pH and thus is equal to the intrinsic dissociation rate. The intrinsic association rates may be calculated applying the same equations describing the fractions of binding-ready species as in the thermodynamic calculations above.

fourth ligand. The crystal structure of Zn-free CA II was first described in 1992 (Haakansson *et al.*, 1992), the water network was compared with CA II at different pH with inorganic ligands. Removal of Zn^{II} has an influence on the protein stability and flexibility as shown by Avvaru *et al.* (2009), but not much effect was observed on substrate binding (Domsic *et al.*, 2008).

The mutation of Zn-binding histidine (His94) to aspartate side chain (Kiefer *et al.*, 1993) reduced the affinity to the metal and the catalytic activity of CA II. When the same residue His94 was replaced by cysteine side chain (Alexander *et al.*, 1993), no zinc was found in the crystal structure of the mutant. On the other hand, replacement of two Zn-coordinating residues His94 and His119 by asparagine and glutamine side chains (Lesburg *et al.*, 1997) resulted in an active enzyme, albeit the crystal structures of these mutants revealed the distorted geometry of Zn^{II} ligands. The effects of Zn-binding histidine replacements by cysteine and aspartate side chains were described by Ippolito and Christianson (1994), though the crystal structures are of limited resolution (2.2–2.4 Å).

Mutation of Thr199 side chain to cysteine was performed as an attempt to modify the metal-binding site (Ippolito and Christianson, 1993). The measured affinity to Zn^{II} was increased, cysteine side chain displaced Zn-bound water, reducing the catalytic activity of the mutant. The mutation of Thr199 to hydrophobic valine (Krebs *et al.*, 1993) led to the conclusion that Thr199 is important in the formation of H-bond to the transition state and van der Waals contacts with HCO_3^-. Femtomolar affinity to zinc was achieved by Thr199 replacement with aspartate (Ippolito *et al.*, 1995). Mutational studies of residues Thr199 and Glu106 (Xue *et al.*, 1993*a*) revealed the dependence of the catalytic activity on the direction of H-bond between residues 199 and 106.

The effect of Zn replacement by other metals was also studied in detail (Haakansson and Wehnert, 1992; Haakansson *et al.*, 1994*b*). A study could be mentioned, where Co-CA II was used for the enhancement of the pH effect on the visible spectra (Avvaru *et al.*, 2010*a*). The effect of high ionic strength and especially of citrate anion used in crystallization was discussed and the crystal structures revealed changes in the coordination sphere of Co due to pH variation.

The 'secondary coordination sphere' of zinc has an effect on the stability of the Zn-binding by histidines (Lesburg and Christianson, 1995; Huang *et al.*, 1996). Mutations in the 'secondary coordination sphere' do not distort significantly the protein conformation, but changing of H-bond network around Zn-binding histidines has an effect on the affinity to metal (Q117E mutant has higher affinity to Zn^{II}) and on the 'fine tuning' of the pK_a of the Zn-bound water. A comprehensive mutational study (Cox *et al.*, 2000) where mutations of several hydrophobic residues forming the 'secondary coordination sphere' influenced the affinity of CA II to metal ions has demonstrated that the protein can accommodate large changes in the hydrophobic core, but the optimized geometry of Zn^{II} ligation is distorted by these mutations.

The importance of the metal coordinating residues was summarized in the review (Martin *et al.*, 2013). Mutants H94C and H94D were compared with the WT enzyme while screening small molecule inhibitors. The crystal structures of the mutants soaked with benzenesulfonamide and 1-hydroxy-2-sulfanylpyridinium that represents another metal-binding group are compared.

Proton transfer

After noticing the flexible conformation of the His64 side chain (Krebs *et al.*, 1991; Nair and Christianson, 1991) at different pH, the proton transfer pathway was proposed and confirmed analyzing numerous mutants of CA II by McKenna and Christianson groups (Nair and Christianson, 1991; Scolnick and Christianson, 1996; Tu *et al.*, 2002; Bhatt *et al.*, 2005, Fisher *et al.*, 2005; Zheng *et al.*, 2008; Domsic *et al.*, 2010; Mikulski *et al.*, 2011*a*, 2011*b*, 2013).

https://doi.org/10.1017/S0033583518000082

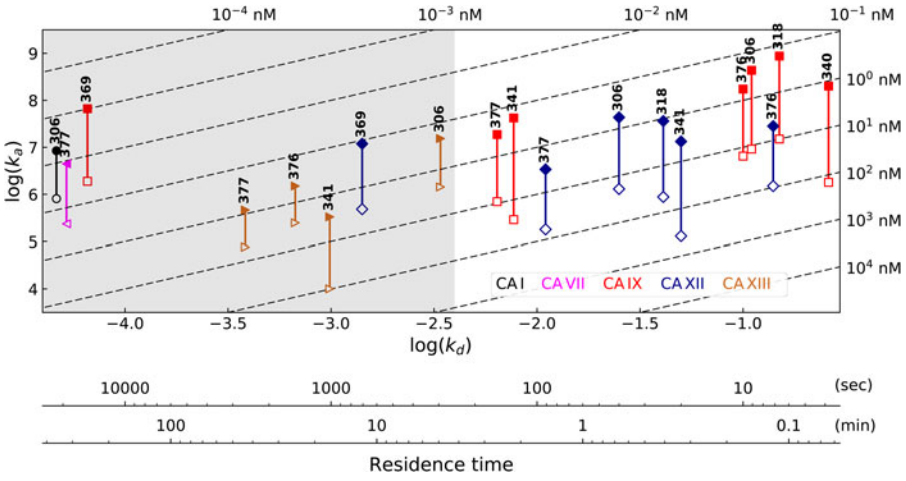

Fig. 23. Association-dissociation rates for a series of compound interaction with several CA isoforms. Each compound-CA interaction is described by two points connected by a vertical line. The upper point describes the intrinsic k_a and the lower point describes the observed k_a. The dissociation rate k_d is the same, observed or intrinsic, therefore there is only one point on the horizontal axis. Observed k_a and k_d values in the right side of the graph were obtained using SPR, while k_ds in the grey-shaded area could not be determined with the desired precision by SPR and thus were calculated using K_D obtained by FTSA and k_a obtained by SPR. The leftmost three compounds exhibit extremely slow dissociation and their residence times are in the order of several hours. Dashed diagonal lines represent isoaffinity lines with the thermodynamic K_d values listed above and on the right side of the graph. Different colors and symbol shapes represent compound binding kinetic parameters to several CA isoforms.

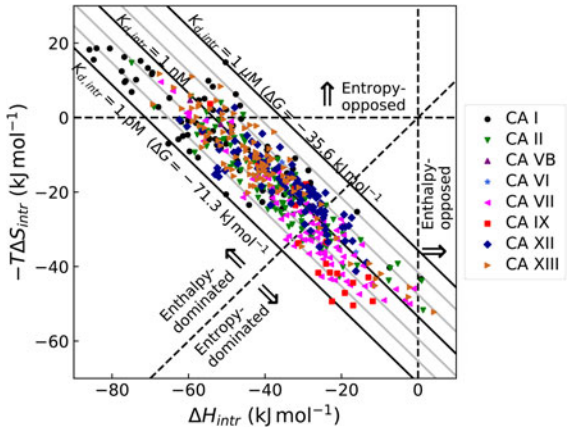

Fig. 24. The enthalpy–entropy compensation plot for all inhibitors listed in Supplementary Table 2. Different colors and symbol shapes represent binding data to various CA isoforms. Most compounds bound to CAs both due to favorable enthalpies and favorable entropy contributions. However, there were few that bound with enthalpy-opposed and entropy-opposed thermodynamics. Note that despite significant differences in compound chemical structures, the values grouped according to CA isoform: CA I binders were mostly on the top-left corner while CA IX – on the right-lower part of the plot.

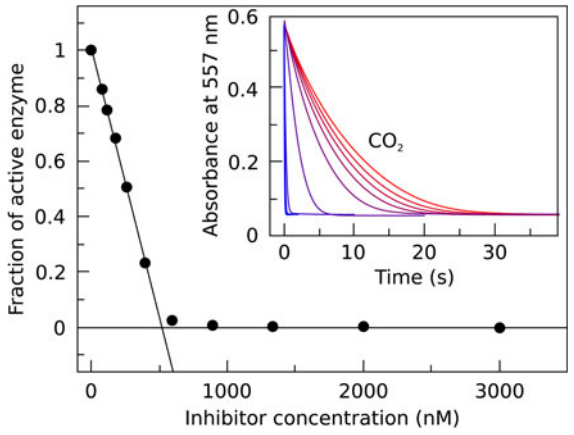

Fig. 25. Determination of the catalytically active fraction of the preparation of CA XIV as previously described by Juozapaitienė *et al.* (2016), performed according to Copeland (2005). Two straight lines intersected at exactly 500 nM concentration equal to the added concentration of CA XIV thus confirming that the entire preparation of CA XIV was enzymatically active. The inset shows the decrease in absorbance lines at various inhibitor concentrations (steep blue lines – no inhibitor, shallow red lines – largest inhibitor concentration added). The red CO_2 curve shows spontaneous hydration of CO_2 in the absence of enzyme.

Proton transfer pathway studies were greatly enhanced by neutron diffraction crystallography that can visualize deuterium. In the case of CA II, very large crystals of a very good quality could be grown, that made it possible to collect neutron diffraction datasets. Crystals were also stable enough to survive soaking in D_2O-based solution in order to exchange labile protons for deuterium (Budayova-Spano *et al.*, 2006). Results from McKenna group involved in this study shed more light on the protonation state of the catalytically important residues (Fisher *et al.*, 2010, 2011, 2012*a*; Michalczyk *et al.*, 2015).

Substrate binding

The binding of HCO_3^- was for the first time observed in the T200H mutant of CA II (Xue *et al.*, 1993*b*). The bicarbonate was bound as a bidentate ligand in the active site of this mutant, that has an increased affinity for HCO_3^-. Bicarbonate ion was found also in several crystal structures of CA I (Kumar and Kannan, 1994) and CA II (Haakansson and Wehnert, 1992; Xue *et al.*, 1993*a*, 1993*b*; Huang *et al.*, 2002), whereas the binding of CO_2 at the active site of CA II (WT and Zn-free) was described in the crystals pressured with CO_2 (Domsic *et al.*, 2008). The interconversion of CO_2 into bicarbonate was also directly observed at 100 K (Sjöblom *et al.*, 2009).

The comparison of acetate binding by CA II, WT as well as Q106E mutant, helped to understand the H-bond network Glu106-Thr199 (Haakansson *et al.*, 1994*a*). The role of hydrophobic residues in substrate binding site was elucidated by the mutational analysis of CA II residues Val121 (Nair *et al.*, 1991) and Val143 (Alexander *et al.*, 1991). In order to clarify the role of the main chain amino group of Thr199, the crystal structures of the double mutant T199P/C206S with small ligands were analyzed (Huang *et al.*, 2002). Substitutions of the Leu198 side chain had an effect on substrate binding and catalytic activity (Nair and Christianson, 1993; Nair *et al.*, 1995). Mutations of residues Asp75 and Gln74 were also investigated (Kannan, 1981).

CA III

The structural studies of CA III isoform were begun, most probably, by the crystallization of the reduced bovine CA III from red

https://doi.org/10.1017/S0033583518000082

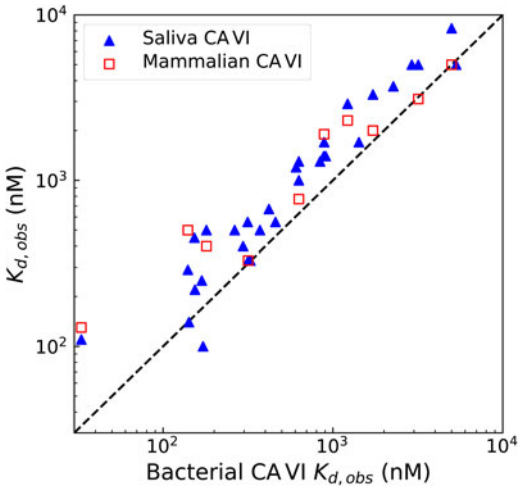

Fig. 26. Correlation between observed inhibitor binding affinities to CA VI produced by three different paths (Kazokaitė *et al.*, 2015). Human recombinant CA VI was prepared in bacterial and mammalian cell cultures. The native human CA VI was also affinity-purified from human volunteer saliva. Comparing the affinities of the compounds to the three kinds of CA VI we see that affinities are highly similar and identical within an error margin with the exception of bacterial preparation that bound the compounds with systematically higher affinity by approximately 2–3 fold. This difference could be caused by the different dimerization pattern of various CA VI preparations.

muscle (Eriksson and Liljas, 1993). The S-glutathionated form of the rat liver enzyme was also described (Mallis *et al.*, 2000). Two surface cysteines, Cys183 and Cys188, were modified and the significance of this modification in the oxidative stress was discussed.

The mechanism of proton transfer by human CA III was elucidated in mutational and structural studies (Duda *et al.*, 2002, 2005). The replacement of Phe198 side chain by leucine has increased the catalytic activity of CA III. An interesting feature of the CA III crystal structures is the ordered C-terminal His-tag that is bound in the active site cavity of the crystallographic symmetry-related subunit. In the WT enzyme, there is a stacking between one of the Zn-coordinating histidines and the phenyl group of Phe198. The possible mechanism of proton donor activation is discussed (Duda *et al.*, 2005). The role of Lys64 and Arg67 side chains, which are the structural analogs of CA II His64 and Asn67, respectively, in the proton transfer was attempted to clarify (Elder *et al.*, 2007).

CA IV

The first crystal structure of the membrane-associated CA IV was reported by Stams *et al.* (1996). The soluble secreted mutant of CA IV with the C-terminal deletion was crystallized with a limited resolution. The conformation of the N-terminal domain was stabilized by two disulfide bonds: Cys6–Cys11 and Cys23–Cys203. The crystal structures of murine CA IV (also a truncated form) were solved by the same group later and compared with CA II (Stams *et al.*, 1998). The protein contains intramolecular disulfide bond typical for trans-membrane and secreted CAs (Cys23–Cys203 in CA I) (Stams *et al.*, 1996). The N-terminal insertion of 5 amino acids in the murine CA IV was compared with other CAs (Stams *et al.*, 1996, 1998).

CA VI

In the only published crystal structure of the catalytic domain of CA VI (Pilka *et al.*, 2012) the intramolecular disulfide bond (Cys42–Cys224) was also found. Such disulfide bonds are typical in membrane-bound CA IV, CA XII, and CA XIV. It is interesting that the octahedrally coordinated Mg^{II} was found in the active site instead of Zn^{II}. The NCS dimer was found in the crystal structure and both active sites face each other, differently from CA IX and CA XII. His85 in this structure is a good candidate for the proton shuttle.

CA VII

There are two crystal structures of CA VII found in the PDB database: the unpublished complex with ethoxzolamide **1** (PDB ID: 3MDZ) and the complex with acetazolamide **2** (Fiore *et al.*, 2010*a*). The mutant with two cysteine residues replaced with serine side chains was used in the crystallization. Intramolecular disulfide bond was found in the crystal (Cys54–Cys178), but authors argued that it is an artifact, because no conserved homologous disulfide was found and such bonds are rare in the cytosolic proteins. **2** makes H-bonds with the protein main chain atoms, water molecules, Gln92 side chain, and van der Waals contacts with the Phe131 side chain.

CA VIII (Carbonic Anhydrase Related Protein, CARP)

The crystal structure of the only structurally characterized CARP, CA VIII, was solved in 2009 (Picaud *et al.*, 2009). The CARP proteins lost their catalytic activity because Zn-coordinating residue His94 (CA II numbering) is replaced by Arg116. The N-terminal Glutamine-rich loop (residues 24–36), a peculiar feature of CA VIII, is partially resolved in the structure. This loop forms contacts with another unique feature of CA VIII, an α3 – β15 loop. Both structural elements contribute to the relatively negatively charged surface of the protein. Two bulky residues restrain a cavity near the active site (Arg116 and Ile224) (homologous to Thr200 of CA II). The residue Glu114 replaces in CA VIII the CA II residue Gln92. Substitutions of the active site residues by more bulky side chains probably preclude the binding of CO_2. Chloride anion is modeled in the crystal structure instead of zinc.

CA IX

The structure of Fab fragment of anti-CA IX mAb M75 with the peptide representing epitope, the proteoglycan-like (PG) segment of CA IX was described (Kral *et al.*, 2008) and the problems of epitope recognition by the antibody are discussed. The first crystal structure of the catalytic domain of CA IX with bound AZM drug appeared in Alterio *et al.* (2009). The protein was produced using the Baculovirus expression system. The residue Cys41, responsible for intermolecular disulfide bond, that stabilizes a dimer, was replaced by serine. The dimerization interface differs from that of CA XII. Active sites of monomers are located on the same side of the dimer. AZM makes several H-bonds with side chains Thr199-200 and Gln92.

Crystallization of CA IX even with a published structure in view, was not an easy task, but finally, it was solved (Leitans *et al.*, 2015). The protein was expressed in yeast and the binding of a series of 2-thiophene-sulfonamide compounds to CA IX was characterized structurally. Binding of one ligand by CA IX was compared with CA II (Leitans *et al.*, 2013). The tail part of thiophenes interacts with the side chain of Phe131 in CA II, that corresponds to the Val130 in CA IX. The presence of phenylalanine

https://doi.org/10.1017/S0033583518000082

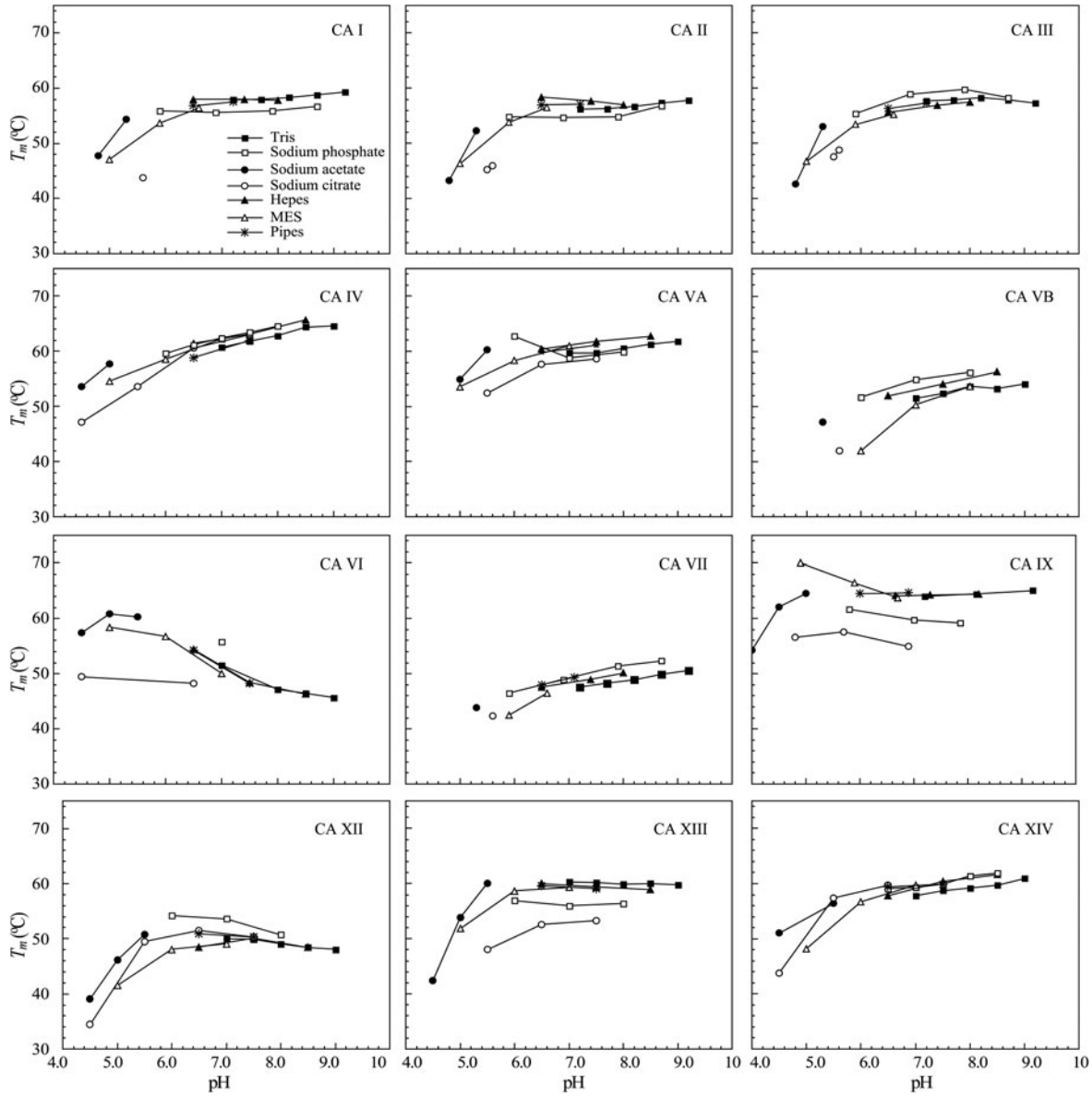

Fig. 27. Characterization of CA isoform stability in various buffers at various pHs. The isoform stability profiles look similar with the greatest stability near pH 7, but there are several notable exceptions, especially CA VI that exhibits stability maximum around slightly acidic pH 5. Note that citrate buffer is destabilizing all CAs because it is complexating Zn^{II} and thus destabilizing the native conformation of CA. Experiments were performed in 100 mM buffer containing 2 mM NaCl and 0.5% DMSO as previously described in: CA I and CA II (Morkūnaitė *et al.*, 2015), CA IV (Mickevičiūtė *et al.*, 2017), CA VB (Kasiliauskaitė *et al.*, 2016), CA VI (Kazokaitė *et al.*, 2015), CA VII (Pilipuitytė and Matulis, 2015), CA IX (Linkuvienė *et al.*, 2016*b*), CA XII (Jogaitė *et al.*, 2013), CA XIII (Baranauskienė and Matulis, 2012), and CA XIV (Juozapaitienė *et al.*, 2016). All panels are drawn at the same scale to help visualize the differences in stabilities among CA isoforms.

in CA II is the main reason for the differences in the binding mode.

CA XII

The first crystal structures of CA XII and CA XII-AZM complex were reported in 2001 (Whittington *et al.*, 2001). In the first structure, acetate ion is present as the fifth ligand of zinc. Its position mimics the binding of bicarbonate. AZM is bound in the other structure of CA XII. As in CA II, AZM interacts with a Phe131 side chain, that is absent in CA XII, the position of ligand differs between two isoforms. CA XII was used for the comparison of binding of various compounds with different human CA isoforms in the search of isoform-specific inhibitors (Čapkauskaitė *et al.*, 2013; Dudutienė *et al.*, 2013, 2014, 2015; Zubrienė *et al.*, 2015).

CA XIII

The first published structures of CA XIII contained acetate and AZM bound in the active site (Fiore *et al.*, 2009). In the structure with acetate, the zinc is penta-coordinated (with acetate and water molecule). The other structure contains **2**. No H-bonds with **2** were evident in the structure. Recently several series of benzenesulfonamide-based inhibitors were analyzed bound in CA XIII in the search for isoform-specific ligands (Čapkauskaitė *et al.*, 2013; Dudutienė *et al.*, 2013, 2015; Kišonaitė *et al.*, 2014).

https://doi.org/10.1017/S0033583518000082

CA XIV

The structural characterization of mammalian CA XIV was started by the crystal structures of the extracellular catalytic domain of murine CA XIV (Whittington *et al.*, 2004). The S–S bond characteristic for other membrane-bound CA (Cys23–Cys203) is found in the murine enzyme. The *N*-glycosylation is detected at the residue Asn195. Murine CA XIV in the crystal structure is monomeric. In the structure of the CA XIV complex with **2**, H-bonds are detected between **2** and Thr199-200. The human CA XIV was first characterized by the crystal structure of its extracellular domain in complex with **2** (Alterio *et al.*, 2013). The H-bonds of **2** with water are found besides H-bonds to Thr199–200.

Summary of the X-ray crystallographic structures of unliganded human CA isoforms

The X-ray crystallographic structures of the 10 out of 12 catalytically active human CA isoforms that are available in the PDB are shown in the Supplementary Fig. 1. There are no structures of CA VA and CA VB available in the PDB. Seven of the 10 structures are monomers, while CA VI, CA IX, and CA XII are dimers.

Studies of CA stability and mimicking the active site of another isoform

Improving the stability of CA II

CAs are some of the most efficient enzymes that make them a good choice for industrial applications. One of the proposed applications could be a large-scale fixation of greenhouse gases. Reaction conditions used in modern technology are rather rigorous, so it makes sense to try to improve the performance of CAs by mutations using all the wealth of the structural information available. A lot of crystallographic studies were performed in order to improve the thermostability (Fisher et al., 2012*b*; Boone *et al.*, 2013*b*, 2015) of human CAs, by introducing mutations as proposed by thermostable CA structures (Fiore *et al.*, 2013; Diaz-Torres *et al.*, 2015; Simone *et al.*, 2015).

The role of cis-Pro202 in CA II was accessed by mutation to alanine (Tweedy *et al.*, 1993), the catalytic activity of the mutant remained unchanged, but its stability was reduced. Interesting to note, that the cis-peptidyl conformation remained in the crystal structure of the mutant. Mutational analysis of the aromatic residues clustered around Phe226 (Boone *et al.*, 2013*a*) revealed its importance for the stability of the protein, with no effect on the activity.

There were also studies (Monnard *et al.*, 2013; Heinisch *et al.*, 2015) aimed to create an artificial transfer hydrogenase.

Mimicking of the active site of CA IX in CA II

The high similarity of α-class CAs and the difficulties with the crystallization of recombinant CA IX prior to 2015 prompted the construction of CA II point mutants-chimeras that were intended to mimic the CA IX active site. All these studies were used in the search of CA IX-specific inhibitors that have low affinity to CA I and CA II.

The crystallographic study of chimeric CA IX was started by McKenna group with two mutations: S65A, Q67N (Genis *et al.*, 2009; Sippel *et al.*, 2011; Tars *et al.*, 2013). In the next version of CA IX chimera, 8 mutations was introduced: A9K, S65A, Q67N, T69E, L91I, V131F, E170K, A204L (Pinard *et al.*, 2013). Chimeric CA IX containing 6 mutations (S65A, Q67N, L91I, V130F, L134V, A203L) was also designed by our group and its interaction with the fluorinated benzenesulfonamides was compared with other human CAs (Dudutienė *et al.*, 2014). Slightly different set of seven mutations (S65A, Q67N, T69E, L91I, V130F, E169K, A203L) was also designed (Moeker *et al.*, 2014*a*; Mahon *et al.*, 2015*a*; Pinard *et al.*, 2015) and an additional mutation (Q214E) was added to this set (Mahon *et al.*, 2015*b*).

The crystal structures of CA IX purified by Tars group from yeast (Leitans *et al.*, 2015) which could be easily co-crystallized with ligands of interest seem to make this direction in human CA research less important.

Mimicking of the active site of CA XII in CA II

Our group also reported the crystal structure of CA II mimicking CA XII (chimeric CA XII) with mutations S65A, K67N, T91I, A130F, S134V, N203L (Dudutienė *et al.*, 2014). The purpose of this construct was to illustrate the suitability and relevance of the chimeric CAs for inhibition studies. The chimeric CA XII both structurally and thermodynamically bound ligands like a real CA XII in a manner that significantly differed from CA II thus proving the approach to be highly suitable for the testing of compound selectivity.

X-Ray crystallographic studies of human CA complexes with inhibitors

The main purpose of crystallographic studies is to design isoform-selective compounds that could be used for the treatment of various human disorders in which CAs are involved.

Sulfonamides

The relatively small compound trifluoromethane sulfonamide (TFS) binds to CAs very effectively due to its low pK_a (5.9–6.2) and its complex with CA II was crystallized (Haakansson and Liljas, 1994). The position of the ligand was compared with the crystal structure of CA II-**2** complex (Vidgren *et al.*, 1990). It is interesting that the oxygen atoms of sulfonamide in $CF_3SO_2NH_2$ were directed opposite to oxygen atoms in **2**. CF_3 fits into the hydrophobic cleft, whereas the aromatic inhibitor must be oriented outwards. Another small molecule, *N*-hydroxysulfonamide, is bound in the crystal structure of CA II (Temperini *et al.*, 2007*c*).

Benzene non-primary sulfonamides

Two crystal structures of benzenesulfonamide with OH or methoxy substitution at N of sulfonamide in CA II are presented by Fiore *et al.* (2011).

para-Benzenesulfonamides

Bio-sensors and fluorescent labels. The binding of benzenesulfonamide with various attached fluorophores and other compounds was tested with CA II as a component of various bio-sensors.

In the crystal structure of fluorophore dansylamide (5-dimethylamino-1-naphthalene sulfonamide) when bound to CA II, the unusual orientation of the naphtyl ring towards the hydrophobic pocket of the active site requires conformational shift of Leu198 (Nair *et al.*, 1996). The use of fluorescent sulfonamide compounds in CA II-based zinc bio-sensors is discussed.

In addition to dansylamide fluorophore (Nair *et al.*, 1996), fluorescein-derivatized arylsulfonamide was tested as a part of

https://doi.org/10.1017/S0033583518000082

zinc bio-sensor based on benzenesulfonamide–CA II interaction (Elbaum *et al.*, 1996). The fluorescein-containing compound and its precursor bound to CA II via benzenesulfonamide, but the fluorescein moiety was not resolved in the crystal. The similar compound was used for the development of hypoxic tumor imaging system, but the linker connecting the benzenesulfonamide and fluorescein moieties was shorter (Alterio *et al.*, 2006). Fluorescein is clearly visible in the structure and exposed out of the active site cavity and interacts with the helix 130–135.

The high affinity of benzenesulfonamides for CA II was used in an unusual way for the structural visualization of the Xe-caging agent cryptophane (Aaron *et al.*, 2008). The cryptophane with caged Xe atom was fairly visible in the CA II crystal pressured with Xe.

CA II binding with benzenesulfonamides was also used in the development of specific protein detection strategy using TFG (two-faced guest) approach. TFG is a bifunctional compound that binds cucurbit[6]uril. When TFG is captured by the enzyme, unreacted cucurbit[6]uril binds Xe in solution for quantification by NMR (Wang *et al.*, 2016). The binding of three TFG candidate compounds to CA II was compared. All of them were bound in the active site hydrophobically.

Model systems. CA II is also used as a model system for purely biophysical research: a crystallographer has a good chance to see in the crystal structure various small molecules as well as sulfonamides with various substituents.

Benzenesulfonamides with aliphatic and fluorinated hydrocarbon tails were used in the study of the hydrophobic effect (Mecinović *et al.*, 2011). It was found that fluorocarbons are indistinguishable from hydrocarbons when bound to CA II, and all the differences in binding affinities are explained by hydrophobic surface changing between ligands. Similar research was performed with tricycled sulfonamides (Snyder *et al.*, 2011; Lockett *et al.*, 2013).

Another direction of the research was the use of CA II as a tool for investigation of Hoffmeister series ions (Fox *et al.*, 2015). Four structures presented in this study were analyzed with respect to water network changes upon the binding of anions and interaction of anions with the protein surface. Anions are known to be weak inhibitors of CAs. Br^-, I^-, SCN^-, and ClO_4^- have different hydration abilities. For example, I^- and Br^- were found associated with hydrophobic parts of the active site cavity and significantly changed the water network.

The effect of fluorination on the interaction with CA II Phe131 was also investigated in detail using crystal structures of CA II with series of *N*-(4-Sulfamylbenzoyl)-benzylamines (Kim *et al.*, 2000, 2001). *N*-(4-Sulfamylbenzoyl)-benzylamines were produced systematically introducing fluorine atoms into the second benzene ring that in the WT enzyme forms edge-to-face interaction with Phe131. Crystal structures of WT CA II were compared with structures of the F131V mutant with the same inhibitors. So the CA II-benzenesulfonamide ligand system was used successfully to study weak interactions. Comparing binding of ligands with varied degree of fluorination, the authors observed the different variants of aromatic interactions in mutant CA II.

CA II interaction with benzenesulfonamide was used in order to verify the computational approach for drug design (Combinatorial small molecule growth algorithm) (Grzybowski *et al.*, 2002). Two molecules were predicted to bind to CA II in a different way and structures presented in the study confirmed the predictions.

A tethered azide/alkyl cycloaddition reaction was performed using target-guided synthesis in the active site of CA II mutant H64C (Wischeler *et al.*, 2011). CA II was used as a model system in the click chemistry. Azide component was attached to the Cys64 by a disulfide bond and alkyl was coordinated at zinc via benzenesulfonamide. Crystal structures of reactants and product in CA II are presented. The reaction was stereo-selective and no Cu(I) was added.

Recognition of protein surfaces by synthetic foldamers was studied using CA II (Buratto *et al.*, 2014). Foldamers were functionalized by benzenesulfonamide in order to keep at the protein surface. Interestingly, foldamers bound to two protein chains dimerized through the stacking interactions of two helices. Foldamers are additionally fixed at the surface of the protein by coordination of zinc located at the secondary Zn-binding site

The crystal structure of CA II–benzenesulfonamide with a bulky thiophene-containing tail was described as a part of the purely crystallographic analysis of high-resolution structures of CA II (Behnke *et al.*, 2010). The crystal structure was compared with 13 high-resolution structures of CA II and refined to the resolution of 0.9 Å. Benzenesulfonamide moiety has a good electron density, whereas the tail is rather flexible, as seen from the poor density and highly anisotropic *B*-factors. The paper discusses the variable parts of the protein by comparison of 14 high-resolution structures. The inhibitor was chosen just to fill up most of the active site.

Inhibitors of CA II. A series of homologous benzenesulfonamides having ethylene glycol tail with attached amino acids in *para*-position of the benzene ring was investigated as CA II inhibitors (Boriack *et al.*, 1995). Ethylene glycol tails were bound in the active site hydrophobically, amino acids were protruded from the active site cavity and were disordered in the crystals.

A new class of 'two-prong' inhibitors of CAs was proposed, which carry the cupric iminodiacetate that can bind solvent-exposed histidines besides benzenesulfonamide moiety that binds to Zn^{II} (Jude *et al.*, 2006). Structures demonstrated the binding of the inhibitors to His64 in CA II and His200 in CA I. All compounds were bound also at the secondary binding site near the N-terminus of the protein.

Inhibitor based on benzenesulfonamide with glycosyl moiety was tested as a promising antiglaucoma agent (Fiore *et al.*, 2007). The compound bound to CA II with the glycosyl moiety oriented towards a hydrophilic part of the active site cavity. This study paralleled the research, where sugars were directly derivatized by sulfonamide (Lopez *et al.*, 2009), and monosaccharides containing sulfamate as a zinc-binding group (Lopez *et al.*, 2011; Moeker *et al.*, 2014*a*; Mahon *et al.*, 2015*b*, 2015*c*). Crystal structures of 4-substituted-ureidobenzenesulfonamides demonstrated variable hydrophobic interaction in the active site (Pacchiano *et al.*, 2010).

Ferrocene and ruthenocenes were co-crystallized with CA II as benzenesulfonamide derivatives (Salmon *et al.*, 2012). The idea was to occupy more fully the hydrophobic part of the active site using bulky hydrophobic organometallics. Complexes fit well, the hydrophilic part is occupied with glycerol or solvent. Yet another exotic CA II inhibitor is the hexamethylcyclohexane at ruthenium in the piano stool-Ru complex (Monnard *et al.*, 2011). The complex makes π-aromatic interaction with Phe131. Yet another crystal structure of the different piano-stool complex with rhenium was also presented with the view of inhibition of

https://doi.org/10.1017/S0033583518000082

cancer-relevant CAs and its technetium analog could be useful in tumor imaging (Can *et al.*, 2012).

4-Sulfamoylphenyl-ω-aminoalkyl ethers with varied linkers were tested as antiglaucoma agents. Structures of one of them and its Boc-protected variant were solved when bound in CA II (Bozdag *et al.*, 2014*b*), both ligands bound in the same way, between Phe131 and Pro202. In crystal structures of benzenesulfonamide containing lipophilic 4-alkoxy- and 4-aryloxy moieties, the compounds coincide perfectly in the active site and are bound hydrophobically (Carta *et al.*, 2015). The pain modulating activity of one of the ligands was demonstrated *in vivo*. The crystal structure of photochromic azobenzene benzenesulfonamide with various electron-donating or withdrawing groups (Runtsch *et al.*, 2015) have demonstrated that azo-group is not perfectly planar and second benzene ring is located between Pro202 and Phe131.

Inhibitors discriminating CA I and CA II. A significant problem of selectivity between the active sites of CA I and CA II was approached with a series of simple benzenesulfonamide containing *para*-substituents of a variable charge (Srivastava *et al.*, 2007). Positive charges are less tolerated in CA I, whereas negatively charged compounds bind equally well in both isoforms. Three crystal structures of CA I with compounds of interest were provided.

Anticonvulsant 4-aminobenzenesulfonamides with branched-alkylamide moieties were tested as inhibitors of CA I, CA II, CA VII, and CA XIV, expressed in the brain. Three compounds were co-crystallyzed in CA II and showed a similar binding mode, mostly by hydrophobic interactions (Hen *et al.*, 2011).

Seven crystal structures of 4-[*N*-(substituted-4-pyrimidinyl)-amino]-benzene-sulfonamides were presented in a crystallographic and binding thermodynamic study of several human CA isoforms (CA I, CA II, CA VII, and CA XIII) (Sūdžius *et al.*, 2010). Electron-withdrawing groups were introduced in order to enhance the interaction of ligands with the hydrophilic part of the active site and the linker length was varied.

The ligand combining two Zn-binding groups was developed as the possible isoform-selective inhibitor (D'Ambrosio *et al.*, 2012). In the presented crystal structure benzenesulfonamide is bound to zinc via sulfonamide, whereas sulfamide moiety made H-bonds with water in the active site. Interestingly, a secondary molecule of the ligand was found at the entrance of the active site in the crystal structure.

A series of *N*-aryl-β-alanine derivatives and diazobenzenesulfonamides were synthesized and their binding affinities towards several CAs were investigated (Rutkauskas *et al.*, 2014). In the crystal structures of two compounds, the first benzene ring is positioned in the same way, second rings are bound similarly between Pro202 and Phe131.

Inhibitory activity of 1,1′-biphenylsulfonamides was tested against CA I, CA II, CA IX, CA XII and CA XIV (La Regina *et al.*, 2015). These larger compounds were aimed towards interaction with residues 127–136 which differ in CA II and CA XIV. Compound with the highest K_i for CA XIV was crystallized in CA II and CA XIV. First rings of the compounds were positioned similarly in both isoforms, second rings differed, whereas the third rings were resolved poorly. H-bond is found between Ser132 in CA XIV and the carbonyl group of the linker.

Isoform-selective inhibitors of CA IX. Many binding, inhibition and structural studies of human CAs were devoted to the design of inhibitors of CA IX and CA XII, the targets against certain types of cancer (Pastorekova *et al.*, 2008). Such inhibitors should be isoform-specific in order not to interfere with the ubiquitous CA I and CA II.

One of the candidate compounds was benzenesulfonamide with the positively charged trimethylpyridinium *para*-substituent. The compound was tested for anti-tumor activity and crystallized in CA II (Menchise *et al.*, 2005). The charge made the compound membrane-impermeant. The pyridinium moiety made a face-to-face stacking with Phe131 and was bound at the hydrophilic part of the active site.

Another interesting approach for creating CA IX-selective inhibitors is based on the design of hypoxia-activated inhibitors containing mercapto-group. Benzenesulfonamide containing 3,3′-dithiodipropionamide- or 2,2′-dithiodibenzamido- moieties were tested and one of the compounds was crystallized in the reduced (thiolic) form with CA II (De Simone *et al.*, 2006).

Two selective arylsulfonamide inhibitors of CA VII, CA IX, and CA XIV were crystallized bound to CA II (Gitto *et al.*, 2012). The second rings of both compounds have alternate positions in the active site. Heteroaryl-benzenesulfonamides were tested as isoform-specific inhibitors with several CA isoforms and their binding to CA II was analyzed in five crystal structures (Buemi *et al.*, 2015). Ligands in all five structures coincided well and were bound hydrophobically.

The adamantyl-containing benzenesulfonamide (Biswas *et al.*, 2013*a*) was compared as an isoform-selective compound with its thiadiazole-counterpart (Avvaru *et al.*, 2010*c*). The replacement of the tricyclic ring with benzene improved the inhibition profile. On the other hand, the first ring of ligands in superimposed structures occupies the same position, but the adamantyl groups are positioned on different sides of the Phe131.

Another example of aryl-benzenesulfonamide (Güzel-Akdemir *et al.*, 2013) ligand was compared with several other aryl-benzenesulfonamides (De Simone *et al.*, 2006; Pacchiano *et al.*, 2010; Carta *et al.*, 2011; Hen *et al.*, 2011). Inhibitor bound at the hydrophobic part of the active site between the side chains of Phe131 and Pro202.

Coumarinyl-substituted benzenesulfonamides were tested against several human CA isoforms (Wagner *et al.*, 2010). The crystal structure of one ligand in CA II was described. Coumarinyl group attached to benzenesulfonamide interacted with the active site like any other benzenesulfonamide in contrast to coumarins lacking the sulfonamide group. The stacking interaction was found between coumarine ring and phenyl group of Phe131.

1,3,5-Triazinyl-substituted benzenesulfonamides discussed as potential inhibitors of human CA and β-class bacterial CAs (Carta *et al.*, 2011) were crystallized in CA II. Triazine ring was found stacked with the side chain of Phe131. Two compounds were located in the CA II active site in a very similar way.

The crystal structure of an anticancer drug E7070, which is a para-substituted benzenesulfonamide was reported, but not found in the PDB database (Abbate *et al.*, 2004*a*).

para-meta-*Benzenesulfonamides*

Inhibitors of CA II. One of the earliest crystallographic studies of inhibitors bound to CA II was the 4-aminobenzenesulfonamide with mercury at the 3rd position of the benzene ring (Eriksson *et al.*, 1988*b*).

Two human CA inhibitors that differ only by the fluorine at *meta*-position of the benzene ring showed different conformations of the second ring in the complex with CA II (Biswas

https://doi.org/10.1017/S0033583518000082

et al., 2011). The interaction of inhibitors with CA II was designed by a new strategy of 'virtual screening' as an alternative to the high-throughput screening (Grüneberg *et al.*, 2002). The method was based on the analysis and docking of known structures. Two predicted compounds were analyzed structurally.

Isoform-selective inhibitors. 1-*N*-Alkylated-6-sulfamoyl saccharin derivative that was unintentionally hydrolyzed during X-ray experiment was further developed into the inhibitor showing selectivity between CA isoforms (Ivanova *et al.*, 2015).

Benzenesulfonamides containing TEMPO (2,2,6,6-tetramethylpiperidine-1-oxyl) moiety in the *para*- or *meta*-positions and Cl in the *meta*-position showed inhibition of human CAs (Ciani *et al.*, 2009). Such compounds could be used for spin-labeling studies. ESR (electron spin resonance) spectra differed between isoforms. The TEMPO moiety was slightly disordered in the crystal structure.

The crystal structure of sulpiride, an anti-psychotic drug, bound to CA II is reported, but not found in the PDB database (Abbate *et al.*, 2004*b*).

ortho-*Benzenesulfonamides*

The binding of halogenated benzenesulfonamide was characterized thermodynamically and crystallographically (Scott *et al.*, 2009). Both 2-substituted benzenesulfonamides showed very different binding profiles and positions in the active site of CA II. Whereas the position of benzenesulfonamide ring was the same in both structures, the orientation of the thiophene tails differed.

Fluorinated para-*benzenesulfonamides*

A detailed binding and crystallographic study of fluorinated *para*-substituted benzenesulfonamides were supplemented by three crystal structures of the compounds bound to CA II, CA XII, and CA XIII (Dudutienė *et al.*, 2013). Fluorination of the benzene ring especially enhanced the binding to CA I. Two possible orientations of benzene ring were revealed in the crystal structures of CA XII and CA XIII with ligands.

The studies of fluorinated *para*-substituted benzenesulfonamides were continued further (Zubrienė *et al.*, 2015). These compounds showed exceptionally strong binding to CA I because the fluorination increased the fraction of deprotonated ligand. Three crystal structures of CA I and the structures of CA II and CA XII in complex with four ligands were described and compared with related compounds (Dudutienė *et al.*, 2013). The study revealed variation in the positions of the first ring of inhibitors in CA II and CA I.

Fluorinated para-meta-*benzenesulfonamides*

Structural and thermodynamic investigations of fluorinated benzenesulfonamides were continued with crystal structures of three compounds containing substituents in *meta*- and *para*-positions bound in CA II, CA XII, and CA XIII (Dudutienė *et al.*, 2015). In CA XIII, fluorinated benzene ring was found only in a single position, whereas in CA II and CA XII the position of the benzene ring could vary.

Chlorinated meta-*benzenesulfonamides*

Compound 5-nitro-2-Cl-benzenesulfonamide as a precursor of the series of ligands could be reduced, thus aiming towards the hypoxia-inducible CA IX (D'Ambrosio *et al.*, 2008*a*). The crystal structure supplemented the inhibition studies.

A face-to-face stacking interaction with Phe131 was found in the crystal structure of sulfonamide-based diuretic drug indapamide (Temperini *et al.*, 2008*b*). The comparison with the crystal structure of other diuretic drug chlorthalidone bound to CA II (Temperini *et al.*, 2009) showed the different binding mode of the drug in its enol form, making H-bonds with waters ordered in the active site and the side chain of Asn67.

The series of indapamide-like *N*-alkylated benzimidazoles was compared with S-alkylated benzimidazole derivatives thermodynamically and structurally in crystal structures with CA II (Čapkauskaitė *et al.*, 2010). The position of the Cl-benzene ring in all crystal structures was determined by Cl atom bound to the hydrophobic pocket of the active site, and tails were directed in the same way as indapamide itself making H-bonds with the residue Asn62 by linker atoms. Analysis of the thermodynamic parameters of binding showed that S-alkylated compounds were more effective CA inhibitors, probably due to better H-bond pattern and larger hydrophobic area.

Chlorinated para-meta-*benzenesulfonamides*

Four crystal structures of *para-meta*-substituted chlorinated benzenesulfonamides were presented in the comprehensive research trying to connect the intrinsic thermodynamic parameters of ligand binding to several CA isoforms with the structural information (Kišonaitė *et al.*, 2014). The influence of chlorine in *ortho*-position and positions of the four different tails on the thermodynamic parameters of binding was analyzed.

The binding of two series of inhibitors, namely, [(2-pyrimidinyl-thio)-acetyl]benzenesulfonamides, that contained Cl at the position 2 of the benzene ring and tail at the *meta*-position and Cl-free ligands substituted at *para*-position of the benzene ring, were compared thermodynamically and structurally (Čapkauskaitė *et al.*, 2012). Chlorine atom determined the positioning of the first ring and analysis of the binding thermodynamic parameters showed better selectivity of the first group of compounds towards CA I, CA II, CA VII, and CA XIII. Cl-free ligands showed better binding but lower selectivity. These studies were continued further (Čapkauskaitė *et al.*, 2013). Two series of ligands described already (Čapkauskaitė *et al.*, 2012) were complemented with *meta*-benzenesulfonamide without Cl and *para*-benzenesulfonamide with Cl. Crystal structures of three compounds with CA II, CA XII, and CA XIII were described in this work. In common, the binding affinities of *para*-substituted compounds were higher. One of the compounds was the selective nanomolar inhibitor of CA I.

di-Benzenesulfonamides

Crystal structures of three benzene-1,3-disulfonamide derivatives bound in CA II demonstrated that the sulfonamide group in *meta*-position is directed towards the hydrophilic part of the active site and made H-bonds with residues His64, Asn67, Gln92, and Thr200 (Alterio *et al.*, 2007). The benzene ring was found in the position, that was relatively rare in known structures of benzenesulfonamide inhibitors bound to CA II.

Heterocycles

Thiophenes and thiazines

Three crystal structures of thiophenesulfonamides with substituents of varied length at the 4-amino group were analyzed (Smith *et al.*, 1994). One of these compounds was the dorzolamide drug. The only difference in the binding of these ligands

https://doi.org/10.1017/S0033583518000082

in CA II was the displacement by the dorzolamide of the proton shuttle residue of CA II–His64.

Inhibitors based on the structure of the topical antiglaucoma drug brinzolamide were compared as inhibitors of CA II and CA IV (Kim *et al.*, 2002). These compounds are nanomolar inhibitors of CA II. Morpholino group and the hydrophobic tail were located at the residue Val135. Positions of the heterocyclic ring depended on the second substituent.

The binding of bicyclic thienothiazene-6-sulfonamide-1,1-dioxide nanomolar inhibitors to CA II was structurally compared with monocyclic 2,5-thiophenedisulfonamides (Boriack-Sjodin *et al.*, 1998). The second sulfonamide group served for the introduction of substituents that interact mostly with the hydrophobic pocket of CA II active site. These structures helped to understand the mechanism of action of the perspective antiglaucoma drug brinzolamide (Stams *et al.*, 1998).

The crystal structure of CA II with another variation of the dorzolamide scaffold was presented (Steele *et al.*, 2009), where the nitric oxide donating moiety is combined with the drug with the aim to develop a dual action antiglaucoma drug.

The crystal structure of thiophenesulfonamide with naphtalene substituted triazole ring represents a group of inhibitors, that were synthesized by click-chemistry (Leitans *et al.*, 2013). These compounds were micromolar inhibitors of CA I and nanomolar – of CA II. Bulky substituents at triazole were proposed to mediate the selectivity towards CA II. Their tails were differently located in crystals.

Thiazoles and thiadiazoles

The use of thiadiazole-based ligands in human CA inhibition studies represented a further development of acetazolamide drug that is in a clinical use for decades.

The linker between sulfonamide group and thiadiazole ring can influence the binding mode of the inhibitor in CA II as was demonstrated in several studies (Fisher *et al.*, 2006; Temperini *et al.*, 2008*a*). Two crystal structures of CA II complexed with thiadiazolesulfonamide with halogenated benzene tail were compared (Menchise *et al.*, 2006). One of them was found in the structure lacking any substituent, probably due to the hydrolysis. The crystal structure of thiadiazolesulfonamide with a very long tail of nitrooxybutylbenzoate in CA II (Mincione *et al.*, 2011) illustrated the inhibition studies of a series of nitric oxide-donating CA inhibitors that could be antiglaucoma drugs. This study paralleled a research of imidazolesulfamides containing the nitro group (Rami *et al.*, 2013).

Sugars

Mono- and disaccharides derivatized by sulfonamide were studied as putative isoform-selective CA inhibitors and their binding to CA II was compared with the sulfamate Zn-binding group containing drug topiramate (Lopez *et al.*, 2009). The hydrophilic sugar moiety has low membrane permeability. Therefore, it is thought to provide *in vivo* selectivity towards transmembrane CA IX and CA XII.

Other heterocycles

A crystal structure of a tricyclic sulfonamide (benzimidazo[1,2-c][1,2,3]thiadiazole-7-sulfonamide) bound to CA II was described (Baranauskienė *et al.*, 2010). This relatively rigid compound is fixed by van der Waals interactions within the active site.

A crystallographic analysis of a series of homologous heterocyclic compounds with sulfonamide group bound in CA II was used in the studies of the hydrophobic effect (Snyder *et al.*, 2011). Crystal structures illustrated regular changes in the binding thermodynamic parameters of homologous ligands. Heterocyclic sulfonamides based on furan, imidazole, thiazole, and thiophene were also extended with the benzene ring in order to increase the hydrophobic surface. The conclusion was that the distortion of structured water was the main driving force of binding. This study was continued with a series of fluorinated heterocyclic compounds (Lockett *et al.*, 2013), and the crystal structure of CA II with fluorinated benzothiazole was described and compared with the previous study. No influence of fluorination on binding was detected.

Indanesulfonamide-based series of human CA inhibitors was analyzed (D'Ambrosio *et al.*, 2008*b*) with two crystal structures of CA II. Indane rings oriented differently in these structures due to the different substituents. In the crystal structure of CA II with indolesulfonamide-based ligand, a nanomolar inhibitor of CA I and CA II (Güzel *et al.*, 2008), the indole ring was accommodated at the hydrophilic side of the active site and made H-bonds with Asn62 and Asn67 side chains as well as with water molecules.

In the crystal structure illustrating an inhibition study of a series of 1-(cyclo)alkylisoquinolinesulfonamides against human CA isoforms (Gitto *et al.*, 2010), isoquinoline ring was fixed in the active site by van der Waals interactions. In the crystal structure of a related compound that differs from the previous study only by the methyl group (Mader *et al.*, 2011), the ring was located in a different way. The observation that very small structural differences could result in relatively large variations of inhibitory profiles was further illustrated by a comparison of two compounds: pyridinesulfonamide and benzenesulfonamide (Bozdag *et al.*, 2014*a*). Compounds have the same tails but were bound very differently in the active site of CA II, and pyridinylsulfonamide had a steric clash with hydroxyl group of Thr200.

Sulfamides

One of the simplest inhibitors structurally characterized was *N*-hydroxysulfamide (Temperini *et al.*, 2007*c*), that is the more effective inhibitor of CA I and CA II than sulfamide. The compound is bound to zinc like all other sulfonamides by the nitrogen atom, but not by the hydroxyl group.

Sulfamides comprise yet another variant of the Zn-binding group and are widely represented in CA crystallography. The positioning of these ligands has an additional degree of flexibility with respect to benzenesulfonamides (or other heterocyclesulfonamides, because of the additional rotation around the nitrogen atom).

The borolane-containing benzenesulfamide was co-crystallized with CA II due to its possible use in boron neutron capture in the anticancer therapy (Fiore *et al.*, 2010*b*). Carboranes bound through a flexible linker to the sulfamide (Brynda *et al.*, 2013) also can be effectively bound by CAs and therefore, considered to have pharmaceutical perspectives. The length of linkers was chosen in order to fill the active site by the icosahedral carborane in an optimal way. Crystal structures confirmed the predicted binding position of ligands by van der Waals interactions with the protein side chains. This study was continued further (Mader *et al.*, 2014). Here, high-resolution structure of carboranesulfamide bound in CA II was described and used for the modeling of the interaction with CA IX.

A series of nitroimidazole derivatives with sulfamide, sulfonamide, and sulfamate groups for anchoring to CA were discussed

https://doi.org/10.1017/S0033583518000082

in numerous studies. Crystal structure with one of nitroimidazolesulfamides confirmed the inhibition studies (Rami *et al.*, 2013). These compounds were chosen as possible chemo- or radiosensitizing agents in an anticancer therapy. The electron density was good and H-bonds of the nitro group with Thr200 and His64 were found.

The other research (De Simone *et al.*, 2014) described inhibitory properties of other series of compounds: phenylmethylsulfamide with substituents optimized to make interactions in the active site. But-2-yn-1-yloxy tail was found to provide strong interactions with CA II active site.

Sulfamates

Sulfamates like sulfamides are derivatives of the sulfamic acid where the substituent is bound via one of three oxygen atoms at sulfur atom. Most of the sulfamate inhibitors studied are perspective anticancer steroid or non-steroid drugs or their homologs.

Many non-steroid drugs initially designed for other targets possess sulfamate Zn-binding group. One of the examples is the anti-convulsant drug RWJ- 37 497, an analog of topiramate crystallized bound to CA II (Recacha *et al.*, 2002). The interaction of topiramate that belongs to this group of compounds with CA II is also described (Lopez *et al.*, 2009) as well as its sulfamide analog (Winum *et al.*, 2006). The crystal structure of 667-coumate, a potent non-steroidal inhibitor of steroid sulfatase (anticancer drug) based on a coumarine ring bound to CA II was reported and the mechanism of the drug stability *in vivo* due to its sequestration by CA II in blood was proposed. The tricyclic coumarine was proposed to mimic steroid structure. The electron density of the 7-membered ring was not very good due to flexibility (Lloyd *et al.*, 2005*a*). In the structures of CA II with aromatase-steroid sulfatase inhibitor analogs possessing sulfamate Zn-binding group (Lloyd *et al.*, 2005*b*), the sulfamate-containing rings in both cases nearly coincided, but the *para*-substituents differ in binding to the protein. Steroid sulfatase inhibitors were sequestered in blood by binding to CA II via sulfamate moiety. This interaction is favorable from the pharmacokinetics point of view and several structures of CA II complexes with similar ligands were reported (Leese *et al.*, 2006; Woo *et al.*, 2008, 2010; Cozier *et al.*, 2010).

Microtubule disruptor crystal structure in complex with CA II (Leese *et al.*, 2008, 2010) was yet another example of the anticancer drug which bioavailability was increased by interaction with CA. Antiproliferative bis-sulfamates and steroid sulfatase inhibitor-CA II structure (Leese *et al.*, 2006) revealed the binding of two molecules in the active site. One molecule was coordinated at zinc by sulfamate in an unusual way, the other filled the rest of the cavity. The binding of estradiol-sulfamate compounds in CA II and its double mutant, mimic of CA IX, were compared (Sippel *et al.*, 2011). These compounds could have an antiproliferative effect, and the aim of the study was to find a CA IX-specific inhibitor that binds stronger to CA IX, but still could be sequestered by CA II.

Rather an unusual set of aliphatic mono- and bis-sulfamates were studied in the search of isoform-specific inhibitors (Vitale *et al.*, 2009). Four compounds were bound in a similar way in CA II. The second sulfamate was exposed out of the cavity and was mobile as could be judged from the increased *B*-factors.

Monosaccharides with one of the hydrophilic groups derivatized to sulfamate described as inhibitors of human CAs (Lopez *et al.*, 2011) were also subject to CA II esterase activity. The loss of acyl groups was observed as well as an inversion of stereochemistry. Carbohydrates carrying sulfamate as a Zn-binding group containing various linkers were studied with the goal of designing CA IX-specific compounds (Moeker *et al.*, 2014*a*). Binding of two compounds with CA II and CA IX mimic (Pinard *et al.*, 2015) was studied crystallographically. Carbohydrate moiety as a tail group was chosen due to its lower membrane permeability. The topic hydrocarbonate-based sulfamates as isoform-selective human CA inhibitors were developed further (Mahon *et al.*, 2015*b*, 2015*c*). Together with the analysis of the ligand binding in CA II and CA IX mimic, the artifact of acetylation of the surface lysine and its effect on the protein stability was discussed (Mahon *et al.*, 2015*c*).

Abbate *et al.* (2004*c*) reported the crystal structure of antiendocrine drug showing both CA and estrone sulfatase inhibition activity: EMATE-sulfamate complex with CA II.

Natural products: alternative metal-binding groups and products of hydrolysis

Small organic Zn-binding groups

Small organic compounds often bind to zinc in a position similar to bicarbonate substrate. One of the examples is acetate. Acetate mimics the binding of substrate (Haakansson *et al.*, 1994*a*), but the latter different position of acetate in the CA active site was also found (Mazumdar *et al.*, 2008). Azide and bromide have an affinity to zinc and were also co-crystallized with CA II (Jonsson *et al.*, 1993). Sulfide and nitrate in CA II were bound at zinc forming a trigonal bipyramide coordination sphere (Mangani and Hakansson, 1992). In the complex of CA II with SCN^- at pH 8.5 (Eriksson *et al.*, 1988*b*) sulfur displaced the deep water. Zn-bound water remained in this structure and zinc was pentacoordinated (Eriksson *et al.*, 1988*b*). Bisulfite and formate complexes in CA II were crystallized at neutral pH (Haakansson *et al.*, 1992). Bisulfite was bound to zinc by an oxygen atom, replacing the Zn-bound water. Formate, lacking a hydroxyl group, bound in a similar position and made H-bond with the main chain nitrogen of Thr199 between the zinc ion and the hydrophobic part of the active site.

Cyanate was reported to bind in a CO_2 binding site, where Zn-bound water kept the position as a metal ligand (Lindahl, *et al.*, 1993). Different ways of cyanate binding were found in the structures of WT CA II and V207I mutant with cyanate (West *et al.*, 2014). The anion was bound directly to Zn finishing a tetrahedral coordination sphere.

The positioning of CS_3^{2-} Zn-binding group was investigated by solving the structure of CA II with trithiocarbonate (Temperini *et al.*, 2010). The trithiocarbonate was bound in a monodentate way to zinc and its position was the same as that of bicarbonate but differed by orientation from urea (Briganti *et al.*, 1999), which made two H-bonds with the main chain nitrogen of Thr199 and its hydroxyl group and with two water molecules.

1,2,4-triazole bound in CA II also replaced Zn-bound water, formed H-bonds with Thr199–200 and filled the proposed position of the substrate (Mangani and Liljas, 1993). Dithiocarbamates investigated as potential inhibitors of human CAs were bound to zinc in a monodentate way by sulfur atom and made interactions with active site residues (Carta *et al.*, 2012*a*, 2012*b*).

Crystal structures of several inhibitors based on hydroxybenzoic acid and phenol bound to CA II were determined (Martin

https://doi.org/10.1017/S0033583518000082

and Cohen, 2012). Phenol and benzoic acid derivatives made a H-bond with the Zn-bound water. Some of them formed H-bonds with water molecules and active site residues as well.

Polyamines as a Zn-binding group were also studied (Carta *et al.*, 2010). Spermine was not coordinated directly to zinc, the terminal aminogroup formed an H-bond with the Zn-bound water and Thr199. Other aminogroups also formed H-bonds with Thr200-Pro201 and had a clash with the side chain of Gln92.

Hydroxamates

Several compounds previously characterized to inhibit other metalloenzymes but were found to influence the activity of CA as well. Example of such ligand was acetohydroxamic and trifluoroacetohydroxamic acid (Scolnick *et al.*, 1997). The monodentate binding of the compound through its nitrogen atom (deprotonated) is similar to bicarbonate. *N*-Hydroxyurea differs from the acetohydroxamic acid by CH_3 replaced with NH_2. *N*-Hydroxyurea representing yet another Zn-binding group was bound to zinc in a bidentate way by nitrogen and oxygen atoms (Temperini *et al.*, 2006*b*). Hydroxamates were investigated further with the crystal structure of benzhydroxamic acid bound in the active site of CA II (Di Fiore *et al.*, 2012).

Cyanamides were hydrolyzed by CA II (Briganti *et al.*, 1999; Guerri *et al.*, 2000). After incubation of CA II with cyanamide, urea was found in the crystal structure. Cyanamide is isoelectronic with CO_2 and subject to hydrolysis by CA II (Briganti *et al.*, 1999). Ureate was bound to zinc as a monodentate ligand and made H-bond with hydroxyl of Thr199 and several H-bonds with water molecules.

Thioxolone: hydrolysis products

The antipsoriatic drug thioxolone was shown to be hydrolyzed by CA II (Barrese *et al.*, 2008). The resulting compound 4-mercaptobenzene-1,3-diol or 2-mercaptophenol remained bound to zinc as a fourth ligand by the thiol group. The intermediate compound S-(2,4-thiophenyl)hydrogen thiocarbonate was located in the structure at the entrance to the active site. An interesting case of oxidation of the thioxolone hydrolysis product by X-ray generated radicals bound to CA II was published (Sippel *et al.*, 2010). The resulting compound was bound to zinc via the hydroxyl group.

Other metal-binding groups were explored: 1-hydroxy-2-sulfanylpyridinium was studied crystallographically with the aim to find alternative metal-binding groups that would bind zinc in a bidentate way (Wischeler *et al.*, 2010). Indeed it was found in the crystal structure of CA II that zinc coordinated sulfur and hydroxyl. The compound is a part of the H-bond network involving several water molecules.

A series of compounds based on the similar Zn-binding group, but having different heterocycle, namely allothiomaltol and thiomaltol, was also studied (Martin *et al.*, 2014*a*). Compounds differ only by the methyl group position. Both ligands were bound directly to zinc but in a different way. Thiomaltol was bound in monodentate mode by sulfur and two conformations were modeled, whereas allothiomaltol was in the crystal structure as a bidentate ligand. The binding of thiomaltol would be expected to be similar to 2-mercaptophenol (Barrese *et al.*, 2008). Allothiomaltol nearly coincided with 1-hydroxy-2-sulfanylpyridinium (Wischeler *et al.*, 2010). Its methyl group fitted well into the hydrophobic cavity in the active site. It is an interesting study trying to show that interaction with local protein active site environment may influence the metal binding with rather significant effects.

A comprehensive crystallographic study of pharmacophores related to 1-hydroxy-2-sulfanylpyridinium was undertaken by systematically varying the position of the methyl group in relatively small compounds (Martin *et al.*, 2014*b*). Small structural differences between ligands resulted in dramatic changes in the position of ligands due to the interaction with highly ordered water network in the active site. The mono- or bidentate binding was ruled mostly by the local interaction of the substituents with protein and correlated with the inhibitor efficiency.

Coumarins: products of hydrolysis

An interesting example of the inhibition by hydrolysis product was described in an attempt to get crystal structure of coumarin derivative with CA II (Maresca *et al.*, 2009, 2010). The product of hydrolysis, a derivative of cis-2-hydroxycinnamic acid was found in the structure. Surprisingly, no interaction with zinc was found, but the compound blocked the entrance to the active site (Maresca *et al.*, 2009). The structure of CA II with the product of hydrolysis of unsubstituted coumarin was also discussed (Maresca *et al.*, 2010). The compound also did not contact with zinc but formed H-bonds to the side chains of His64, Gln92, and Asn62.

Phenols

The library of phenol-based natural products was analyzed with respect to inhibition of β-class CAs from human pathogens and CA I/CA II (Davis *et al.*, 2011). Phenols were chosen because in the published crystal structure of CA II phenol was bound to the Zn-bound water by its hydroxyl group (Nair, *et al.*, 1994). The similar binding mode was found in the structure of CA II with one of the compounds from the library. The structure of benzenesulfonamide-derivative of this compound in CA II was also solved for comparison.

Saccharines

As saccharines were found to be inhibitors of CAs, it was very natural to try to crystallize CAs with them (Köhler *et al.*, 2007). Compounds were bound to zinc with the nitrogen atom and one of sulfanyl oxygen atoms and made the fifth ligand of zinc, with a rather distorted geometry. Two structures were presented with the similar binding of a ligand, and the secondary binding site of saccharine was found in one of the structures. The perspectives of the saccharine analogs as isoform-selective inhibitors were further investigated in Moeker *et al.* (2014*b*). A relatively long tail was added to the benzene moiety through triazole. A crystal structure of this saccharine derivative was presented when bound to CA II. The tail was completely unresolved in the electron density probably due to multiple conformations.

Saccharine modified by sulfonamide moiety was found in CA II bound to zinc by sulfonamide, as all other sulfonamide compounds (Alterio *et al.*, 2015). A crystal structure of saccharine modified with carboxymethyl as Zn-binding group in CA II was also published (Langella *et al.*, 2015), thus representing a new Zn-binding group. Carboxylate was bound to zinc as a monodentate ligand.

Cholines

Cholic acid is a naturally occurring inhibitor of human CAs in the gastroenteric tract, therefore it was interesting to determine its crystal structure in complex with CA II (Boone *et al.*, 2014). Bidentate binding of cholate carboxyl to zinc displaced the Zn-bound water and shifted the deep water. Hydroxyl groups

https://doi.org/10.1017/S0033583518000082

made a lot of water-mediated H-bonds with the protein side chains in the active site, but no direct H-bonds were found. The changes on the ordered water network were discussed.

Sulfonamides as drugs

CA I

Protein interaction of CA I with clinically used drugs was studied rather intensively. There were not many structures of CA I with inhibitors as a part of drug design studies, probably due to the relatively low catalytic activity of CA I compared with ubiquitous CA II, which was a subject of intensive inhibitor search.

Three crystal structures of CA I with commercial drugs were reported (Chakravarty and Kannan, 1994). The **2, 3** and benzenesulfonamide-Hg compounds were bound to zinc, but sulfonamide group was differently oriented. **3** disrupts the H-bond network. Antiviral drug foscarnet was crystallized bound to CA I (Temperini *et al.*, 2007*a*). The drug is interesting because of an unusual Zn-binding phosphonate group. Foscarnet had some activator activity on CA I, whereas it is a weak inhibitor of several other isoforms as revealed by kinetics measurements (Rusconi *et al.*, 2004). The drug bound to zinc in the inhibitor-like manner that contradicted the kinetics data. The crystal structure of CA I with topiramate (Alterio *et al.*, 2010) showed the rearrangement of the active site compared with CA II, that means conformations of side chains of Trp5, His67, and His200 differed between the native CA I and the complex.

CA II

Nonsteroidal anti-inflammatory drugs, inhibitors of the inducible cyclooxygenase COX-2 were described as inhibitors of several human CAs (Weber *et al.*, 2004). A crystal structure of CA II with celecoxib drug was presented. The affinity for CA II could be expected, as the drug bears the sulfonamide group. Trifluoromethyl moiety was bound to the hydrophobic wall of the active site, methylbenzene made contacts with Asn62, Glu69, and Gln92. The related drug valdecoxib was also crystallized bound to CA II (Fiore *et al.*, 2006). It bounds in a different way, making stacking interaction with Phe131.

The high-resolution crystal structure of **2** in CA II was presented (Sippel *et al.*, 2009). Three **2** molecules were found in the structure. Acetazolamide is used usually as a reference compound in various inhibitor studies or in order to check the effects of mutations. In crystal structures of L198 CA II mutants in the unliganded form and with **2** were compared in order to elucidate the role of this side chain in substrate binding (Nair and Christianson, 1993; Nair *et al.*, 1995). One of the mutations, L198F, was a variant that was present in CA III, and significant conformational changes of Phe side chain occurred upon binding of inhibitor. A binding of a modified version of **2**, which is more selective towards CA II was presented (Biswas *et al.*, 2013*b*). Further modifications of **2** scaffold producing dual-tail inhibitors were described (Tanpure *et al.*, 2015), where the hydrophilic glucosyl-tail and hydrophobic phenyl-tail were found in the corresponding parts of the active site. Crystal structure of **1**, a compound preceding the dorzolamide and brinzolamide drugs bound to CA II was also described (Di Fiore *et al.*, 2008).

Interaction of an antiepileptic drug topiramate (**4**) and its sulfamate and sulfamide analogs was intensively studied (Recacha *et al.*, 2002; Winum *et al.*, 2006; Lopez *et al.*, 2009). Another antiepileptic drug lacozamide has no traditional Zn-binding groups and nevertheless, it was an inhibitor of human CAs. The complex of the drug with CA II was crystallized and showed that the binding mode is similar to the products of hydrolysis of coumarin (Temperini *et al.*, 2010). It makes no contacts with zinc. There was another example of the antimetastatic drug not contacting zinc in CA II, the Ru (III) complex compound NAMI-A [tetrachloro(DMSO)(imidazole)-ruthenate(III)] (Casini *et al.*, 2010). The complex compound was disrupted in the protein, imidazole was found at Zn^{II} and Ru^{III} was located far away in the entrance as well as DMSO.

Antihelmint drug thiabendazole was modified with sulfonamide and its activity was checked against human CAs and *Caenorhabditis elegans* α-CAH-4b (Crocetti *et al.*, 2009). The crystal structure of CA II with this compound was presented and discussed in view of human parasite CA inhibition and probably with clinical perspectives for some human CA isoforms.

CA IV

The structure of murine CA IV (Stams *et al.*, 1998) and also truncated version was compared with human CA IV (Stams *et al.*, 1996). Murine CA IV was crystallized in complex with brinzolamide and compared with CA II (Stams *et al.*, 1998). The affinity of binding differed significantly between two proteins, structural differences were discussed: the position of the drug was very similar, but in murine CA IV there were fewer contacts with the inhibitor than in CA II. There was interaction with Phe131, H-bond with water in CA IV, and tail of the ligand was disordered in the murine enzyme. An attempt to optimize the dorzolamide with respect to the binding to CA IV and solubility was reported (Vernier *et al.*, 2010). Resulting compounds were *para-meta*-substituted pyrimidinesulfonamides.

Activators

Activator molecules bind mostly at the entrance of the active site and participate in the proton transfer pathway. Activator compounds include amino acids, peptides, and amines that may be easily protonated.

CA I

The first reported case of an activator molecule in the active site of CA I was the crystal structure of the complex with histidine (Temperini *et al.*, 2006*a*). The activation effect of histidine was explained by the binding to the imidazole ring of His 200 and involvement to the water network. The binding differed from that in CA II-His structure (Temperini *et al.*, 2005).

The antiviral drug foscarnet, a weak inhibitor of human CAs, acted as an activator of CA I (Temperini *et al.*, 2007*a*). The compound was coordinated to zinc by phosphonate moiety. The phosphonate made a weak H-bond with imidazole ring of His200 in CA I active site. The presence of His200 (corresponds to Thr200 in CA II) made the CA I active site more narrow compared with other CAs and unusual orientation of foscarnet in CA I could be the reason for its role as an activator.

CA II

The first crystallographically characterized activator of CA II was histamine (Briganti *et al.*, 1997). The activator bound at the entrance of the active site cavity and the imidazole moiety was connected through water network to the proton shuttle residue His64. The molecule 1-[2-(1*H*-imidazol-4-yl)-ethyl]-2,4,6-trimethylpyridinium resulted from an optimization of histamine (Dave *et al.*, 2011). Unexpectedly, in the crystal structure with

https://doi.org/10.1017/S0033583518000082

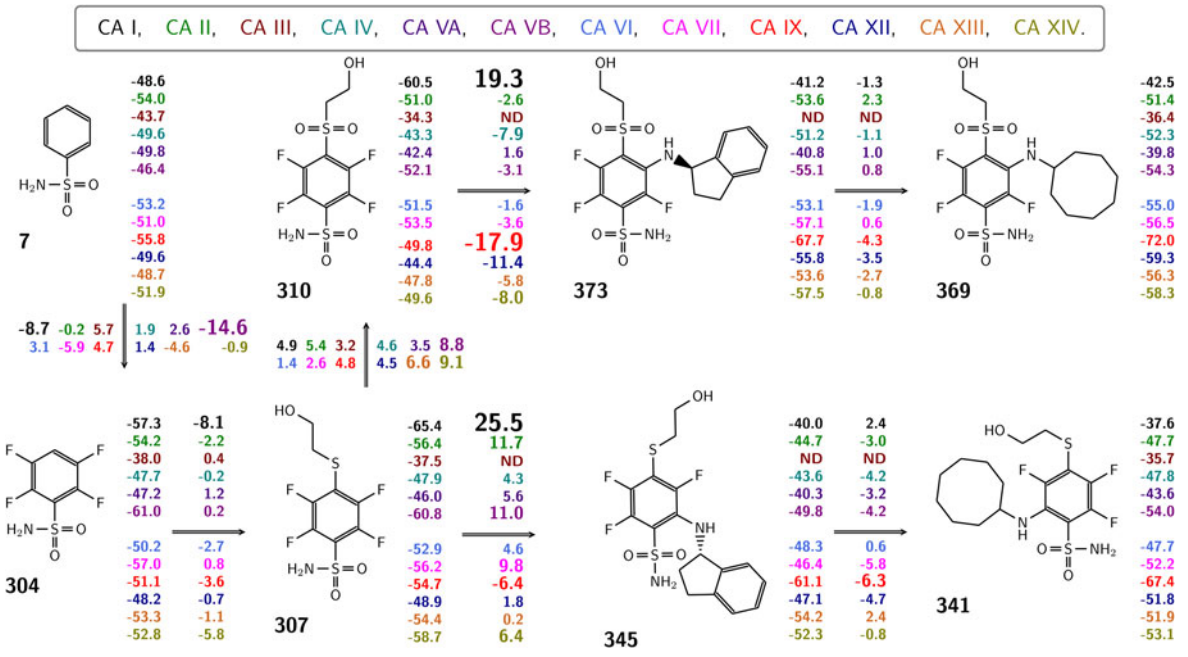

Fig. 28. Binding Gibbs energy contributions of compound functional groups in the search of fluorinated compounds that would selectively bind and inhibit CA IX. The map shows a series of compounds connected by arrows beginning with benzenesulfonamide as the weakest inhibitor and ending with the best inhibitors on the right. Numbers next to the structures show the intrinsic Gibbs energies of compound binding to each recombinant human CA isoform. Numbers at the arrows show the differences between the affinities to two connected isoforms. Larger differences are depicted in larger font size to emphasize the largest energy gains upon chemical modifications of the compounds.

CA II, the compound was found with the pyridinyl moiety directed to zinc and making contacts with Phe131 and Pro202.

Imidazole ring of L-histidine was involved in H-bonds with His64 (and other amino acids), and water molecules connected the activator to the Zn-bound water (Temperini *et al.*, 2005). The binding of the stereoisomer D-histidine also made a H-bond with His64, but otherwise, contacts were different. D-histidine in the crystal structure was also connected through water molecules with the Zn-bound water (Temperini *et al.*, 2006*d*).

The D- and L-tryptophans were investigated as activators of various human CA isoforms (Temperini *et al.*, 2008*c*). In the crystal structure of D-tryptophan in CA II, the activator was bound in an unusual way as compared with other structurally characterized activators. The amino acid was bound at the edge of the active site and contacted to a symmetry-related protein molecule. The binding of tryptophans was compared with the crystal structure of CA II with L-adrenaline (Temperini *et al.*, 2007*b*).

L- and D-phenylalanine, another pair of stereoisomers whose binding to CA II could be compared structurally. The position of both ligands differed. Both made H-bond to the His64 residue by carboxylate (D-phenylalanine) and by an amino group (L-phenylalanine) (Temperini *et al.*, 2006*c*).

Addition of the exogenous donor/acceptor of protons could rescue the proton transfer in H64A mutant of CA II (Duda *et al.*, 2001, 2003). In this case, 4-methylimidazole was used as an activator. The water network that could help understand the mechanism of rescue was visualized in the crystal structures. The same small molecule. 4-Methylimidazole was used for the rescue of another CA II double mutant H64W, W5A (Bhatt *et al.*, 2007). 4-Methylimidazole made a π-interaction with Trp64. A regular crystallographic study of catalytic activity rescue of CA II mutant H64A described the binding of four imidazole derivatives (Aggarwal *et al.*, 2014). Imidazoles were found in multiple binding sites.

In search for correlations between the X-ray crystallographic structures of inhibitor-CA complexes and the intrinsic thermodynamic parameters of their interaction

Crystallographic studies of CA inhibitors that was reviewed in the preceding sections provided the structural modes of various compounds binding in the active site of CA. However, crystallographic investigations can provide only the structural information and do not provide the energetic picture of binders. Weakly binding and weakly inhibiting millimolar compounds that do not have potential to be developed as drugs would be indistinguishable in the crystallographic structures from nanomolar or picomolar compounds that have potential to be developed as drugs. In the process of crystal growth in the presence of a binding compound or crystal soaking with an inhibitor, the concentration of the compound used in the experiment usually is in the millimolar range. The electron density of the bound compounds can be clearly visible both for weak and tight binders.

Therefore, as discussed above, it is important to use biochemical and biophysical methods together and accurately determine the affinities of compounds. The primary sulfonamides stand-out among various inhibitors as ones that bind to CAs specifically and significantly stronger than other reviewed compounds. Therefore, in the search for the 3D (crystallographic complex) structure – energetics correlations, the primary sulfonamides is the focus, similarly to 2D (chemical structure) – energetics correlations described in previous sections. In this section, all CA crystal structures available in the PDB that have sulfonamide compounds bound and the intrinsic binding information is available, are

https://doi.org/10.1017/S0033583518000082

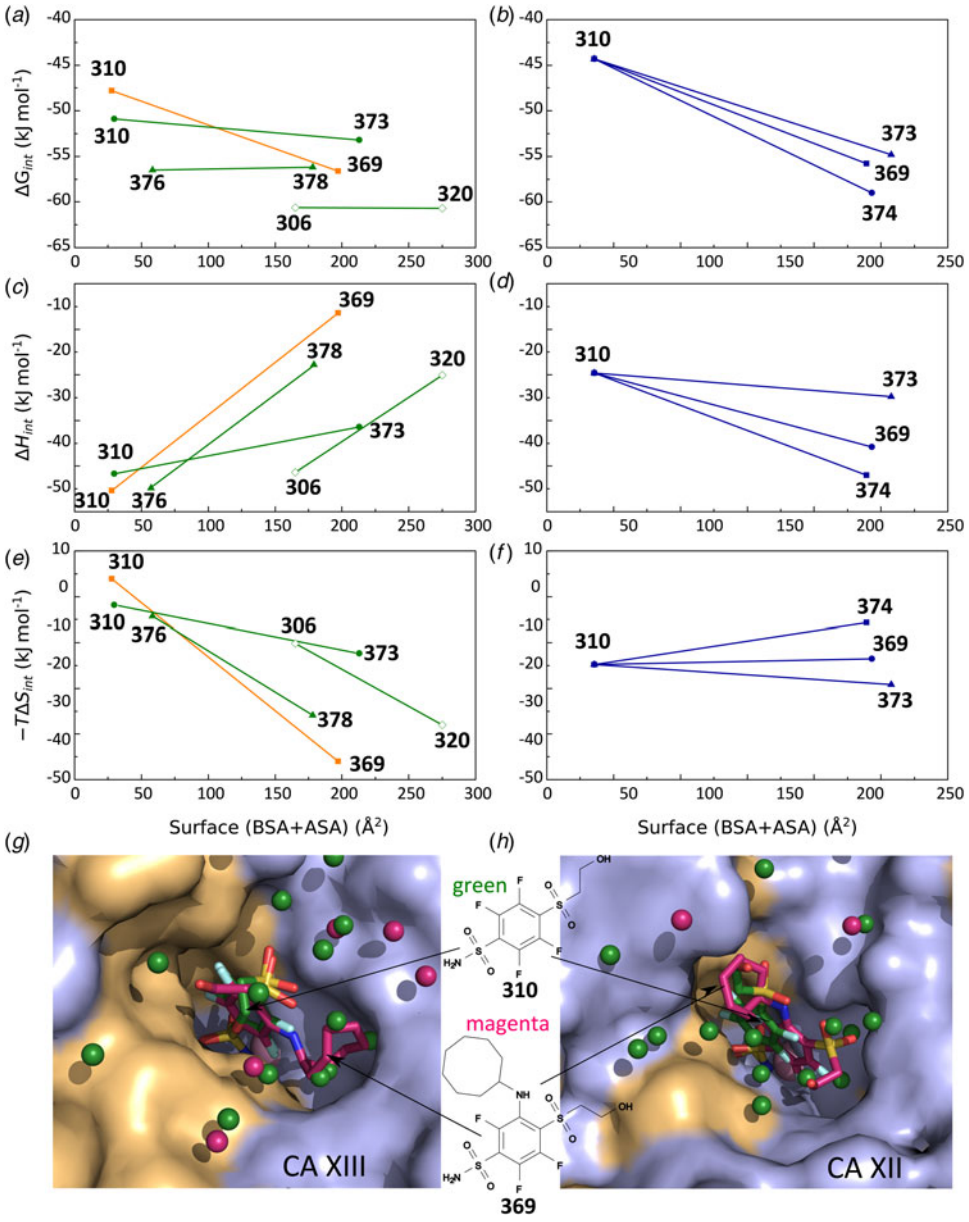

Fig. 29. Comparison of the binding thermodynamic parameters in structurally-related compound pairs arranged according to the buried and accessible surface areas (BSA + ASA) which were calculated from the crystal structures as described by Smirnov *et al.* (2018). Panels (*a*) and (*b*) show the Gibbs energies of binding, (*c*) and (*d*) the intrinsic enthalpies of binding, and (*e*) and (*f*) – the entropies multiplied by the absolute temperature. Panels on the left show the pairs that are called similar, meaning that the sulfonamide benzene ring is positioned identically in both crystal structures, while the panels on the right show dissimilar binders, where the position of the benzene ring is different in the pair. In the similar binders, there is a significant loss of exothermic enthalpy observed upon addition of a hydrophobic group on a compound. However, in dissimilar binders, the opposite tendency is observed – the enthalpy is gained upon the addition of a hydrophobic surface. The bottom two panels G and H show the crystallographic positions of the similar (G) and dissimilar (H) pairs of binders.

reviewed by listing the structures next to the intrinsic thermodynamic parameters of binding. Such correlations may describe the physical reasons behind the affinities and could lead to rational design of compounds with desired binding properties to any protein target, not limited to CA. The goal is to search for correlations that would be of general importance for any compound interaction with its target protein.

Figures 1–9 in supplementary figures file show the Pymol renderings of compounds bound to human CAs. The CA crystal structures from the PDB are shown next to the compound chemical structure together with the intrinsic binding data. Each figure arranges the structures of inhibitors bound to one CA isoform. The crystal structures are shown in the same orientation to visualize the entrance of the compound. Hydrophobic residue surface area is colored yellow, while the charged and polar amino acid surface is blue.

The crystal structure–thermodynamic parameter correlations show that the compounds span many orders of magnitude in affinity, from mM to pM, and small structural changes may lead to large changes in the binding energetics that are not fully understood. It seems that not only the positions of each atom at the protein–ligand interface are important, but probably also the water molecules that are being displaced by the bound ligand from the protein and ligand surface. All these contributions are not clear and therefore it is not yet possible to predict the affinities, enthalpies, and entropies from the structural arrangement of the ligand and vice versa – the structural arrangement from the thermodynamic parameters.

Quite a few observations and conclusions may be made based on a comparison of compounds with similar chemical structure. When a large collection of crystal structures confirms that all studied primary sulfonamide compounds bind to CAs via a coordination bond between the amino nitrogen and Zn^{II}, we can draw the structure–thermodynamics maps showing the functional group contributions to the binding energies and extend the maps to compounds whose crystal structures are not available.

https://doi.org/10.1017/S0033583518000082

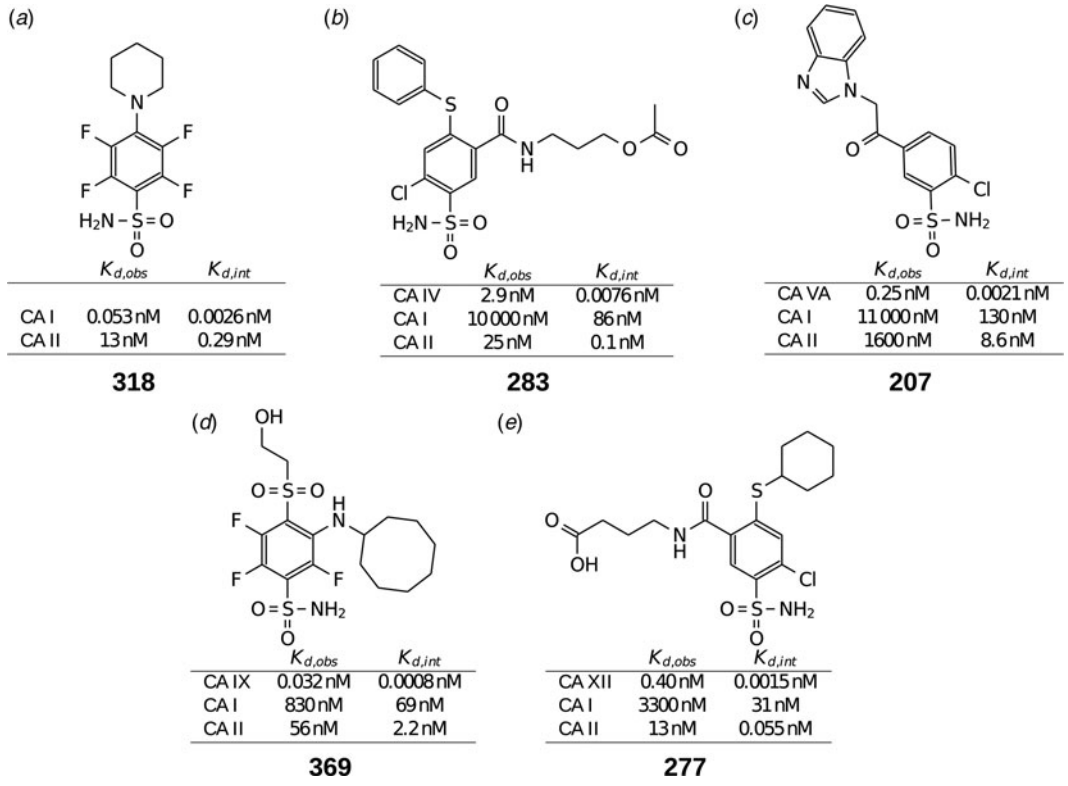

Fig. 30. Several compounds that exhibit high affinity towards one CA isoform and significant selectivity over CA I and CA II. The observed and intrinsic K_ds of the compounds to the most important CAs are shown below.

The sulfonamide groups will always be oriented towards the Zn^{II} in the active site and the remaining tail part of the compound would extend towards the entrance of the protein or bind to the surface areas nearby which may differ in each isoform, being hydrophobic or hydrophilic.

The development of compounds of VD series containing fluorine atoms in the benzenesulfonamide ring that led to the discovery of CA IX inhibitors of pM affinity and significant selectivity over other CA isoforms is shown in Fig. 28. This compound comparison map shows the intrinsic Gibbs energies of binding to each CA isoform and the differences in the energies between two adjacent compounds. The adjacent compounds in the map have small structural differences that lead to energetic changes of binding. It could be helpful to remember that the gain of -6 kJ mol^{-1} of Gibbs energy is equivalent to a 10-fold gain in K_d. Starting with benzenesulfonamide on the left upper corner of the map, it is clear that this compound exhibits strong affinity towards CA IX and is slightly selective over other isoforms. Addition of four fluorines did not improve the intrinsic binding (though improved the observed affinities). Further addition of *para* tail practically did not have an effect on affinity towards CA IX. The main gain in both the affinity and selectivity was achieved by an addition of *para* or *meta* bulky substituents that were designed to bind in the hydrophobic pocket on CA IX, based on the chimeric CA IX structure (Dudutienė *et al.*, 2014). Furthermore, the addition of these substituents significantly diminished the binding of these compounds to CA I, thus reducing an undesired side effect in a possible anticancer therapy targeting CA IX.

Development of another series, the chlorinated EA compounds towards CA XII is shown in Supplementary Fig. 11. At the end of this series is a compound that exhibits subnanomolar affinity and significant selectivity towards CA XII, another anticancer target. The logic of the development is the same – the search of functional groups that would selectively bind to the desired isoform but would not bind as strongly to non-desired isoforms.

The enthalpies of binding are still poorly understood, but they should provide information on the contacts between the ligand and protein. The larger negative exothermic enthalpy would indicate that the compound makes better contacts with the protein and the binding is more specific. Enthalpic development of high-affinity CA IX inhibitors of VD series is shown in Supplementary Fig. 12. The enthalpies of binding of the best compounds actually were not the most exothermic. However, the dissection of enthalpic and entropic contributions helped to provide the directions of compound design.

Correlations between the buried surface areas and the changes in enthalpies and entropies of binding of several compounds are shown in Fig. 29. The compounds were arranged in structurally similar pairs where there is an increase in the hydrophobic surface area when comparing them. In the case of *similar* binders, there was a tendency to observe a less exothermic enthalpy change and increased the entropy of binding. However, in the case of *dissimilar* binders, there was an opposite tendency observed. Significantly more data would be needed to ensure that such observations are of general use for the rational design of ligands that would bind the desired protein.

High-affinity and selective inhibitors of CA isoforms

One of the main practically-useful outcomes of this structure-activity correlation study of CAs is a series of

https://doi.org/10.1017/S0033583518000082

compounds that were designed and exhibited high affinity for one CA isoform and thousand-fold selectivity over most or all remaining human CA isoforms, especially CA I and CA II. The structures of five such compounds are shown in Fig. 30 together with the observed K_ds towards a particular CA isoform and compared with the affinities for CA I and CA II. Note that here we chose to list the observed affinities in addition to the intrinsic ones because for a pharmaceutical developer of lead structures it is important to know what is the potency/affinity of the compound under physiological conditions such as pH 7.0. The affinities of our best compounds towards CA I and CA IX reached from 10 to 100 pM, while for CA IV, CA VA, and CA XII – around 1nM. These compounds have a potential to be further developed as pharmaceuticals.

Conclusions

In this paper, we have reviewed and provided our opinion on the state-of-the-art in the design of small molecule inhibitors of human CAs. Among the techniques that are most often used and are of most importance in the experimental assessment of compound interaction with CAs and inhibition of their enzymatic activity are stopped-flow assay of the inhibition of CA enzymatic activity, isothermal titration calorimetry, fluorescent thermal shift assay, and SPR. Every one of these methods has advantages and disadvantages and it is advised to obtain data by several orthogonal techniques that complement each other and increase our knowledge in various aspects of interaction. For example, FTSA has the widest affinity range, SFA is the only method that directly determines the inhibition of enzymatic activity, ITC is the only method that directly determines the enthalpy of interaction, and SPR is the only technique from this list that determines the kinetic parameters of binding.

The interaction between the best-known inhibitors of CAs, primary sulfonamides, is hindered by the binding-linked reactions, such as deprotonation of the sulfonamide amino group or protonation of the CA-Zn(II)-bound hydroxide. It seems that in many cases a non-dominant form of the compound or protein is binding and, therefore, the binding is strongly influenced by buffer or pH. It is important to subtract all such binding-linked reactions in order to obtain the intrinsic thermodynamic and kinetic binding parameters. Such parameters are necessary to obtain correlations between compound chemical structures and binding efficiency. It is not fully correct to develop compound structures based only on the observed binding parameters.

The 85 X-ray crystallographic structures of 60 compounds bound to six CA isoforms together with a database of 400 primary sulfonamide compound binding to 12 recombinant human catalytically active CAs provided insight in the chemical structural features that strengthen compound binding and in some cases make the compounds more selective towards a particular CA isoform that is a potential drug target. The data should also be of use for computational modelers that build approaches to design novel compounds *in silico*. Compounds that reached pM to nM affinity towards CA I, CA IV, CA VA, CA IX, and CA XII and exhibited thousands of fold selectivity towards these isoforms were proposed as compounds suitable for further development as drugs targeting these isoforms.

Supplementary material. The supplementary material for this article can be found at https://doi.org/10.1017/S0033583518000082

Acknowledgements. This research was funded by a grant from the Research Council of Lithuania (S-MIP-17-87). The authors thank the local contacts at the EMBL beamlines Dr. G. Bourenkov and Dr. M. Cianci for the help with P13 and P14 EMBL beamline operations at PETRA III storage ring (DESY, Hamburg). Instant JChem was used for structure database management, search and prediction, Instant JChem 6.1.3, 2013, ChemAxon (http://www.chemaxon.com). Authors acknowledge Povilas Norvaišas for maintaining and supporting the Instant JChem database. The authors thank Audronė Rukšėnaitė, Vytautas Smirnovas, and Zita Liutkevičiūtė for performing HRMS experiments on part of the compounds and proteins.

References

Aaron JA, Chambers JM, Jude KM, Costanzo LD, Dmochowski IJ and Christianson DW (2008) Structure of a 129Xe-cryptophane biosensor complexed with human carbonic anhydrase II. *Journal of the American Chemical Society* **130**, 6942–6943.

Abbate F, Casini A, Owa T, Scozzafava A and Supuran CT (2004*a*) Carbonic anhydrase inhibitors: E7070, a sulfonamide anticancer agent, potently inhibits cytosolic isozymes I and II, and transmembrane, tumor-associated isozyme IX. *Bioorganic & Medicinal Chemistry Letters* **14**, 217–223.

Abbate F, Coetzee A, Casini A, Ciattini S, Scozzafava A and Supuran CT (2004*b*) Carbonic anhydrase inhibitors: X-ray crystallographic structure of the adduct of human isozyme II with the antipsychotic drug sulpiride. *Bioorganic & Medicinal Chemistry Letters* **14**, 337–341.

Abbate F, Winum JY, Potter BV, Casini A, Montero JL, Scozzafava A and Supuran CT (2004*c*) Carbonic anhydrase inhibitors: X-ray crystallographic structure of the adduct of human isozyme II with EMATE, a dual inhibitor of carbonic anhydrases and steroid sulfatase. *Bioorganic & Medicinal Chemistry Letters* **14**, 231–234.

Abellán-Flos M, Tanç M, Supuran CT and Vincent SP (2015) Multimeric xanthates as carbonic anhydrase inhibitors. *Journal of Enzyme Inhibition and Medicinal Chemistry* **31**, 1–7.

Aggarwal M, Kondeti B and McKenna R (2013) Anticonvulsant/antiepileptic carbonic anhydrase inhibitors: a patent review. *Expert Opinion on Therapeutic Patents* **23**, 717–724.

Aggarwal M, Kondeti B, Tu C, Maupin CM, Silverman DN and McKenna R (2014) Structural insight into activity enhancement and inhibition of H64A carbonic anhydrase II by imidazoles. *IUCrJ* **1**, 129–135.

Ahmad M, Helms V, Lengauer T and Kalinina OV (2015) Enthalpy–entropy compensation upon molecular conformational changes. *Journal of Chemical Theory and Computation* **11**, 1410–1418.

Ahmed A, Smith RD, Clark JJ, Dunbar JB and Carlson HA (2015) Recent improvements to binding MOAD: a resource for protein–ligand binding affinities and structures. *Nucleic Acids Research* **43**, D465–D469.

Alexander RS, Nair SK and Christianson DW (1991) Engineering the hydrophobic pocket of carbonic anhydrase II. *Biochemistry* **30**, 11064–11072.

Alexander RS, Kiefer LL, Fierke CA and Christianson DW (1993) Engineering the zinc binding site of human carbonic anhydrase II: structure of the His-94–Cys apoenzyme in a new crystalline form. *Biochemistry* **32**, 1510–1518.

Alp C, Maresca A, Alp NA, Gültekin MS, Ekinci D, Scozzafava A and Supuran CT (2013) Secondary/tertiary benzenesulfonamides with inhibitory action against the cytosolic human carbonic anhydrase isoforms I and II. *Journal of Enzyme Inhibition and Medicinal Chemistry* **28**, 294–298.

Alterio V, Vitale RM, Monti SM, Pedone C, Scozzafava A, Cecchi A, Simone GD and Supuran CT (2006) Carbonic anhydrase inhibitors: X-ray and molecular modeling study for the interaction of a fluorescent antitumor sulfonamide with isozyme II and IX. *Journal of the American Chemical Society* **128**, 8329–8335.

Alterio V, De Simone G, Monti SM, Scozzafava A and Supuran CT (2007) Carbonic anhydrase inhibitors: inhibition of human, bacterial, and archaeal isozymes with benzene-1,3-disulfonamides–solution and crystallographic studies. *Bioorganic & Medicinal Chemistry Letters* **17**, 4201–4207.

Alterio V, Hilvo M, Di Fiore A, Supuran CT, Pan P, Parkkila S, Scaloni A, Pastorek J, Pastorekova S, Pedone C, Scozzafava A, Monti SM and De Simone G (2009) Crystal structure of the catalytic domain of the tumor-

associated human carbonic anhydrase IX. *Proceedings of the National Academy of Sciences of the United States of America* **106**, 16233–16238.

Alterio V, Monti SM, Truppo E, Pedone C, Supuran CT and Simone GD (2010) The first example of a significant active site conformational rearrangement in a carbonic anhydrase-inhibitor adduct: the carbonic anhydrase I-topiramate complex. *Organic & Biomolecular Chemistry* **8**, 3528–3533.

Alterio V, Pan P, Parkkila S, Buonanno M, Supuran CT, Monti SM and De Simone G (2013) The structural comparison between membrane-associated human carbonic anhydrases provides insights into drug design of selective inhibitors. *Biopolymers* **101**, 769–778.

Alterio V, Tanc M, Ivanova J, Zalubovskis R, Vozny I, Monti SM, Fiore AD, Simone GD and Supuran CT (2015) X-ray crystallographic and kinetic investigations of 6-sulfamoyl-saccharin as a carbonic anhydrase inhibitor. *Organic & Biomolecular Chemistry* **13**, 4064–4069.

Anderson SR and Weber G (1969) Fluorescence polarization of the complexes of 1-anilino-8-naphthalenesulfonate with bovine serum albumin. Evidence for preferential orientation of the ligand. *Biochemistry* **8**, 371–377.

Avvaru BS, Busby SA, Chalmers MJ, Griffin PR, Venkatakrishnan B, Agbandje-McKenna M, Silverman DN and McKenna R (2009) Apo-human carbonic anhydrase II revisited: implications of the loss of a metal in protein structure, stability, and solvent network. *Biochemistry* **48**, 7365–7372.

Avvaru BS, Arenas DJ, Tu C, Tanner DB, McKenna R and Silverman DN (2010*a*) Comparison of solution and crystal properties of Co(II)-substituted human carbonic anhydrase II. *Archives of Biochemistry and Biophysics* **502**, 53–59.

Avvaru BS, Kim CU, Sippel KH, Gruner SM, Agbandje-McKenna M, Silverman DN and McKenna R (2010*b*) A short, strong hydrogen bond in the active site of human carbonic anhydrase II. *Biochemistry* **49**, 249–251.

Avvaru BS, Wagner JM, Maresca A, Scozzafava A, Robbins AH, Supuran CT and McKenna R (2010*c*) Carbonic anhydrase inhibitors. The X-ray crystal structure of human isoform II in adduct with an adamantyl analogue of acetazolamide resides in a less utilized binding pocket than most hydrophobic inhibitors. *Bioorganic & Medicinal Chemistry Letters* **20**, 4376–4381.

Baird Jr T, Waheed A, Okuyama T, Sly WS and Fierke CA (1997) Catalysis and inhibition of human carbonic anhydrase IV. *Biochemistry* **36**, 2669–2678.

Baranauskienė L and Matulis D (2012) Intrinsic thermodynamics of ethoxzolamide inhibitor binding to human carbonic anhydrase XIII. *BMC Biophysics* **5**, 12.

Baranauskienė L, Hilvo M, Matulienė J, Golovenko D, Manakova E, Dudutienė V, Michailovienė V, Torresan J, Jachno J, Parkkila S, Maresca A, Supuran CT, Gražulis S and Matulis D (2010) Inhibition and binding studies of carbonic anhydrase isozymes I, II and IX with benzimidazo[1,2-c][1,2,3]thiadiazole-7-sulphonamides. *Journal of Enzyme Inhibition and Medicinal Chemistry* **25**, 863–870.

Barbosa S, Taboada P and Mosquera V (2003) Protein–ligand interactions: volumetric and compressibility characterization of the binding of two anionic penicillins to human serum albumin. *Langmuir* **19**, 1446–1448.

Barrese AA, Genis C, Fisher SZ, Orwenyo JN, Kumara MT, Dutta SK, Phillips E, Kiddle JJ, Tu C, Silverman DN, Govindasamy L, Agbandje-McKenna M, McKenna R and Tripp BC (2008) Inhibition of carbonic anhydrase II by thioxolone: a mechanistic and structural study. *Biochemistry* **47**, 3174–3184.

Behnke CA, Le Trong I, Godden JW, Merritt EA, Teller DC, Bajorath J and Stenkamp RE (2010) Atomic resolution studies of carbonic anhydrase II. *Acta Crystallographica. Section D, Biological Crystallography* **66**, 616–627.

Bhatt D, Tu C, Fisher SZ, Prada JAH, McKenna R and Silverman DN (2005) Proton transfer in a Thr200His mutant of human carbonic anhydrase II. *Proteins* **61**, 239–245.

Bhatt D, Fisher SZ, Tu C, McKenna R and Silverman DN (2007) Location of binding sites in small molecule rescue of human carbonic anhydrase II. *Biophysical Journal* **92**, 562–570.

Biswas S, Aggarwal M, Güzel Ö, Scozzafava A, McKenna R and Supuran CT (2011) Conformational variability of different sulfonamide inhibitors with thienyl-acetamido moieties attributes to differential binding in the active site of cytosolic human carbonic anhydrase isoforms. *Bioorganic & Medicinal Chemistry* **19**, 3732–3738.

Biswas S, Carta F, Scozzafava A, McKenna R and Supuran CT (2013*a*) Structural effect of phenyl ring compared to thiadiazole based adamantylsulfonamides on carbonic anhydrase inhibition. *Bioorganic & Medicinal Chemistry* **21**, 2314–2318.

Biswas S, McKenna R and Supuran CT (2013*b*) Effect of incorporating a thiophene tail in the scaffold of acetazolamide on the inhibition of human carbonic anhydrase isoforms I, II, IX and XII. *Bioorganic & Medicinal Chemistry Letters* **23**, 5646–5649.

Block P (2006) AffinDB: a freely accessible database of affinities for protein–ligand complexes from the PDB. *Nucleic Acids Research* **34**, D522–D526.

Boone CD, Gill S, Tu C, Silverman DN and McKenna R (2013*a*) Structural, catalytic and stabilizing consequences of aromatic cluster variants in human carbonic anhydrase II. *Archives of Biochemistry and Biophysics* **539**, 31–37.

Boone CD, Habibzadegan A, Tu C, Silverman DN and McKenna R (2013*b*) Structural and catalytic characterization of a thermally stable and acid-stable variant of human carbonic anhydrase II containing an engineered disulfide bond. *Acta Crystallographica. Section D, Biological Crystallography* **69**, 1414–1422.

Boone CD, Chingkuang Tu C and McKenna R (2014) Structural elucidation of the hormonal inhibition mechanism of the bile acid cholate on human carbonic anhydrase II. *Acta Crystallographica. Section D, Biological Crystallography* **70**, 1758–1763.

Boone CD, Rasi V, Tu C and McKenna R (2015) Structural and catalytic effects of proline substitution and surface loop deletion in the extended active site of human carbonic anhydrase II. *FEBS Journal* **282**, 1445–1457.

Boriack PA, Christianson DW, Kingery-Wood J and Whitesides GM (1995) Secondary interactions significantly removed from the sulfonamide binding pocket of carbonic anhydrase II influence inhibitor binding constants. *Journal of Medicinal Chemistry* **38**, 2286–2291.

Boriack-Sjodin PA, Zeitlin S, Chen HH, Crenshaw L, Gross S, Dantanarayana A, Delgado P, May JA, Dean T and Christianson DW (1998) Structural analysis of inhibitor binding to human carbonic anhydrase II. *Protein Science* **7**, 2483–2489.

Bozdag M, Ferraroni M, Nuti E, Vullo D, Rossello A, Carta F, Scozzafava A and Supuran CT (2014*a*) Combining the tail and the ring approaches for obtaining potent and isoform-selective carbonic anhydrase inhibitors: solution and X-ray crystallographic studies. *Bioorganic & Medicinal Chemistry* **22**, 334–340.

Bozdag M, Pinard M, Carta F, Masini E, Scozzafava A, McKenna R and Supuran CT (2014*b*) A class of 4-sulfamoylphenyl – aminoalkyl ethers with effective carbonic anhydrase inhibitory action and antiglaucoma effects. *Journal of Medicinal Chemistry* **57**, 9673–9686.

Brandts JF and Lin LN (1990) Study of strong to ultratight protein interactions using differential scanning calorimetry. *Biochemistry* **29**, 6927–6940.

Briganti F, Mangani S, Orioli P, Scozzafava A, Vernaglione G and Supuran CT (1997) Carbonic anhydrase activators: X-ray crystallographic and spectroscopic investigations for the interaction of isozymes I and II with histamine. *Biochemistry* **36**, 10384–10392.

Briganti F, Mangani S, Scozzafava A, Vernaglione G and Supuran CT (1999) Carbonic anhydrase catalyzes cyanamide hydration to urea: is it mimicking the physiological reaction? *Journal of Biological Inorganic Chemistry* **4**, 528–536.

Brynda J, Mader P, Sicha V, Fabry M, Poncova K, Bakardiev M, Gruner B, Cigler P and Rezacova P (2013) Carborane-based carbonic anhydrase inhibitors. *Angewandte Chemie (International ed. in English)* **52**, 13760–13763.

Budayova-Spano M, Fisher SZ, Dauvergne MT, Agbandje-McKenna M, Silverman DN, Myles DAA and McKenna R (2006) Production and X-ray crystallographic analysis of fully deuterated human carbonic anhydrase II. *Acta Crystallographica, Section F: Structural Biology and Crystallization Communications* **62**, 6–9.

Buemi MR, De Luca L, Ferro S, Bruno E, Ceruso M, Supuran CT, Pospíšilová K, Brynda J, Řezáčová P and Gitto R (2015) Carbonic anhydrase inhibitors: design, synthesis and structural characterization of new heteroaryl-*N*-carbonylbenzenesulfonamides targeting druggable human carbonic anhydrase isoforms. *European Journal of Medicinal Chemistry* **102**, 223–232.

https://doi.org/10.1017/S0033583518000082

Buratto J, Colombo C, Stupfel M, Dawson SJ, Dolain C, d'Estaintot BL, Fischer L, Granier T, Laguerre M, Gallois B and Huc I (2014) Structure of a complex formed by a protein and a helical aromatic oligoamide foldamer at 2.1 Å resolution. *Angewandte Chemie (International ed. in English)* **53**, 883–887.

Callies O and Daranas AH (2016) Application of isothermal titration calorimetry as a tool to study natural product interactions. *Natural Product Reports* **33**, 881–904.

Can D, Spingler B, Schmutz P, Mendes F, Raposinho P, Fernandes C, Carta F, Innocenti A, Santos I, Supuran CT and Alberto R (2012) $[(Cp\text{-}R)M(CO)_3]$ (M = Re or 99mTc) arylsulfonamide, arylsulfamide, and arylsulfamate conjugates for selective targeting of human carbonic anhydrase IX. *Angewandte Chemie (International ed. in English)* **51**, 3354–3357.

Čapkauskaitė E, Baranauskienė L, Golovenko D, Manakova E, Gražulis S, Tumkevičius S and Matulis D (2010) Indapamide-like benzenesulfonamides as inhibitors of carbonic anhydrases I, II, VII, and XIII. *Bioorganic & Medicinal Chemistry* **18**, 7357–7364.

Čapkauskaitė E, Zubrienė A, Baranauskienė L, Tamulaitienė G, Manakova E, Kairys V, Gražulis S, Tumkevičius S and Matulis D (2012) Design of [(2-pyrimidinylthio)acetyl]benzenesulfonamides as inhibitors of human carbonic anhydrases. *European Journal of Medicinal Chemistry* **51**, 259–270.

Čapkauskaitė E, Zubrienė A, Smirnov A, Torresan J, Kišonaitė M, Kazokaitė J, Gylytė J, Michailovienė V, Jogaitė V, Manakova E, Gražulis S, Tumkevičius S and Matulis D (2013) Benzenesulfonamides with pyrimidine moiety as inhibitors of human carbonic anhydrases I, II, VI, VII, XII, and XIII. *Bioorganic & Medicinal Chemistry* **21**, 6937–6947.

Čapkauskaitė E, Linkuvienė V, Smirnov A, Milinavičiūtė G, Timm DD, Kasiliauskaitė A, Manakova E, Gražulis S and Matulis D (2017) Combinatorial design of isoform-selective *N*-alkylated benzimidazole-based inhibitors of carbonic anhydrases. *ChemistrySelect* **2**, 5360–5371.

Carey FG, Knowles F and Gibson QH (1977) Effect of hydrostatic pressure on ligand binding to hemoglobin. *Journal of Biological Chemistry* **252**, 4102–4107.

Carta F, Temperini C, Innocenti A, Scozzafava A, Kaila K and Supuran CT (2010) Polyamines inhibit carbonic anhydrases by anchoring to the zinc-coordinated water molecule. *Journal of Medicinal Chemistry* **53**, 5511–5522.

Carta F, Garaj V, Maresca A, Wagner J, Avvaru BS, Robbins AH, Scozzafava A, McKenna R and Supuran CT (2011) Sulfonamides incorporating 1,3,5-triazine moieties selectively and potently inhibit carbonic anhydrase transmembrane isoforms IX, XII and XIV over cytosolic isoforms I and II: solution and X-ray crystallographic studies. *Bioorganic & Medicinal Chemistry* **19**, 3105–3119.

Carta F, Aggarwal M, Maresca A, Scozzafava A, McKenna R and Supuran CT (2012*a*) Dithiocarbamates: a new class of carbonic anhydrase inhibitors. Crystallographic and kinetic investigations. *Chemical Communications (Cambridge, U. K.)* **48**, 1868–1870.

Carta F, Aggarwal M, Maresca A, Scozzafava A, McKenna R, Masini E and Supuran CT (2012*b*) Dithiocarbamates strongly inhibit carbonic anhydrases and show antiglaucoma action *in vivo*. *Journal of Medicinal Chemistry* **55**, 1721–1730.

Carta F, Akdemir A, Scozzafava A, Masini E and Supuran CT (2013) Xanthates and trithiocarbonates strongly inhibit carbonic anhydrases and show antiglaucoma effects *in vivo*. *Journal of Medicinal Chemistry* **56**, 4691–4700.

Carta F, Supuran CT and Scozzafava A (2014) Sulfonamides and their isosters as carbonic anhydrase inhibitors. *Future Medicinal Chemistry* **6**, 1149–1165.

Carta F, Di Cesare Mannelli L, Pinard M, Ghelardini C, Scozzafava A, McKenna R and Supuran CT (2015) A class of sulfonamide carbonic anhydrase inhibitors with neuropathic pain modulating effects. *Bioorganic & Medicinal Chemistry* **23**, 1828–1840.

Casini A, Temperini C, Gabbiani C, Supuran CT and Messori L (2010) The X-ray structure of the adduct between NAMI-A and carbonic anhydrase provides insights into the reactivity of this metallodrug with proteins. *ChemMedChem* **5**, 1989–1994.

Chaires JB (2008) Calorimetry and thermodynamics in drug design. *Annual Review of Biophysics* **37**, 135–151.

Chakravarty S and Kannan KK (1994) Drug-protein interactions. Refined structures of three sulfonamide drug complexes of human carbonic anhydrase I enzyme. *Journal of Molecular Biology* **243**, 298–309.

Chalikian TV and Filfil R (2003) How large are the volume changes accompanying protein transitions and binding? *Biophysical Chemistry* **104**, 489–499.

Chazalette C, Riviere-Baudet M, Scozzafava A, Abbate F, Ben Maarouf Z and Supuran CT (2001) Carbonic anhydrase inhibitors, interaction of boron derivatives with isozymes I and II: a new binding site for hydrophobic inhibitors at the entrance of the active site as shown by docking studies. *Journal of Enzyme Inhibition* **16**, 125–133.

Chegwidden WR, Carter ND and Edwards YH (eds) (2000) *The Carbonic Anhydrases*. Basel: Birkhäuser Basel.

Chodera JD and Mobley DL (2013) Entropy–enthalpy compensation: role and ramifications in biomolecular ligand recognition and design. *Annual Review of Biophysics* **42**, 121–142.

Ciani L, Cecchi A, Temperini C, Supuran CT and Ristori S (2009) Dissecting the inhibition mechanism of cytosolic versus transmembrane carbonic anhydrases by ESR. *Journal of Physical Chemistry B* **113**, 13998–14005.

Cimmperman P and Matulis D (2011) Protein thermal denaturation measurements via a fluorescent dye. *RSC Biomolecular Sciences* **22**, 247–274.

Cimmperman P, Baranauskienė L, Jachimovičiūtė S, Jachno J, Torresan J, Michailovienė V, Matulienė J, Sereikaitė J, Bumelis V and Matulis D (2008) A quantitative model of thermal stabilization and destabilization of proteins by ligands. *Biophysical Journal* **95**, 3222–3231.

Coleman JE (1967) Mechanism of action of carbonic anhydrase substrate, sulfonamide, and anion binding. *Journal of Biological Chemistry* **242**, 5212–5219.

Copeland RA (2005) *Evaluation of Enzyme Inhibitors in Drug Discovery: A Guide for Medicinal Chemists and Pharmacologists*. Hoboken, N.J.: Wiley-Interscience.

Cox JD, Hunt JA, Compher KM, Fierke CA and Christianson DW (2000) Structural influence of hydrophobic core residues on metal binding and specificity in carbonic anhydrase II. *Biochemistry* **39**, 13687–13694.

Cozier GE, Leese MP, Lloyd MD, Baker MD, Thiyagarajan N, Acharya KR and Potter BVL (2010) Structures of human carbonic anhydrase II/inhibitor complexes reveal a second binding site for steroidal and nonsteroidal inhibitors. *Biochemistry* **49**, 3464–3476.

Crocetti L, Maresca A, Temperini C, Hall RA, Scozzafava A, Muhlschlegel FA and Supuran CT (2009) A thiabendazole sulfonamide shows potent inhibitory activity against mammalian and nematode alpha-carbonic anhydrases. *Bioorganic & Medicinal Chemistry Letters* **19**, 1371–1375.

D'Ambrosio K, Vitale RM, Dogné JM, Masereel B, Innocenti A, Scozzafava FA, De Simone G and Supuran CT (2008*a*) Carbonic anhydrase inhibitors: bioreductive nitro-containing sulfonamides with selectivity for targeting the tumor associated isoforms IX and XII. *Journal of Medicinal Chemistry* **51**, 3230–3237.

D'Ambrosio K, Masereel B, Thiry A, Scozzafava A, Supuran CT and De Simone G (2008*b*) Carbonic anhydrase inhibitors: binding of indanesulfonamides to the human isoform II. *ChemMedChem* **3**, 473–477.

D'Ambrosio K, Smaine F-Z, Carta F, De Simone G, Winum J-Y and Supuran CT (2012) Development of potent carbonic anhydrase inhibitors incorporating both sulfonamide and sulfamide groups. *Journal of Medicinal Chemistry* **55**, 6776–6783.

D'Ambrosio K, Carradori S, Monti SM, Buonanno M, Secci D, Vullo D, Supuran CT and De Simone G (2015) Out of the active site binding pocket for carbonic anhydrase inhibitors. *Chemical Communications*. **51**, 302–305.

D'Ascenzio M, Carradori S, De Monte C, Secci D, Ceruso M and Supuran CT (2014) Design, synthesis and evaluation of *N*-substituted saccharin derivatives as selective inhibitors of tumor-associated carbonic anhydrase XII. *Bioorganic & Medicinal Chemistry* **22**, 1821–1831.

Dave K, Ilies MA, Scozzafava A, Temperini C, Vullo D and Supuran CT (2011) An inhibitor-like binding mode of a carbonic anhydrase activator within the active site of isoform II. *Bioorganic & Medicinal Chemistry Letters* **21**, 2764–2768.

https://doi.org/10.1017/S0033583518000082

Davenport HW (1984) The early days of research on carbonic anhydrase. *Annals of the New York Academy of Sciences* **429**, 4–9.

Davis RA, Hofmann A, Osman A, Hall RA, Mühlschlegel FA, Vullo D, Innocenti A, Supuran CT and Poulsen S-A (2011) Natural product-based phenols as novel probes for mycobacterial and fungal carbonic anhydrases. *Journal of Medicinal Chemistry* **54**, 1682–1692.

Davis RA, Vullo D, Supuran CT and Poulsen S-A (2014) Natural product polyamines that inhibit human carbonic anhydrases. *BioMed Research International* **2014**, 374079.

De Simone G, Vitale RM, Di Fiore A, Pedone C, Scozzafava A, Montero J-L, Winum J-Y and Supuran CT (2006) Carbonic anhydrase inhibitors: hypoxia-activatable sulfonamides incorporating disulfide bonds that target the tumor-associated isoform IX. *Journal of Medicinal Chemistry* **49**, 5544–5551.

De Simone G, Alterio V and Supuran CT (2013) Exploiting the hydrophobic and hydrophilic binding sites for designing carbonic anhydrase inhibitors. *Expert Opinion on Drug Discovery* **8**, 793–810.

De Simone G, Pizika G, Monti SM, Di Fiore A, Ivanova J, Vozny I, Trapencieris P, Zalubovskis R, Supuran CT and Alterio V (2014) Hydrophobic substituents of the phenylmethylsulfamide moiety can be used for the development of new selective carbonic anhydrase inhibitors. *Biomed Research International* **2014**, 523210.

Diaz-Torres NA, Mahon BP, Boone CD, Pinard MA, Tu C, Ng R, Agbandje-McKenna M, Silverman D, Scott K and McKenna R (2015) Structural and biophysical characterization of the -carbonic anhydrase from the gammaproteobacterium Thiomicrospira Crunogena Xcl-2: insights into engineering thermostable enzymes for Co2 sequestration. *Acta Crystallographica. Section D, Biological Crystallography* **71**, 1745–1756.

Di Fiore A, Pedone C, Antel J, Waldeck H, Witte A, Wurl M, Scozzafava A, Supuran CT and De Simone G (2008) Carbonic anhydrase inhibitors: the X-ray crystal structure of ethoxzolamide complexed to human isoform II reveals the importance of thr200 and gln92 for obtaining tight-binding inhibitors. *Bioorganic & Medicinal Chemistry Letters* **18**, 2669–2674.

Di Fiore A, Maresca A, Supuran CT and De Simone G (2012) Hydroxamate represents a versatile zinc binding group for the development of new carbonic anhydrase inhibitors. *Chemical Communications (Cambridge, U. K.)* **48**, 8838–8840.

Dodgson SJ, Tashian RE, Gros G and Carter ND (eds) (1991) *The Carbonic Anhydrases*. Springer US, Boston, MA, pp. 1–379.

Domsic JF, Avvaru BS, Kim CU, Gruner SM, Agbandje-McKenna M, Silverman DN and McKenna R (2008) Entrapment of carbon dioxide in the active site of carbonic anhydrase II. *Journal of Biological Chemistry* **283**, 30766–30771.

Domsic JF, Williams W, Fisher SZ, Tu C, Agbandje-McKenna M, Silverman DN and McKenna R (2010) Structural and kinetic study of the extended active site for proton transfer in human carbonic anhydrase II. *Biochemistry* **49**, 6394–6399.

Dragan AI, Read CM and Crane-Robinson C (2017) Enthalpy–entropy compensation: the role of solvation. *European Biophysics Journal with Biophysics Letters* **46**, 301–308.

Duda D, Tu C, Qian M, Laipis P, Agbandje-McKenna M, Silverman DN and McKenna R (2001) Structural and kinetic analysis of the chemical rescue of the proton transfer function of carbonic anhydrase II. *Biochemistry* **40**, 1741–1748.

Duda D, Govindasamy L, Agbandje-McKenna M, Tu C, Silverman DN and McKenna R (2003) The refined atomic structure of carbonic anhydrase II at 1.05 A resolution: implications of chemical rescue of proton transfer. *Acta Crystallographica. Section D, Biological Crystallography* **59**, 93–104.

Duda DM, Yoshioka C, Govindasamy L, An H, Tu C, Silverman DN and McKenna R (2002) Crystallization and preliminary X-ray analysis of human carbonic anhydrase III. *Acta Crystallographica. Section D, Biological Crystallography* **58**, 849–852.

Duda DM, Tu C, Fisher SZ, An H, Yoshioka C, Govindasamy L, Laipis PJ, Agbandje-McKenna M, Silverman DN and McKenna R (2005) Human carbonic anhydrase III: structural and kinetic study of catalysis and proton transfer. *Biochemistry* **44**, 10046–10053.

Dudutiene V, Baranauskiene L and Matulis D (2007) Benzimidazo[1,2-c][1,2,3]thiadiazole-7-sulfonamides as inhibitors of carbonic anhydrase. *Bioorganic & Medicinal Chemistry Letters* **17**, 3335–3338.

Dudutienė V, Zubrienė A, Smirnov A, Gylytė J, Timm D, Manakova E, Gražulis S and Matulis D (2013) 4-Substituted-2,3,5,6-tetrafluorobenzenesulfonamides as inhibitors of carbonic anhydrases I, II, VII, XII, and XIII. *Bioorganic & Medicinal Chemistry* **21**, 2093–2106.

Dudutienė V, Matulienė J, Smirnov A, Timm DD, Zubrienė A, Baranauskienė L, Morkūnaite V, Smirnovienė J, Michailovienė V, Juozapaitienė V, Mickevičiūtė A, Kazokaitė J, Bakšytė S, Kasiliauskaitė A, Jachno J, *et al.* (2014) Discovery and characterization of novel selective inhibitors of carbonic anhydrase IX. *Journal of Medicinal Chemistry* **57**, 9435–9446.

Dudutienė V, Zubrienė A, Smirnov A, Timm DD, Smirnovienė J, Kazokaitė J, Michailovienė V, Zakšauskas A, Manakova E, Gražulis S and Matulis D (2015) Functionalization of fluorinated benzenesulfonamides and their inhibitory properties toward carbonic anhydrases. *ChemMedChem* **10**, 662–687.

Earnhardt JN, Qian M, Tu C, Lakkis MM, Bergenhem NCH, Laipis PJ, Tashian RE and Silverman DN (1998) The catalytic properties of murine carbonic anhydrase VII. *Biochemistry* **37**, 10837–10845.

Elbaum D, Nair S, Patchan M, Thompson R and Christianson D (1996) Structure-based design of a sulfonamide probe for fluorescence anisotropy detection of zinc with a carbonic anhydrase-based biosensor. *Journal of the American Chemical Society* **118**, 8381–8387.

Elder I, Fisher Z, Laipis PJ, Tu C, McKenna R and Silverman DN (2007) Structural and kinetic analysis of proton shuttle residues in the active site of human carbonic anhydrase III. *Proteins* **68**, 337–343.

Engberg P and Lindskog S (1984) Effects of pH and inhibitors on the absorption spectrum of cobalt(II)-substituted carbonic anhydrase III from bovine skeletal muscle. *FEBS Letters* **170**, 326–330.

Engstrand C, Jonsson B-H and Lindskog S (1995) Catalytic and inhibitor-binding properties of some active-site mutants of human carbonic anhydrase I. *European Journal of Biochemistry* **229**, 696–702.

Eriksson AE and Liljas A (1993) Refined structure of bovine carbonic anhydrase III at 2.0 A resolution. *Proteins* **16**, 29–42.

Eriksson AE, Jones TA and Liljas A (1988*a*) Refined structure of human carbonic anhydrase II at 2.0 A resolution. *Proteins* **4**, 274–282.

Eriksson AE, Kylsten PM, Jones TA and Liljas A (1988*b*) Crystallographic studies of inhibitor binding sites in human carbonic anhydrase II: a pentacoordinated binding of the SCN- ion to the zinc at high pH. *Proteins* **4**, 283–293.

Falconer RJ (2016) Applications of isothermal titration calorimetry – the research and technical developments from 2011 to 2015: review of isothermal titration calorimetry from 2011 to 2015. *Journal of Molecular Recognition* **29**, 504–515.

Ferraroni M, Tilli S, Briganti F, Chegwidden WR, Supuran CT, Wiebauer KE, Tashian RE and Scozzafava A (2002) Crystal structure of a zinc-activated variant of human carbonic anhydrase I, CA I Michigan 1: evidence for a second zinc binding site involving arginine coordination. *Biochemistry* **41**, 6237–6244.

Ferraroni M, Carta F, Scozzafava A and Supuran CT (2016) Thioxocoumarins show an alternative carbonic anhydrase inhibition mechanism compared to coumarins. *Journal of Medicinal Chemistry* **59**, 462–473.

Fiore AD, Pedone C, D'Ambrosio K, Scozzafava A, Simone GD and Supuran CT (2006) Carbonic anhydrase inhibitors: valdecoxib binds to a different active site region of the human isoform II as compared to the structurally related cyclooxygenase II 'selective' inhibitor celecoxib. *Bioorganic & Medicinal Chemistry Letters* **16**, 437–442.

Fiore AD, Scozzafava A, Winum J-Y, Montero J-L, Pedone C, Supuran CT and Simone GD (2007) Carbonic anhydrase inhibitors: binding of an antiglaucoma glycosyl-sulfanilamide derivative to human isoform II and its consequences for the drug design of enzyme inhibitors incorporating sugar moieties. *Bioorganic & Medicinal Chemistry Letters* **17**, 1726–1731.

Fiore AD, Monti SM, Hilvo M, Parkkila S, Romano V, Scaloni A, Pedone C, Scozzafava A, Supuran CT and Simone GD (2009) Crystal structure of human carbonic anhydrase XIII and its complex with the inhibitor acetazolamide. *Proteins* **74**, 164–175.

Fiore AD, Truppo E, Supuran CT, Alterio V, Dathan N, Bootorabi F, Parkkila S, Monti SM and De Simone G (2010*a*) Crystal structure of

https://doi.org/10.1017/S0033583518000082

the C183S/C217S mutant of human CA VII in complex with acetazolamide. *Bioorganic & Medicinal Chemistry Letters* **20**, 5023–5026.

Fiore AD, Monti SM, Innocenti A, Winum J-Y, Simone GD and Supuran CT (2010*b*) Carbonic anhydrase inhibitors: crystallographic and solution binding studies for the interaction of a boron-containing aromatic sulfamide with mammalian isoforms I-XV. *Bioorganic & Medicinal Chemistry Letters* **20**, 3601–3605.

Fiore AD, Maresca A, Alterio V, Supuran CT and Simone GD (2011) Carbonic anhydrase inhibitors: X-ray crystallographic studies for the binding of *N*-substituted benzenesulfonamides to human isoform II. *Chemical Communications (Cambridge, U. K.)* **47**, 11636–11638.

Fiore AD, Capasso C, Luca VD, Monti SM, Carginale V, Supuran CT, Scozzafava A, Pedone C, Rossi M and Simone GD (2013) X-ray structure of the first 'extremo – carbonic anhydrase', a dimeric enzyme from the thermophilic bacterium Sulfurihydrogenibium yellowstonense YO3AOP1. *Acta Crystallographica. Section D, Biological Crystallography* **69**, 1150–1159.

Fisher SZ, Govindasamy L, Boyle N, Agbandje-McKenna M, Silverman DN, Blackburn GM and McKenna R (2006) X-ray crystallographic studies reveal that the incorporation of spacer groups in carbonic anhydrase inhibitors causes alternate binding modes. *Acta Crystallographica, Section F: Structural Biology and Crystallization Communications* **62**, 618–622.

Fisher SZ, Maupin CM, Budayova-Spano M, Govindasamy L, Tu C, Agbandje-McKenna M, Silverman DN, Voth GA and McKenna R (2007*a*) Atomic crystal and molecular dynamics simulation structures of human carbonic anhydrase II: insights into the proton transfer mechanism. *Biochemistry* **46**, 2930–2937.

Fisher SZ, Tu C, Bhatt D, Govindasamy L, Agbandje-McKenna M, McKenna R and Silverman DN (2007*b*) Speeding up proton transfer in a fast enzyme: kinetic and crystallographic studies on the effect of hydrophobic amino acid substitutions in the active site of human carbonic anhydrase II. *Biochemistry* **46**, 3803–3813.

Fisher SZ, Kovalevsky AY, Domsic JF, Mustyakimov M, McKenna R, Silverman DN and Langan PA (2010) Neutron structure of human carbonic anhydrase II: implications for proton transfer. *Biochemistry* **49**, 415–421.

Fisher SZ, Aggarwal M, Kovalevsky AY, Silverman DN and McKenna R (2012*a*) Neutron diffraction of acetazolamide-bound human carbonic anhydrase II reveals atomic details of drug binding. *Journal of the American Chemical Society* **134**, 14726–14729.

Fisher Z, Prada JAH, Tu C, Duda D, Yoshioka C, An H, Govindasamy L, Silverman DN and McKenna R (2005) Structural and kinetic characterization of active-site histidine as a proton shuttle in catalysis by human carbonic anhydrase II. *Biochemistry* **44**, 1097–1105.

Fisher Z, Kovalevsky AY, Mustyakimov M, Silverman DN, McKenna R and Langan P (2011) Neutron structure of human carbonic anhydrase II: a hydrogen-bonded water network 'switch' is observed between pH 7.8 and 10.0. *Biochemistry* **50**, 9421–9423.

Fisher Z, Boone CD, Biswas SM, Venkatakrishnan B, Aggarwal M, Tu C, Agbandje-McKenna M, Silverman D and McKenna R (2012*b*) Kinetic and structural characterization of thermostabilized mutants of human carbonic anhydrase II. *Protein Engineering, Design & Selection* **25**, 347–355.

Forster RE (2000) Remarks on the discovery of carbonic anhydrase. In Chegwidden WR, Carter ND and Edwards YH (eds), *The Carbonic Anhydrases*. Birkhäuser, Basel: EXS **90**, pp. 1–11.

Fox JM, Kang K, Sherman W, Héroux A, Sastry M, Baghbanzadeh M, Lockett MR and Whitesides GM (2015) Interactions between Hofmeister anions and the binding pocket of a protein. *Journal of the American Chemical Society* **137**, 3859–3866.

Frost SC and McKenna R (eds) (2014) *Carbonic Anhydrase: Mechanism, Regulation, Links to Disease, and Industrial Applications*. Dordrecht: Springer Netherlands.

Genis C, Sippel KH, Case N, Cao W, Avvaru BS, Tartaglia LJ, Govindasamy L, Tu C, Agbandje-McKenna M, Silverman DN, Rosser CJ and McKenna R (2009) Design of a carbonic anhydrase IX active-site mimic to screen inhibitors for possible anticancer properties. *Biochemistry* **48**, 1322–1331.

Geschwindner S, Ulander J and Johansson P (2015) Ligand binding thermodynamics in drug discovery: still a hot tip? *Journal of Medicinal Chemistry* **58**, 6321–6335.

Gilson MK, Liu T, Baitaluk M, Nicola G, Hwang L and Chong J (2016) BindingDB in 2015: a public database for medicinal chemistry, computational chemistry and systems pharmacology. *Nucleic Acids Research* **44**, D1045–D1053.

Gitto R, Agnello S, Ferro S, De Luca L, Vullo D, Brynda J, Mader P, Supuran CT and Chimirri A (2010) Identification of 3,4-dihydroisoquinoline-2(1*H*)-sulfonamides as potent carbonic anhydrase inhibitors: synthesis, biological evaluation, and enzyme–ligand X-ray studies. *Journal of Medicinal Chemistry* **53**, 2401–2408.

Gitto R, Damiano FM, Mader P, De Luca L, Ferro S, Supuran CT, Vullo D, Brynda J, Rezacova P and Chimirri A (2012) Synthesis, structure-activity relationship studies, and X-ray crystallographic analysis of arylsulfonamides as potent carbonic anhydrase inhibitors. *Journal of Medicinal Chemistry* **55**, 3891–3899.

Goldberg RN, Kishore N and Lennen RM (2002) Thermodynamic quantities for the ionization reactions of buffers. *Journal of Physical and Chemical Reference Data* **31**, 231–370.

Grüneberg S, Stubbs MT and Klebe G (2002) Successful virtual screening for novel inhibitors of human carbonic anhydrase: strategy and experimental confirmation. *Journal of Medicinal Chemistry* **45**, 3588–3602.

Grzybowski BA, Ishchenko AV, Kim C-Y, Topalov G, Chapman R, Christianson DW, Whitesides GM and Shakhnovich EI (2002) Combinatorial computational method gives new picomolar ligands for a known enzyme. *Proceedings of the National Academy of Sciences of the United States of America* **99**, 1270–1273.

Guerri A, Briganti F, Scozzafava A, Supuran CT and Mangani S (2000) Mechanism of cyanamide hydration catalyzed by carbonic anhydrase II suggested by cryogenic X-ray diffraction. *Biochemistry* **39**, 12391–12397.

Güzel Ö, Temperini C, Innocenti A, Scozzafava A, Salman A and Supuran CT (2008) Carbonic anhydrase inhibitors. Interaction of 2-(hydrazinocarbonyl)-3-phenyl-1*H*-indole-5-sulfonamide with 12 mammalian isoforms: kinetic and X-ray crystallographic studies. *Bioorganic & Medicinal Chemistry Letters* **18**, 152–158.

Güzel-Akdemir Ö, Biswas S, Lastra K, McKenna R and Supuran CT (2013) Structural study of the location of the phenyl tail of benzene sulfonamides and the effect on human carbonic anhydrase inhibition. *Bioorganic & Medicinal Chemistry* **21**, 6674–6680.

Haakansson K and Liljas A (1994) The structure of a complex between carbonic anhydrase II and a new inhibitor, trifluoromethane sulphonamide. *FEBS Letters* **350**, 319–322.

Haakansson K and Wehnert A (1992) Structure of cobalt carbonic anhydrase complexed with bicarbonate. *Journal of Molecular Biology* **228**, 1212–1218.

Haakansson K, Carlsson M, Svensson LA and Liljas A (1992) Structure of native and apo carbonic anhydrase II and structure of some of its anion-ligand complexes. *Journal of Molecular Biology* **227**, 1192–1204.

Haakansson K, Briand C, Zaitsev V, Xue Y and Liljas A (1994*a*) Wild-type and E106Q mutant carbonic anhydrase complexed with acetate. *Acta Crystallographica. Section D, Biological Crystallography* **50**, 101–104.

Haakansson K, Wehnert A and Liljas A (1994*b*) X-ray analysis of metal-substituted human carbonic anhydrase II derivatives. *Acta Crystallographica. Section D, Biological Crystallography* **50**, 93–100.

Heinisch T, Pellizzoni M, Dürrenberger M, Tinberg CE, Köhler V, Klehr J, Häussinger D, Baker D and Ward TR (2015) Improving the catalytic performance of an artificial metalloenzyme by computational design. *Journal of the American Chemical Society* **137**, 10414–10419.

Hen N, Bialer M, Yagen B, Maresca A, Aggarwal M, Robbins AH, McKenna R, Scozzafava A and Supuran CT (2011) Anticonvulsant 4-aminobenzenesulfonamide derivatives with branched-alkylamide moieties: X-ray crystallography and inhibition studies of human carbonic anhydrase isoforms I, II, VII, and XIV. *Journal of Medicinal Chemistry* **54**, 3977–3981.

Hilvo M, Baranauskiene L, Salzano AM, Scaloni A, Matulis D, Innocenti A, Scozzafava A, Monti SM, Di Fiore A, De Simone G, Lindfors M, Janis J, Valjakka J, Pastorekova S, Pastorek J, Kulomaa MS, Nordlund HR, Supuran CT and Parkkila S (2008) Biochemical characterization of CA IX, one of the most active carbonic anhydrase isozymes. *Journal of Biological Chemistry* **283**, 27799–27809.

Huang CC, Lesburg CA, Kiefer LL, Fierke CA and Christianson DW (1996) Reversal of the hydrogen bond to zinc ligand histidine-119 dramatically

https://doi.org/10.1017/S0033583518000082

diminishes catalysis and enhances metal equilibration kinetics in carbonic anhydrase II. *Biochemistry* **35**, 3439–3446.

Huang S, Sjoblom B, Sauer-Eriksson AE and Jonsson B-H (2002) Organization of an efficient carbonic anhydrase: implications for the mechanism based on structure-function studies of a T199P/C206S mutant. *Biochemistry* **41**, 7628–7635.

Hurt JD, Tu C, Laipis PJ and Silverman DN (1997) Catalytic properties of Murine Carbonic Anhydrase IV. *Journal of Biological Chemistry* **272**, 13512–13518.

Inhester T and Rarey M (2014) Protein–ligand interaction databases: advanced tools to mine activity data and interactions on a structural level: protein–ligand interaction databases. *WIREs Computational Molecular Science* **4**, 562–575.

Innocenti A, Pastorekova S, Pastorek J, Scozzafava A, Simone GD and Supuran CT (2009) The proteoglycan region of the tumor-associated carbonic anhydrase isoform IX acts as anintrinsic buffer optimizing CO_2 hydration at acidic pH values characteristic of solid tumors. *Bioorganic & Medicinal Chemistry Letters* **19**, 5825–5828.

Innocenti A, Beyza Oztürk Sarikaya S, Gülçin I and Supuran CT (2010) Carbonic anhydrase inhibitors. Inhibition of mammalian isoforms I-XIV with a series of natural product polyphenols and phenolic acids. *Bioorganic & Medicinal Chemistry* **18**, 2159–2164.

Innocenti A, Durdagi S, Doostdar N, Strom TA, Barron AR and Supuran CT (2010*a*) Nanoscale enzyme inhibitors: Fullerenes inhibit carbonic anhydrase by occluding the active site entrance. *Bioorganic and Medicinal Chemistry* **18**, 2822–2828.

Ippolito JA and Christianson DW (1993) Structure of an engineered His3Cys zinc binding site in human carbonic anhydrase II. *Biochemistry* **32**, 9901–9905.

Ippolito JA and Christianson DW (1994) Structural consequences of redesigning a protein-zinc binding site. *Biochemistry* **33**, 15241–15249.

Ippolito JA, Baird TT, McGee SA, Christianson DW and Fierke CA (1995) Structure-assisted redesign of a protein-zinc-binding site with femtomolar affinity. *Proceedings of the National Academy of Sciences of the United States of America* **92**, 5017–5021.

Ivanova J, Leitans J, Tanc M, Kazaks A, Zalubovskis R, Supuran CT and Tars K (2015) X-ray crystallography-promoted drug design of carbonic anhydrase inhibitors. *Chemical Communications (Cambridge, U. K.)* **51**, 7108–7111.

Jewell DA, Tu C, Paranawithana SR, Tanhauser SM, LoGrasso PV, Laipis PJ and Silverman DN (1991) Enhancement of the catalytic properties of human carbonic anhydrase III by site-directed mutagenesis. *Biochemistry* **30**, 1484–1490.

Jogaitė V, Zubrienė A, Michailovienė V, Gylytė J, Morkūnaitė V and Matulis D (2013) Characterization of human carbonic anhydrase XII stability and inhibitor binding. *Bioorganic & Medicinal Chemistry* **21**, 1431–1436.

Jonsson BM, Hakansson K and Liljas A (1993) The structure of human carbonic anhydrase II in complex with bromide and azide. *FEBS Letters* **322**, 186–190.

Jude KM, Banerjee AL, Haldar MK, Manokaran S, Roy B, Mallik S, Srivastava DK and Christianson DW (2006) Ultrahigh resolution crystal structures of human carbonic anhydrases I and II complexed with 'Two-prong' inhibitors reveal the molecular basis of high affinity. *Journal of the American Chemical Society* **128**, 3011–3018.

Juozapaitienė V, Bartkutė B, Michailovienė V, Zakšauskas A, Baranauskienė L, Satkūnė S and Matulis D (2016) Purification, enzymatic activity and inhibitor discovery for recombinant human carbonic anhydrase XIV. *Journal of Biotechnology* **240**, 31–42.

Kannan K (1981) Structure and function of carbonic anhydrases. *Biomolecular Structure, Conformation, Function and Evolution* **1**, 165–170.

Kannan KK, Fridborg K, Bergsten PC, Liljas A, Lovgren S, Petef M, Strandberg B, Waara I, Adler L, Falkbring SO, Göthe PO and Nyman PO (1972*a*) Structure of human carbonic anhydrase B. I. Crystallization and heavy atom modifications. *Journal of Molecular Biology* **63**, 601–604.

Kannan KK, Liljas A, Waara I, Bergsten PC, Lovgren S, Strandberg B, Bengtsson U, Carlbom U, Fridborg K, Jarup L and Petef M (1972*b*) Crystal structure of human erythrocyte carbonic anhydrase C. VI. The three-dimensional structure at high resolution in relation to other mammalian carbonic anhydrases. *Cold Spring Harbor Symposia on Quantitative Biology* **36**, 221–231.

Kannan KK, Notstrand B, Fridborg K, Lovgren S, Ohlsson A and Petef M (1975) Crystal structure of human erythrocyte carbonic anhydrase B. Three-dimensional structure at a nominal 2.2-Å resolution. *Proceedings of the National Academy of Sciences of the United States of America* **72**, 51–55.

Kannan KK, Ramanadham M and Jones TA (1984) Structure, refinement, and function of carbonic anhydrase isozymes: refinement of human carbonic anhydrase I. *Annals of the New York Academy of Sciences* **429**, 49–60.

Karioti A, Carta F and Supuran CT (2016) Phenols and polyphenols as carbonic anhydrase inhibitors. *Molecules* **21**, 1649.

Kasiliauskaitė A, Časaitė V, Juozapaitienė V, Zubrienė A, Michailovienė V, Revuckienė J, Baranauskienė L, Meškys R and Matulis D (2016) Thermodynamic characterization of human carbonic anhydrase VB stability and intrinsic binding of compounds. *Journal of Thermal Analysis and Calorimetry* **123**, 2191–2200.

Kazokaitė J, Milinavičiūtė G, Smirnovienė J, Matulienė J and Matulis D (2015) Intrinsic binding of 4-substituted-2,3,5,6-tetrafluorobenezenesulfonamides to native and recombinant human carbonic anhydrase VI. *FEBS Journal* **282**, 972–983.

Khalifah RG (1977) Histidine-200 alters inhibitor binding in human carbonic anhydrase B. A carbon-13 nuclear magnetic resonance identification. *Biochemistry* **16**, 2236–2240.

Khalifah RG, Strader DJ, Bryant SH and Gibson SM (1977) Carbon-13 nuclear magnetic resonance probe of active-site ionizations in human carbonic anhydrase B. *Biochemistry* **16**, 2241–2247.

Kiefer L, Ippolito J, Fierke C and Christianson D (1993) Redesigning the zinc-binding site of human carbonic anhydrase-II – structure of a His2asp-Zn2+ metal coordination polyhedron. *Journal of the American Chemical Society* **115**, 12581–12582.

Kim C, Chang JS, Doyon JB, Baird TTJ, Fierke CA, Jain A and Christianson D (2000) Contribution of fluorine to protein–ligand affinity in the binding of fluoroaromatic inhibitors to carbonic anhydrase II. *Journal of the American Chemical Society* **122**, 12125–12134.

Kim CY, Chandra PP, Jain A and Christianson DW (2001) Fluoroaromatic–fluoroaromatic interactions between inhibitors bound in the crystal lattice of human carbonic anhydrase II. *Journal of the American Chemical Society* **123**, 9620–9627.

Kim C-Y, Whittington DA, Chang JS, Liao J, May JA and Christianson DW (2002) Structural aspects of isozyme selectivity in the binding of inhibitors to carbonic anhydrases II and IV. *Journal of Medicinal Chemistry* **45**, 888–893.

Kišonaitė M, Zubrienė A, Čapkauskaitė E, Smirnov A, Smirnovienė J, Kairys V, Michailovienė V, Manakova E, Gražulis S and Matulis D (2014) Intrinsic thermodynamics and structure correlation of benzenesulfonamides with a pyrimidine moiety binding to carbonic anhydrases I, II, VII, XII, and XIII. *PLoS ONE* **9**, e114106.

Köhler K, Hillebrecht A, Schulze Wischeler J, Innocenti A, Heine A, Supuran CT and Klebe G (2007) Saccharin inhibits carbonic anhydrases: possible explanation for its unpleasant metallic aftertaste. *Angewandte Chemie (International ed. in English)* **46**, 7697–7699.

Krainer G and Keller S (2015) Single-experiment displacement assay for quantifying high-affinity binding by isothermal titration calorimetry. *Methods* **76**, 116–123.

Krainer G, Broecker J, Vargas C, Fanghänel J and Keller S (2012) Quantifying high-affinity binding of hydrophobic ligands by isothermal titration calorimetry. *Analytical Chemistry* **84**, 10715–10722.

Kral V, Mader P, Collard R, Fabry M, Horejsi M, Rezacova P, Kozisek M, Zavada J, Sedlacek J, Rulisek L and Brynda J (2008) Stabilization of antibody structure upon association to a human carbonic anhydrase IX epitope studied by X-ray crystallography, microcalorimetry, and molecular dynamics simulations. *Proteins* **71**, 1275–1287.

Krebs JF, Fierke CA, Alexander RS and Christianson DW (1991) Conformational mobility of His-64 in the Thr-200-Ser mutant of human carbonic anhydrase II. *Biochemistry* **30**, 9153–9160.

https://doi.org/10.1017/S0033583518000082

Krebs JF, Ippolito JA, Christianson DW and Fierke CA (1993) Structural and functional importance of a conserved hydrogen bond network in human carbonic anhydrase II. *Journal of Biological Chemistry* **268**, 27458–27466.

Krimmer SG and Klebe G (2015) Thermodynamics of proteinLigand interactions as a reference for computational analysis: how to assess accuracy, reliability and relevance of experimental data. *Journal of Computer-aided Molecular Design* **29**, 867–883.

Krishnamurthy VM, Kaufman GK, Urbach AR, Gitlin I, Gudiksen KL, Weibel DB and Whitesides GM (2008) Carbonic anhydrase as a model for biophysical and physical-organic studies of proteins and protein–ligand binding. *Chemical Reviews* **108**, 946–1051.

Kumar V and Kannan KK (1994) Enzyme-substrate interactions. Structure of human carbonic anhydrase I complexed with bicarbonate. *Journal of Molecular Biology* **241**, 226–232.

Kumar V, Kannan KK and Sathyamurthi P (1994) Differences in anionic inhibition of human carbonic anhydrase I revealed from the structures of iodide and gold cyanide inhibitor complexes. *Acta Crystallographica. Section D, Biological Crystallography* **50**, 731–738.

Ladbury JE and Doyle ML (eds) (2004) *Biocalorimetry 2: Applications of Calorimetry in the Biological Sciences*. Chichester; Hoboken, NJ: Wiley.

Langella E, D'Ambrosio K, D'Ascenzio M, Carradori S, Monti S, Supuran CT and Simone GD (2015) A combined crystallographic and theoretical study explains the capability of carboxylic acids to adopt multiple binding modes within carbonic anhydrase active site. *Chemistry: A European Journal* **22**, 97–100.

La Regina G, Coluccia A, Famiglini V, Pelliccia S, Monti L, Vullo D, Nuti E, Alterio V, De Simone G, Monti SM, Pan P, Parkkila S, Supuran CT, Rossello A and Silvestri R (2015) Discovery of 1,1′-biphenyl-4-sulfonamides as a new class of potent and selective carbonic anhydrase XIV inhibitors. *Journal of Medicinal Chemistry* **58**, 8564–8572.

Leese MP, Leblond B, Smith A, Newman SP, Di Fiore A, De Simone G, Supuran CT, Purohit A, Reed MJ and Potter BV (2006) 2-substituted estradiol bis-sulfamates, multitargeted antitumor agents: synthesis, *in vitro* SAR, protein crystallography, and *in vivo* activity. *Journal of Medicinal Chemistry* **49**, 7683–7696.

Leese MP, Jourdan FL, Gaukroger K, Mahon MF, Newman SP, Foster PA, Stengel C, Regis-Lydi S, Ferrandis E, Fiore AD, Simone GD, Supuran CT, Purohit A, Reed MJ and Potter BVL (2008) Structure-activity relationships of C-17 cyano-substituted estratrienes as anticancer agents. *Journal of Medicinal Chemistry* **51**, 1295–1308.

Leese MP, Jourdan F, Kimberley MR, Cozier GE, Thiyagarajan N, Stengel C, Regis-Lydi S, Foster PA, Newman SP, Acharya KR, Ferrandis E, Purohit A, Reed MJ and Potter BVL (2010) Chimeric microtubule disruptors. *Chemical Communiations (Cambridge, U. K.)* **46**, 2907–2909.

Leitans J, Sprudza A, Tanc M, Vozny I, Zalubovskis R, Tars K and Supuran CT (2013) 5-Substituted-(1,2,3-triazol-4-yl)Thiophene-2-sulfonamides strongly inhibit human carbonic anhydrases I, II, IX and XII: solution and X-ray crystallographic studies. *Bioorganic & Medicinal Chemistry* **21**, 5130–5138.

Leitans J, Kazaks A, Balode A, Ivanova J, Zalubovskis R, Supuran CT and Tars K (2015) Efficient expression and crystallization system of cancer-associated carbonic anhydrase isoform IX. *Journal of Medicinal Chemistry* **58**, 9004–9009.

Lesburg C and Christianson D (1995) X-Ray crystallographic studies of engineered hydrogen bond networks in a protein-zinc binding site. *Journal of the American Chemical Society* **117**, 6838–6844.

Lesburg CA, Huang C, Christianson DW and Fierke CA (1997) Histidine – carboxamide ligand substitutions in the zinc binding site of carbonic anhydrase II alter metal coordination geometry but retain catalytic activity. *Biochemistry* **36**, 15780–15791.

Liljas A, Kannan KK, Bergsten PC, Waara I, Fridborg K, Strandberg B, Carlbom U, Jarup L, Lovgren S and Petef M (1972) Crystal structure of human carbonic anhydrase C. *Nature: New biology* **235**, 131–137.

Lindahl M, Svensson LA and Liljas A (1993) Metal poison inhibition of carbonic anhydrase. *Proteins* **15**, 177–182.

Linkuvienė V, Krainer G, Chen W-Y and Matulis D (2016*a*) Isothermal titration calorimetry for drug design: precision of the enthalpy and binding constant measurements and comparison of the instruments. *Analytical Biochemistry* **515**, 61–64.

Linkuvienė V, Matulienė J, Juozapaitienė V, Michailovienė V, Jachno J and Matulis D (2016*b*) Intrinsic thermodynamics of inhibitor binding to human carbonic anhydrase IX. *Biochimica et Biophysica Acta (BBA) – General Subjects* **1860**, 708–718.

Linkuvienė V, Talibov VO, Danielson UH and Matulis D (2018) Introduction of intrinsic kinetics of protein–ligand interactions and their implications for drug design. *Journal of Medicinal Chemistry* **61**, 2292–2302.

Liu Z, Li J, Liu J, Liu Y, Nie W, Han L, Li Y and Wang R (2015) Cross-Mapping of protein – ligand binding data between ChEMBL and PDBbind. *Molecular Informatics* **34**, 568–576.

Lloyd MD, Pederick RL, Natesh R, Woo LWL, Purohit A, Reed MJ, Acharya KR and Potter BVL (2005*a*) Crystal structure of human carbonic anhydrase II at 1.95 A resolution in complex with 667-coumate, a novel anti-cancer agent. *Biochemical Journal* **385**, 715–720.

Lloyd MD, Thiyagarajan N, Ho YT, Woo LWL, Sutcliffe OB, Purohit A, Reed MJ, Acharya KR and Potter BVL (2005*b*) First crystal structures of human carbonic anhydrase II in complex with dual aromatase-steroid sulfatase inhibitors. *Biochemistry* **44**, 6858–6866.

Lo M-C, Aulabaugh A, Jin G, Cowling R, Bard J, Malamas M and Ellestad G (2004) Evaluation of fluorescence-based thermal shift assays for hit identification in drug discovery. *Analytical Biochemistry* **332**, 153–159.

Lockett MR, Lange H, Breiten B, Heroux A, Sherman W, Rappoport D, Yau PO, Snyder PW and Whitesides GM (2013) The binding of benzoarylsulfonamide ligands to human carbonic anhydrase is insensitive to formal fluorination of the ligand. *Angewandte Chemie (International ed. in English)* **52**, 7714–7717.

Lomelino C and McKenna R (2016) Carbonic anhydrase inhibitors: a review on the progress of patent literature (20112016). *Expert Opinion on Therapeutic Patents* **26**, 947–956.

Lopez M, Paul B, Hofmann A, Morizzi J, Wu QK, Charman SA, Innocenti A, Vullo D, Supuran CT and Poulsen SA (2009) S-glycosyl primary sulfonamides – a new structural class for selective inhibition of cancer-associated carbonic anhydrases. *Journal of Medicinal Chemistry* **52**, 6421–6432.

Lopez M, Vu H, Wang CK, Wolf MG, Groenhof G, Innocenti A, Supuran CT and Poulsen S-A (2011) Promiscuity of carbonic anhydrase II. Unexpected ester hydrolysis of carbohydrate-based sulfamate inhibitors. *Journal of the American Chemical Society* **133**, 18452–18462.

Lou Y, McDonald PC, Oloumi A, Chia S, Ostlund C, Ahmadi A, Kyle A, auf dem Keller U, Leung S, Huntsman D, Clarke B, Sutherland BW, Waterhouse D, Bally M, Roskelley C, Overall CM, Minchinton A, Pacchiano F, Carta F, Scozzafava A, Touisni N, Winum J-Y, Supuran CT and Dedhar S (2011) Targeting tumor hypoxia: suppression of breast tumor growth and metastasis by novel carbonic anhydrase IX inhibitors. *Cancer Research* **71**, 3364–3376.

Mader P, Brynda J, Gitto R, Agnello S, Pachl P, Supuran CT, Chimirri A and Řezáčová P (2011) Structural basis for the interaction between carbonic anhydrase and 1,2,3,4-tetrahydroisoquinolin-2-ylsulfonamides. *Journal of Medicinal Chemistry* **54**, 2522–2526.

Mader P, Pecina A, Cígler P, Lepšík M, Šícha V, Hobza P, Grüner B, Fanfrlík J, Brynda J and Řezáčová P (2014) Carborane-based carbonic anhydrase inhibitors: insight into CAII/CAIX specificity from a high-resolution crystal structure, modeling, and quantum chemical calculations. *BioMed Research International* **2014**, 389869.

Mahon BP, Hendon AM, Driscoll JM, Rankin GM, Poulsen S-A, Supuran CT and McKenna R (2015*a*) Saccharin: a lead compound for structure-based drug design of carbonic anhydrase IX inhibitors. *Bioorganic & Medicinal Chemistry* **23**, 849–854.

Mahon BP, Lomelino CL, Ladwig J, Rankin GM, Driscoll JM, Salguero AL, Pinard MA, Vullo D, Supuran CT, Poulsen S-A and McKenna R (2015*b*) Mapping selective inhibition of the cancer-related carbonic anhydrase IX using structure-activity relationships of glucosyl-based sulfamates. *Journal of Medicinal Chemistry* **58**, 6630–6638.

Mahon BP, Lomelino CL, Salguero AL, Driscoll JM, Pinard MA and McKenna R (2015*c*) Observed surface lysine acetylation of human carbonic anhydrase II expressed in Escherichia coli. *Protein Science* **24**, 1800–1807.

https://doi.org/10.1017/S0033583518000082

Mallis RJ, Poland BW, Chatterjee TK, Fisher RA, Darmawan S, Honzatko RB and Thomas JA (2000) Crystal structure of S-glutathiolated carbonic anhydrase III. *FEBS Letters* **482**, 237–241.

Mangani S and Hakansson K (1992) Crystallographic studies of the binding of protonated and unprotonated inhibitors to carbonic anhydrase using hydrogen sulphide and nitrate anions. *European Journal of Biochemistry* **210**, 867–871.

Mangani S and Liljas A (1993) Crystal structure of the complex between human carbonic anhydrase II and the aromatic inhibitor 1,2,4-triazole. *Journal of Molecular Biology* **232**, 9–14.

Maresca A, Temperini C, Vu H, Pham NB, Poulsen S-A, Scozzafava A, Quinn RJ and Supuran CT (2009) Non-zinc mediated inhibition of carbonic anhydrases: coumarins are a new class of suicide inhibitors. *Journal of the American Chemical Society* **131**, 3057–3062.

Maresca A, Temperini C, Pochet L, Masereel B, Scozzafava A and Supuran CT (2010) Deciphering the mechanism of carbonic anhydrase inhibition with coumarins and thiocoumarins. *Journal of Medicinal Chemistry* **53**, 335–344.

Maresca A, Akyuz G, Osman SM, AlOthman Z and Supuran CT (2015) Inhibition of mammalian carbonic anhydrase isoforms I-XIV with a series of phenolic acid esters. *Bioorganic & Medicinal Chemistry* **23**, 7181–7188.

Martin DP and Cohen SM (2012) Nucleophile recognition as an alternative inhibition mode for benzoic acid based carbonic anhydrase inhibitors. *Chemical Communications* **48**, 5259–5261.

Martin DP, Hann ZS and Cohen SM (2013) Metalloprotein-inhibitor binding: human carbonic anhydrase II as a model for probing Metal-Ligand interactions in a metalloprotein active site. *Inorganic Chemistry* **52**, 12207–12215.

Martin DP, Blachly PG, Marts AR, Woodruff TM, de Oliveira CAF, McCammon JA, Tierney DL and Cohen SM (2014*a*) 'Unconventional' coordination chemistry by metal chelating fragments in a metalloprotein active site. *Journal of the American Chemical Society* **136**, 5400–5406.

Martin DP, Blachly PG, McCammon JA and Cohen SM (2014*b*) Exploring the influence of the protein environment on metal-binding pharmacophores. *Journal of Medicinal Chemistry* **57**, 7126–7135.

Masini E, Carta F, Scozzafava A and Supuran CT (2013) Antiglaucoma carbonic anhydrase inhibitors: a patent review. *Expert Opinion on Therapeutic Patents* **23**, 705–716.

Matulis D and Lovrien R (1998) 1-Anilino-8-naphthalene sulfonate anion-protein binding depends primarily on Ion pair formation. *Biophysical Journal* **74**, 422–429.

Matulis D and Todd MJ (2004) Thermodynamics – structure correlations of sulfonamide inhibitor binding to carbonic anhydrase. In Ladbury JE and Doyle ML (eds), *Biocalorimetry 2*, Wiley-Blackwell (Verlag), pp. 107–132.

Matulis D, Baumann CG, Bloomfield VA and Lovrien RE (1999) 1-Anilino-8-naphthalene sulfonate as a protein conformational tightening agent. *Biopolymers* **49**, 451–458.

Matulis D, Kranz JK, Salemme FR and Todd MJ (2005) Thermodynamic stability of carbonic anhydrase: measurements of binding affinity and stoichiometry using ThermoFluor. *Biochemistry* **44**, 5258–5266.

Mazumdar PA, Kumaran D, Swaminathan S and Das AK (2008) A novel acetate-bound complex of human carbonic anhydrase II. *Acta Crystallographica, Section F: Structural Biology and Crystallization Communications* **64**, 163–166.

McDonnell PA, Yanchunas J, Newitt JA, Tao L, Kiefer SE, Ortega M, Kut S, Burford N, Goldfarb V, Duke GJ, Shen H, Metzler W, Doyle M, Chen Z, Tarby C, Borzilleri R, Vaccaro W, Gottardis M, Lu S, Crews D, Kim K, Lombardo L and Roussel DL (2009) Assessing compound binding to the Eg5 motor domain using a thermal shift assay. *Analytical Biochemistry* **392**, 59–69.

McKenna R and Supuran CT (2014) Carbonic anhydrase inhibitors drug design. *Subcellular Biochemistry* **75**, 291–323.

Mecinović J, Snyder PW, Mirica KA, Bai S, Mack ET, Kwant RL, Moustakas DT, Héroux A and Whitesides GM (2011) Fluoroalkyl and alkyl chains have similar hydrophobicities in binding to the 'hydrophobic wall' of carbonic anhydrase. *Journal of the American Chemical Society* **133**, 14017–14026.

Meldrum NU and Roughton FJ (1932) Some properties of carbonic anhydrase, the CO_2 enzyme present in blood. *Journal of Physiology* **75**, 15P–16P.

Meldrum NU and Roughton FJW (1933*a*) The state of carbon dioxide in blood. *Journal of Physiology* **80**, 143–170.

Meldrum NU and Roughton FJW (1933*b*) Carbonic anhydrase. Its preparation and properties. *Journal of Physiology* **80**, 113–142.

Menchise V, Simone G, Alterio V, Fiore A, Pedone C, Scozzafava A and Supuran CT (2005) Carbonic anhydrase inhibitors: stacking with Phe131 determines active site binding region of inhibitors As exemplified by the X-ray crystal structure of a membrane-impermeant antitumor sulfonamide complexed with isozyme II. *Journal of Medicinal Chemistry* **48**, 5721–5727.

Menchise V, Simone GD, Fiore AD, Scozzafava A and Supuran CT (2006) Carbonic anhydrase inhibitors: X-ray crystallographic studies for the binding of 5-amino-1,3,4-thiadiazole-2-sulfonamide and 5-(4-amino-3-chloro-5-fluorophenylsulfonamido)-1,3,4-thiadiazole-2-sulfonamide to human isoform II. *Bioorganic & Medicinal Chemistry Letters* **16**, 6204–6208.

Michalczyk R, Unkefer CJ, Bacik J-P, Schrader TE, Ostermann A, Kovalevsky AY, McKenna R and Fisher SZ (2015) Joint neutron crystallographic and NMR solution studies of Tyr residue ionization and hydrogen bonding: implications for enzyme-mediated proton transfer. *Proceedings of the National Academy of Sciences of the United States of America* **112**, 5673–5678.

Mickevičiūtė A, Timm DD, Gedgaudas M, Linkuvienė V, Chen Z, Waheed A, Michailovienė V, Zubrienė A, Smirnov A, Čapkauskaitė E, Baranauskienė L, Jachno J, Revuckienė J, Manakova E, Gražulis S, Matulienė J, Di Cera E, Sly WS and Matulis D (2017) Intrinsic thermodynamics of high affinity inhibitor binding to recombinant human carbonic anhydrase IV. *European Biophysics Journal with Biophysics Letters* **47**, 271–290.

Mikulski R, Avvaru BS, Tu C, Case N, McKenna R and Silverman DN (2011*a*) Kinetic and crystallographic studies of the role of tyrosine 7 in the active site of human carbonic anhydrase II. *Archives of Biochemistry and Biophysics* **506**, 181–187.

Mikulski R, Domsic JF, Ling G, Tu C, Robbins AH, Silverman DN and McKenna R (2011*b*) Structure and catalysis by carbonic anhydrase II: role of active-site tryptophan 5. *Archives of Biochemistry and Biophysics* **516**, 97–102.

Mikulski R, West D, Sippel KH, Avvaru BS, Aggarwal M, Tu C, McKenna R and Silverman DN (2013) Water networks in fast proton transfer during catalysis by human carbonic anhydrase II. *Biochemistry* **52**, 125–131.

Mincione F, Benedini F, Biondi S, Cecchi A, Temperini C, Formicola G, Pacileo I, Scozzafava A, Masini E and Supuran CT (2011) Synthesis and crystallographic analysis of new sulfonamides incorporating NO-donating moieties with potent antiglaucoma action. *Bioorganic & Medicinal Chemistry Letters* **21**, 3216–3221.

Moeker J, Mahon BP, Bornaghi LF, Vullo D, Supuran CT, McKenna R and Poulsen S-A (2014*a*) Structural insights into carbonic anhydrase IX isoform specificity of carbohydrate-based sulfamates. *Journal of Medicinal Chemistry* **57**, 8635–8645.

Moeker J, Peat TS, Bornaghi LF, Vullo D, Supuran CT and Poulsen S-A (2014*b*) Cyclic secondary sulfonamides: unusually good inhibitors of cancer-related carbonic anhydrase enzymes. *Journal of medicinal chemistry* **57**, 3522–3531.

Monnard FW, Heinisch T, Nogueira ES, Schirmer T and Ward TR (2011) Human carbonic anhydrase II as a host for piano-stool complexes bearing a sulfonamide anchor. *Chemical Communications (Cambridge, U. K.)* **47**, 8238–8240.

Monnard FW, Nogueira ES, Heinisch T, Schirmer T and Ward TR (2013) Human carbonic anhydrase II as host protein for the creation of artificial metalloenzymes: the asymmetric transfer hydrogenation of imines. *Chemical Science* **4**, 3269–3274.

Morkūnaitė V, Baranauskienė L, Zubrienė A, Kairys V, Ivanova J, Trapencieris P and Matulis D (2014) Saccharin sulfonamides as inhibitors of carbonic anhydrases I, II, VII, XII, and XIII. *BioMed Research International* **2014**, 638902.

Morkūnaitė V, Gylytė J, Zubrienė A, Baranauskienė L, Kišonaitė M, Michailovienė V, Juozapaitienė V, Todd MJ and Matulis D (2015) Intrinsic thermodynamics of sulfonamide inhibitor binding to human

https://doi.org/10.1017/S0033583518000082

carbonic anhydrases I and II. *Journal of Enzyme Inhibition and Medicinal Chemistry* **30**, 204–211.

Myszka DG and Rich RL (2000) Implementing surface plasmon resonance biosensors in drug discovery. *Pharmaceutical Science & Technology Today* **3**, 310–317.

Nair SK and Christianson DW (1991) Unexpected pH-dependent conformation of His-64, the proton shuttle of carbonic anhydrase II. *Journal of the American Chemical Society* **113**, 9455–9458.

Nair SK and Christianson DW (1993) Structural consequences of hydrophilic amino acid substitutions in the hydrophobic pocket of human carbonic anhydrase II. *Biochemistry* **32**, 4506–4514.

Nair SK, Calderone TL, Christianson DW and Fierke CA (1991) Altering the mouth of a hydrophobic pocket. Structure and kinetics of human carbonic anhydrase II mutants at residue Val-121. *Journal of Biological Chemistry* **266**, 17320–17325.

Nair SK, Ludwig PA and Christianson DW (1994) Two-site binding of phenol in the active site of human carbonic anhydrase II: structural implications for substrate association. *Journal of the American Chemical Society* **116**, 3659–3660.

Nair SK, Krebs JF, Christianson DW and Fierke CA (1995) Structural basis of inhibitor affinity to variants of human carbonic anhydrase II. *Biochemistry* **34**, 3981–3989.

Nair SK, Elbaum D and Christianson DW (1996) Unexpected binding mode of the sulfonamide fluorophore 5-dimethylamino-1-naphthalene sulfonamide to human carbonic anhydrase II. Implications for the development of a zinc biosensor. *Journal of Biological Chemistry* **271**, 1003–1007.

Niesen FH, Berglund H and Vedadi M (2007) The use of differential scanning fluorimetry to detect ligand interactions that promote protein stability. *Nature Protocols* **2**, 2212–2221.

Olaru A, Bala C, Jaffrezic-Renault N and Aboul-Enein HY (2015) Surface plasmon resonance (SPR) biosensors in pharmaceutical analysis. *Critical Reviews in Analytical Chemistry* **45**, 97–105.

Olsson TSG, Williams MA, Pitt WR and Ladbury JE (2008) The thermodynamics of protein–ligand interaction and solvation: insights for ligand design. *Journal of Molecular Biology* **384**, 1002–1017.

Pacchiano F, Aggarwal M, Avvaru BS, Robbins AH, Scozzafava A, McKenna R and Supuran CT (2010) Selective hydrophobic pocket binding observed within the carbonic anhydrase II active site accommodate different 4-substituted-ureido-benzenesulfonamides and correlate to inhibitor potency. *Chemical Communications (Cambridge, U. K.)* **46**, 8371–8373.

Pantoliano MW, Petrella EC, Kwasnoski JD, Lobanov VS, Myslik J, Graf E, Carver T, Asel E, Springer BA, Lane P and Salemme FR (2001) High-density miniaturized thermal shift assays as a general strategy for drug discovery. *Journal of Biomolecular Screening* **6**, 429–440.

Pastorekova S, Kopacek J and Pastorek J (2007) Carbonic anhydrase inhibitors and the management of cancer. *Current Topics in Medicinal Chemistry* **7**, 865–878.

Pastorekova S, Zatovicova M and Pastorek J (2008) Cancer-associated carbonic anhydrases and their inhibition. *Current Pharmaceutical Design* **14**, 685–698.

Patching SG (2014) Surface plasmon resonance spectroscopy for characterisation of membrane proteinLigand interactions and its potential for drug discovery. *Biochimica et Biophysica Acta (BBA) – Biomembranes* **1838**, 43–55.

Petrauskas V, Baranauskienė L, Zubrienė A and Matulis D (2016) Isothermal titration calorimetry and fluorescent thermal and pressure shift assays in protein-ligand interactions. In *Biocalorimetry*. Boca Raton, London, New York, Washington, D.C.: CRC Press, pp. 261–280. ISBN 148224666X, 9781482246667.

Petrauskas V, Gylytė J, Toleikis Z, Cimmperman P and Matulis D (2013) Volume of Hsp90 ligand binding and the unfolding phase diagram as a function of pressure and temperature. *European Biophysics Journal with Biophysics Letters* **42**, 355–362.

Picaud SS, Muniz JRC, Kramm A, Pilka ES, Kochan G, Oppermann U and Yue WW (2009) Crystal structure of human carbonic anhydrase-related protein VIII reveals the basis for catalytic silencing. *Proteins* **76**, 507–511.

Pilipuitytė V and Matulis D (2015) Intrinsic thermodynamics of trifluoromethanesulfonamide and ethoxzolamide binding to human carbonic anhydrase VII: thermodynamics of TFS and EZA binding to CA VII. *Journal of Molecular Recognition* **28**, 166–172.

Pilka ES, Kochan G, Oppermann U and Yue WW (2012) Crystal structure of the secretory isozyme of mammalian carbonic anhydrases CA VI: implications for biological assembly and inhibitor development. *Biochemical and Biophysical Research Communications* **419**, 485–489.

Pinard MA, Boone CD, Rife BD, Supuran CT and McKenna R (2013) Structural study of interaction between brinzolamide and dorzolamide inhibition of human carbonic anhydrases. *Bioorganic & Medicinal Chemistry* **21**, 7210–7215.

Pinard MA, Aggarwal M, Mahon BP, Tu C and McKenna R (2015) A sucrose-binding site provides a lead towards an isoform-specific inhibitor of the cancer-associated enzyme carbonic anhydrase IX. *Acta Crystallographica. Section F, Structural Biology Communications* **71**, 1352–1358.

Qian M, Tu C, Earnhardt JN, Laipis PJ and Silverman DN (1997) Glutamate and aspartate as proton shuttles in mutants of carbonic anhydrase. *Biochemistry* **36**, 15758–15764.

Rami M, Dubois L, Parvathaneni N-K, Alterio V, van Kuijk SJA, Monti SM, Lambin P, De Simone G, Supuran CT and Winum J-Y (2013) Hypoxia-targeting carbonic anhydrase IX inhibitors by a new series of nitroimidazole-sulfonamides/sulfamides/sulfamates. *Journal of Medicinal Chemistry* **56**, 8512–8520.

Recacha R, Costanzo MJ, Maryanoff BE and Chattopadhyay D (2002) Crystal structure of human carbonic anhydrase II complexed with an anticonvulsant sugar sulphamate. *Biochemical Journal* **361**, 437–441.

Redhead M, Satchell R, Morkūnaitė V, Swift D, Petrauskas V, Golding E, Onions S, Matulis D and Unitt J (2015) A combinatorial biophysical approach; FTSA and SPR for identifying small molecule ligands and PAINs. *Analytical Biochemistry* **479**, 63–73.

Renaud J-P, Chung C-w, Danielson UH, Egner U, Hennig M, Hubbard RE and Nar H (2016) Biophysics in drug discovery: impact, challenges and opportunities. *Nature Reviews. Drug discovery* **15**, 679–698.

Robbins AH, Domsic JF, Agbandje-McKenna M and McKenna R (2010) Emerging from pseudo-symmetry: the redetermination of human carbonic anhydrase II in monoclinic P2(1) with a doubled a axis. *Acta Crystallographica. Section D, Biological Crystallography* **66**, 950–952.

Roche J, Caro JA, Norberto DR, Barthe P, Roumestand C, Schlessman JL, Garcia AE, García-Moreno EB and Royer CA (2012) Cavities determine the pressure unfolding of proteins. *Proceedings of the National Academy of Sciences*, **109**, 6945–6950.

Runtsch LS, Barber DM, Mayer P, Groll M, Trauner D and Broichhagen J (2015) Azobenzene-based inhibitors of human carbonic anhydrase II. *Beilstein Journal of Organic Chemistry* **11**, 1129–1135.

Rusconi S, Innocenti A, Vullo D, Mastrolorenzo A, Scozzafava A and Supuran CT (2004) Carbonic anhydrase inhibitors. Interaction of isozymes I, II, IV, V, and IX with phosphates, carbamoyl phosphate, and the phosphonate antiviral drug foscarnet. *Bioorganic & Medicinal Chemistry Letters* **14**, 5763–5767.

Rutkauskas K, Zubrienė A, Tumosienė I, Kantminienė K, Kažemėkaitė M, Smirnov A, Kazokaitė J, Morkūnaitė V, Čapkauskaitė E, Manakova E, Gražulis S, Beresnevičius Z and Matulis D (2014) 4-Amino-substituted benzenesulfonamides as inhibitors of human carbonic anhydrases. *Molecules* **19**, 17356–17380.

Rutkauskas K, Zubrienė A, Tumosienė I, Kantminienė K, Mickevičius V and Matulis D (2017) Benzenesulfonamides bearing pyrrolidinone moiety as inhibitors of carbonic anhydrase IX: synthesis and binding studies. *Medicinal Chemistry Research* **26**, 235–246.

Salmon AJ, Williams ML, Hofmann A and Poulsen S-A (2012) Protein crystal structures with ferrocene and ruthenocene-based enzyme inhibitors. *Chemical Communications (Cambridge, U. K.)* **48**, 2328–2330.

Scolnick L and Christianson D (1996) X-ray crystallographic studies of alanine-65 variants of carbonic anhydrase II reveal the structural basis of compromised proton transfer in catalysis. *Biochemistry* **35**, 16429–16434.

Scolnick L, Clements A, Liao J, Crenshaw L, Hellberg M, May J, Dean T and Christianson D (1997) Novel binding mode of hydroxamate inhibitors to human carbonic anhydrase II. *Journal of the American Chemical Society* **119**, 850–851.

https://doi.org/10.1017/S0033583518000082

Scott AD, Phillips C, Alex A, Flocco M, Bent A, Randall A, O'Brien R, Damian L and Jones LH (2009) Thermodynamic optimisation in drug discovery: a case study using carbonic anhydrase inhibitors. *ChemMedChem* **4**, 1985–1989.

Scozzafava A, Supuran CT and Carta F (2013) Antiobesity carbonic anhydrase inhibitors: a literature and patent review. *Expert Opinion on Therapeutic Patents* **23**, 725–735.

Simone GD, Monti SM, Alterio V, Buonanno M, Luca VD, Rossi M, Carginale V, Supuran CT, Capasso C and Fiore AD (2015) Crystal structure of the most catalytically effective carbonic anhydrase enzyme known, SazCA from the thermophilic bacterium Sulfurihydrogenibium azorense. *Bioorganic & Medicinal Chemistry Letters* **25**, 2002–2006.

Sippel KH, Robbins AH, Domsic J, Genis C, Agbandje-McKenna M and McKenna R (2009) High-resolution structure of human carbonic anhydrase II complexed with acetazolamide reveals insights into inhibitor drug design. *Acta Crystallographica, Section F: Structural Biology and Crystallization Communications* **65**, 992–995.

Sippel KH, Genis C, Govindasamy L, Agbandje-McKenna M, Kiddle JJ, Tripp BC and McKenna R (2010) Synchrotron radiation provides a plausible explanation for the generation of a free radical adduct of thioxolone in mutant carbonic anhydrase II. *Journal of Physical Chemistry Letters* **1**, 2898–2902.

Sippel KH, Stander A, Tu C, Venkatakrishnan B, Robbins AH, Agbandje-McKenna M, Fourie J, Joubert AM and McKenna R (2011) Characterization of carbonic anhydrase isozyme specific inhibition by sulfamated 2-ethylestra compounds. *Letters in Drug Design & Discovery* **8**, 1–25.

Sjöblom B, Polentarutti M and Djinović-Carugo K (2009) Structural study of X-ray induced activation of carbonic anhydrase. *PNAS* **106**, 10609–10613.

Skvarnavičius G, Toleikis Z, Grigaliūnas M, Smirnovienė J, Norvaišas P, Cimmperman P, Matulis D and Petrauskas V (2017) High pressure spectrofluorimetry a tool to determine protein–ligand binding volume. *Journal of Physics: Conference Series* **950**, 042001.

Slavik J (1982) Anilinonaphthalene sulfonate as a probe of membrane composition and function. *Biochimica et Biophysica Acta* **694**, 1–25.

Smirnov A, Zubrienė A, Manakova E, Gražulis S and Matulis D (2018) Crystal structure correlations with the intrinsic thermodynamics of human carbonic anhydrase inhibitor binding. *PeerJ* **6**, e4412.

Smirnovienė J, Smirnovas V and Matulis D (2017) Picomolar inhibitors of carbonic anhydrase: importance of inhibition and binding assays. *Analytical Biochemistry* **522**, 61–72.

Smith DA and Jones RM (2008) The sulfonamide group as a structural alert: a distorted story? *Current Opinion in Drug Discovery & Development* **11**, 72–79.

Smith GM, Alexander RS, Christianson DW, McKeever BM, Ponticello GS, Springer JP, Randall WC, Baldwin JJ and Habecker CN (1994) Positions of His-64 and a bound water in human carbonic anhydrase II upon binding three structurally related inhibitors. *Protein Science* **3**, 118–125.

Snyder PW, Mecinović J, Moustakas DT, Thomas SW, Harder M, Mack ET, Lockett MR, Héroux A, Sherman W and Whitesides GM (2011) Mechanism of the hydrophobic effect in the biomolecular recognition of arylsulfonamides by carbonic anhydrase. *Proceedings of the National Academy of Sciences of the United States of America* **108**, 17889–17894.

Son I, Shek YL, Dubins DN and Chalikian TV (2012) Volumetric characterization of Tri-*N*-Acetylglucosamine Binding to lysozyme. *Biochemistry* **51**, 5784–5790.

Srivastava DK, Jude KM, Banerjee AL, Haldar M, Manokaran S, Kooren J, Mallik S and Christianson DW (2007) Structural analysis of charge discrimination in the binding of inhibitors to human carbonic anhydrases I and II. *Journal of the American Chemical Society* **129**, 5528–5537.

Stadie WC and O'Brien H (1933*a*) The kinetics of carbon dioxide reactions in buffer systems and blood. *Journal of Biological Chemistry* **100**, lxxxviii–lxxxix.

Stadie WC and O'Brien H (1933*b*) The catalysis of the hydration of carbon dioxide and dehydration of carbonic acid by an enzyme isolated from Red blood cells. *Journal of Biological Chemistry* **103**, 521–529.

Stams T, Nair SK, Okuyama T, Waheed A, Sly WS and Christianson DW (1996) Crystal structure of the secretory form of membrane-associated human carbonic anhydrase IV at 2.8-A resolution. *Proceedings of the National Academy of Sciences of the United States of America* **93**, 13589–13594.

Stams T, Chen Y, Boriack-Sjodin PA, Hurt JD, Liao J, May JA, Dean T, Laipis P, Silverman DN and Christianson DW (1998) Structures of murine carbonic anhydrase IV and human carbonic anhydrase II complexed with brinzolamide: molecular basis of isozyme-drug discrimination. *Protein Science* **7**, 556–563.

Steele RM, Benedini F, Biondi S, Borghi V, Carzaniga L, Impagnatiello F, Miglietta D, Chong WK, Rajapakse R, Cecchi A, Temperini C and Supuran CT (2009) Nitric oxide-donating carbonic anhydrase inhibitors for the treatment of open-angle glaucoma. *Bioorganic & Medicinal Chemistry Letters* **19**, 6565–6570.

Sūdžius J, Baranauskienė L, Golovenko D, Matulienė J, Michailovienė V, Torresan J, Jachno J, Sukackaitė R, Manakova E, Gražulis S, Tumkevičius S and Matulis D (2010) 4-[*N*-(Substituted 4-pyrimidinyl) Amino]Benzenesulfonamides as inhibitors of carbonic anhydrase isozymes I, II, VII, and XIII. *Bioorganic & Medicinal Chemistry* **18**, 7413–7421.

Supuran CT (2008) Carbonic anhydrases: novel therapeutic applications for inhibitors and activators. *Nature Reviews Drug Discovery* **7**, 168–181.

Supuran CT (2017) Advances in structure-based drug discovery of carbonic anhydrase inhibitors. *Expert Opinion on Drug Discovery* **12**, 61–88.

Supuran CT, Scozzafava A and Casini A (2003) Carbonic anhydrase inhibitors. *Medicinal Research Reviews* **23**, 146–189.

Supuran CT, Scozzafava A and Conway J (2004) *Carbonic Anhydrase: Its Inhibitors and Activators*. Boca Raton, London, New York, Washington, D.C.: CRC Press.

Talibov VO, Linkuvienė V, Matulis D and Danielson UH (2016) Kinetically selective inhibitors of human carbonic anhydrase isozymes I, II, VII, IX, XII, and XIII. *Journal of Medicinal Chemistry* **59**, 2083–2093.

Tanc M, Carta F, Bozdag M, Scozzafava A and Supuran CT (2013) 7-Substituted-sulfocoumarins are isoform-selective, potent carbonic anhydrase II inhibitors. *Bioorganic & Medicinal Chemistry* **21**, 4502–4510.

Tanpure RP, Ren B, Peat TS, Bornaghi LF, Vullo D, Supuran CT and Poulsen S-A (2015) Carbonic anhydrase inhibitors with dual-tail moieties To match the hydrophobic and hydrophilic halves of the carbonic anhydrase active site. *Journal of Medicinal Chemistry* **58**, 1494–1501.

Tars K, Vullo D, Kazaks A, Leitans J, Lends A, Grandane A, Zalubovskis R, Scozzafava A and Supuran CT (2013) Sulfocoumarins (1,2-benzoxathiine-2,2-dioxides): a class of potent and isoform-selective inhibitors of tumor-associated carbonic anhydrases. *Journal of Medicinal Chemistry* **56**, 293–300.

Taylor PW, King RW and Burgen ASV (1970) Influence of pH on the kinetics of complex formation between aromatic sulfonamides and human carbonic anhydrase. *Biochemistry* **9**, 3894–3902.

Temperini C, Scozzafava A, Puccetti L and Supuran CT (2005) Carbonic anhydrase activators: X-ray crystal structure of the adduct of human isozyme II with L-histidine as a platform for the design of stronger activators. *Bioorganic & Medicinal Chemistry Letters* **15**, 5136–5141.

Temperini C, Scozzafava A and Supuran CT (2006*a*) Carbonic anhydrase activators: the first X-ray crystallographic study of an adduct of isoform I. *Bioorganic & Medicinal Chemistry Letters* **16**, 5152–5156.

Temperini C, Innocenti A, Scozzafava A and Supuran CT (2006*b*) *N*-Hydroxyurea–a versatile zinc binding function in the design of metalloenzyme inhibitors. *Bioorganic & Medicinal Chemistry Letters* **16**, 4316–4320.

Temperini C, Scozzafava A, Vullo D and Supuran CT (2006*c*) Carbonic anhydrase activators. Activation of isoforms I, II, IV, VA, VII, and XIV with L- and D-phenylalanine and crystallographic analysis of their adducts with isozyme II: stereospecific recognition within the active site of an enzyme and its consequences for the drug design. *Journal of Medicinal Chemistry* **49**, 3019–3027.

Temperini C, Scozzafava A, Vullo D and Supuran CT (2006*d*) Carbonic anhydrase activators. Activation of isozymes I, II, IV, VA, VII, and XIV with L- and D-histidine and crystallographic analysis of their adducts with isoform II: engineering proton-transfer processes within the active site of an enzyme. *Chemistry* **12**, 7057–7066.

Temperini C, Innocenti A, Guerri A, Scozzafava A, Rusconi S and Supuran CT (2007*a*) Phosph(on)Ate as a zinc-binding group in

https://doi.org/10.1017/S0033583518000082

metalloenzyme inhibitors: X-ray crystal structure of the antiviral drug foscarnet complexed to human carbonic anhydrase I. *Bioorganic & Medicinal Chemistry Letters* **17**, 2210–2215.

Temperini C, Innocenti A, Scozzafava A, Mastrolorenzo A and Supuran CT (2007*b*) Carbonic anhydrase activators: l-Adrenaline plugs the active site entrance of isozyme II, activating better isoforms I, IV, VA, VII, and XIV. *Bioorganic & Medicinal Chemistry Letters* **17**, 628–635.

Temperini C, Winum J-Y, Montero J-L, Scozzafava A and Supuran CT (2007*c*) Carbonic anhydrase inhibitors: the X-ray crystal structure of the adduct of *N*-hydroxysulfamide with isozyme II explains why this new zinc binding function is effective in the design of potent inhibitors. *Bioorganic & Medicinal Chemistry Letters* **17**, 2795–2801.

Temperini C, Cecchi A, Boyle NA, Scozzafava A, Cabeza JE, Wentworth P, Blackburn GM and Supuran CT (2008*a*) Carbonic anhydrase inhibitors. Interaction of 2-*N*, *N*-dimethylamino-1,3,4-thiadiazole-5-methanesulfonamide with 12 mammalian isoforms: kinetic and X-ray crystallographic studies. *Bioorganic & Medicinal Chemistry Letters* **18**, 999–1005.

Temperini C, Cecchi A, Scozzafava A and Supuran CT (2008*b*) Carbonic anhydrase inhibitors. Interaction of indapamide and related diuretics with 12 mammalian isozymes and X-ray crystallographic studies for the indapamide-isozyme II adduct. *Bioorganic & Medicinal Chemistry Letters* **18**, 2567–2573.

Temperini C, Innocenti A, Scozzafava A and Supuran CT (2008*c*) Carbonic anhydrase activators: kinetic and X-ray crystallographic study for the interaction of D- and L-tryptophan with the mammalian isoforms I-XIV. *Bioorganic & Medicinal Chemistry* **16**, 8373–8378.

Temperini C, Cecchi A, Scozzafava A and Supuran CT (2009) Carbonic anhydrase inhibitors. Comparison of chlorthalidone, indapamide, trichlormethiazide, and furosemide X-ray crystal structures in adducts with isozyme II, when several water molecules make the difference. *Bioorganic & Medicinal Chemistry* **17**, 1214–1221.

Temperini C, Scozzafava A and Supuran CT (2010) Carbonic anhydrase inhibitors. X-ray crystal studies of the carbonic anhydrase II-trithiocarbonate adduct–an inhibitor mimicking the sulfonamide and urea binding to the enzyme. *Bioorganic & Medicinal Chemistry Letters* **20**, 474–478.

Toleikis Z, Cimmperman P, Petrauskas V and Matulis D (2011) Determination of the volume changes induced by ligand binding to heat shock protein 90 using high-pressure denaturation. *Analytical Biochemistry* **413**, 171–178.

Toleikis Z, Cimmperman P, Petrauskas V and Matulis D (2012) Serum albumin ligand binding volumes using high pressure denaturation. *The Journal of Chemical Thermodynamics* **52**, 24–29.

Toleikis Z, Sirotkin VA, Skvarnavičius G, Smirnovienė J, Roumestand C, Matulis D and Petrauskas V (2016) Volume of Hsp90 ProteinLigand binding determined by fluorescent pressure shift assay, densitometry, and NMR. *Journal of Physical Chemistry B* **120**, 9903–9912.

Touisni N, Maresca A, McDonald PC, Lou Y, Scozzafava A, Dedhar S, Winum J-Y and Supuran CT (2011) Glycosyl coumarin carbonic anhydrase IX and XII inhibitors strongly attenuate the growth of primary breast tumors. *Journal of Medicinal Chemistry* **54**, 8271–8277.

Tu C, Qian M, An H, Wadhwa NR, Duda D, Yoshioka C, Pathak Y, McKenna R, Laipis PJ and Silverman DN (2002) Kinetic analysis of multiple proton shuttles in the active site of human carbonic anhydrase. *Journal of Biological Chemistry* **277**, 38870–38876.

Tu CK and Silverman DN (1986) Observation of the visible absorption spectrum of cobalt(II)-carbonic anhydrase III during catalytic hydration of carbon dioxide. *Journal of the American Chemical Society* **108**, 6065–6066.

Tweedy NB, Nair SK, Paterno SA, Fierke CA and Christianson DW (1993) Structure and energetics of a non-proline cis-peptidyl linkage in a proline-202–alanine carbonic anhydrase II variant. *Biochemistry* **32**, 10944–10949.

Ulmasov B, Waheed A, Shah GN, Grubb JH, Sly WS, Tu C and Silverman DN (2000) Purification and kinetic analysis of recombinant CA XII, a membrane carbonic anhydrase overexpressed in certain cancers. *Proceedings of the National Academy of Sciences of the United States of America* **97**, 14212–14217.

Vaškevičienė I, Paketurytė V, Zubrienė A, Kantminienė K, Mickevičius V and Matulis D (2017) *N*-Sulfamoylphenyl- and *N*-sulfamoylphenyl-*N*-thiazolyl – alanines and their derivatives as inhibitors of human carbonic anhydrases. *Bioorganic Chemistry* **75**, 16–29.

Vega S, Abian O and Velazquez-Campoy A (2016) On the link between conformational changes, ligand binding and heat capacity. *Biochimica et Biophysica Acta (BBA) – General Subjects* **1860**, 868–878.

Vernier W, Chong W, Rewolinski D, Greasley S, Pauly T, Shaw M, Dinh D, Ferre RA, Nukui S, Ornelas M and Reyner E (2010) Thioether benzenesulfonamide inhibitors of carbonic anhydrases II and IV: structure-based drug design, synthesis, and biological evaluation. *Bioorganic & Medicinal Chemistry* **18**, 3307–3319.

Vidgren J, Liljas A and Walker NP (1990) Refined structure of the Acetazolamide complex of human carbonic anhydrase II at 1.9 A. *International Journal of Biological Macromolecules* **12**, 342–344.

Vitale RM, Alterio V, Innocenti A, Winum JY, Monti SM, De Simone G and Supuran CT (2009) Carbonic anhydrase inhibitors. Comparison of aliphatic sulfamate/bis-sulfamate adducts with isozymes II and IX as a platform for designing tight-binding, more isoform-selective inhibitors. *Journal of Medicinal Chemistry* **52**, 5990–5998.

Voloshin VP, Medvedev NN, Smolin N, Geiger A and Winter R (2015) Disentangling volumetric and hydrational properties of proteins. *Journal of Physical Chemistry B* **119**, 1881–1890.

Wagner J, Avvaru BS, Robbins AH, Scozzafava A, Supuran CT and McKenna R (2010) Coumarinyl-substituted sulfonamides strongly inhibit several human carbonic anhydrase isoforms: solution and crystallographic investigations. *Bioorganic & Medicinal Chemistry* **18**, 4873–4878.

Wang Y, Roose BW, Philbin JP, Doman JL and Dmochowski IJ (2016) Programming A molecular relay for ultrasensitive biodetection through (129) Xe. *Angewandte Chemie International Edition in English* **55**, 1733–1736.

Weber A, Casini A, Heine A, Kuhn D, Supuran CT, Scozzafava A and Klebe G (2004) Unexpected nanomolar inhibition of carbonic anhydrase by COX-2-selective celecoxib: new pharmacological opportunities due to related binding site recognition. *Journal of Medicinal Chemistry* **47**, 550–557.

West D, Pinard MA, Tu C, Silverman DN and McKenna R (2014) Human carbonic anhydrase II-cyanate inhibitor complex: putting the debate to rest. *Crystallographica. Section F, Structural Biology Communications* **70**, 1324–1327.

Whitney PL and Brandt H (1976) Effects of two ionizing groups on the active site of human carbonic anhydrase B. *Journal of Biological Chemistry* **251**, 3862–3867.

Whittington DA, Waheed A, Ulmasov B, Shah GN, Grubb JH, Sly WS and Christianson DW (2001) Crystal structure of the dimeric extracellular domain of human carbonic anhydrase XII, a bitopic membrane protein overexpressed in certain cancer tumor cells. *Proceedings of the National Academy of Sciences of the United States of America* **98**, 9545–9550.

Whittington DA, Grubb JH, Waheed A, Shah GN, Sly WS and Christianson DW (2004) Expression, assay, and structure of the extracellular domain of murine carbonic anhydrase XIV: implications for selective inhibition of membrane-associated isozymes. *Journal of Biological Chemistry* **279**, 7223–7228.

Wilton DJ, Kitahara R, Akasaka K, Pandya MJ and Williamson MP (2009) Pressure-Dependent structure changes in barnase on ligand binding reveal intermediate rate fluctuations. *Biophysical Journal* **97**, 1482–1490.

Wingo T, Tu C, Laipis PJ and Silverman DN (2001) The catalytic properties of human carbonic anhydrase IX. *Biochemical and Biophysical Research Communications* **288**, 666–669.

Winum JY, Temperini C, Cheikh KE, Innocenti A, Vullo D, Ciattini S, Montero JL, Scozzafava A and Supuran CT (2006) Carbonic anhydrase inhibitors: clash with Ala65 as a means for designing inhibitors with Low affinity for the ubiquitous isozyme II, exemplified by the crystal structure of the topiramate sulfamide analogue. *Journal of Medicinal Chemistry* **49**, 7024–7031.

Winum J-Y, Innocenti A, Scozzafava A, Montero J-L and Supuran CT (2009) Carbonic anhydrase inhibitors. Inhibition of the human cytosolic isoforms I and II and transmembrane, tumor-associated isoforms IX and XII with boronic acids. *Bioorganic & Medicinal Chemistry* **17**, 3649–3652.

Wischeler JS, Innocenti A, Vullo D, Agrawal A, Cohen SM, Heine A, Supuran CT and Klebe G (2010) Bidentate zinc chelators for alpha-carbonic

https://doi.org/10.1017/S0033583518000082

anhydrases that produce a trigonal bipyramidal coordination geometry. *ChemMedChem* **5**, 1609–1615.

Wischeler JS, Sun D, Sandner NU, Linne U, Heine A, Koert U and Klebe G (2011) Stereo- and regioselective azide/alkyne cycloadditions in carbonic anhydrase II via tethering, monitored by crystallography and mass spectrometry. *Chemistry* **17**, 5842–5851.

Wiseman T, Williston S, Brandts JF and Lin LN (1989) Rapid measurement of binding constants and heats of binding using a new titration calorimeter. *Analytical Biochemistry* **179**, 131–137.

Wishart DS, Knox C, Guo AC, Shrivastava S, Hassanali M, Stothard P, Chang Z and Woolsey J (2006) Drugbank: a comprehensive resource for in silico drug discovery and exploration. *Nucleic Acids Research* **34**, D668–D672.

Woo LWL, Fischer DS, Sharland CM, Trusselle M, Foster PA, Chander SK, Fiore AD, Supuran CT, Simone GD, Purohit A, Reed MJ and Potter BVL (2008) Anticancer steroid sulfatase inhibitors: synthesis of a potent fluorinated second-generation agent, *in vitro* and *in vivo* activities, molecular modeling, and protein crystallography. *Molecular Cancer Therapeutics* **7**, 2435–2444.

Woo LWL, Jackson T, Putey A, Cozier G, Leonard P, Acharya KR, Chander SK, Purohit A, Reed MJ and Potter BVL (2010) Highly potent first examples of dual aromatase-steroid sulfatase inhibitors based on a biphenyl template. *Journal of Medicinal Chemistry* **53**, 2155–2170.

Xue Y, Liljas A, Jonsson B and Lindskog S (1993*a*) Structural analysis of the zinc hydroxide-Thr-199-Glu-106 hydrogen-bond network in human carbonic anhydrase II. *Proteins* **17**, 93–106.

Xue Y, Vidgren J, Svensson LA, Liljas A, Jonsson BH and Lindskog S (1993*b*) Crystallographic analysis of Thr-200–His human carbonic anhydrase II and its complex with the substrate, HCO_3^-. *Proteins* **15**, 80–87.

Yanchunas J, Langley DR, Tao L, Rose RE, Friborg J, Colonno RJ and Doyle ML (2005) Molecular basis for increased susceptibility of isolates with atazanavir resistance-conferring substitution I50L to other protease inhibitors. *Antimicrobial Agents and Chemotherapy* **49**, 3825–3832.

Zheng J, Avvaru BS, Tu C, McKenna R and Silverman DN (2008) Role of hydrophilic residues in proton transfer during catalysis by human carbonic anhydrase II. *Biochemistry* **47**, 12028–12036.

Zubrienė A, Čapkauskaitė E, Gylytė J, Kišonaitė M, Tumkevičius S and Matulis D (2014) Benzenesulfonamides with benzimidazole moieties as inhibitors of carbonic anhydrases I, II, VII, XII and XIII. *Journal of Enzyme Inhibition and Medicinal Chemistry* **29**, 124–131.

Zubrienė A, Smirnovienė J, Smirnov A, Morkūnaitė V, Michailovienė V, Jachno J, Juozapaitienė V, Norvaišas P, Manakova E, Gražulis S and Matulis D (2015) Intrinsic thermodynamics of 4-substituted-2,3,5,6-tetrafluorobenzenesulfonamide binding to carbonic anhydrases by isothermal titration calorimetry. *Biophysical Chemistry* **205**, 51–65.

Zubrienė A, Smirnov A, Dudutienė V, Timm DD, Matulienė J, Michailovienė V, Zakšauskas A, Manakova E, Gražulis S and Matulis D (2017) Intrinsic thermodynamics and structures of 2,4- and 3,4-substituted fluorinated benzenesulfonamides binding to carbonic anhydrases. *ChemMedChem* **12**, 161–176.

https://doi.org/10.1017/S0033583518000082